MAGNETIC DATA OVER THE CONTINENTAL MARGIN OF EASTERN CANADA: PREPARATION OF A DATA BASE AND CONSTRUCTION OF A 1:5 MILLION MAGNETIC ANOMALY MAP.

Jacob Verhoef and Ron Macnab
Atlantic Geoscience Centre

GSC Open File 1504

December 20, 1987

Geological Survey of Canada
Dartmouth, Nova Scotia
B2Y 4A2

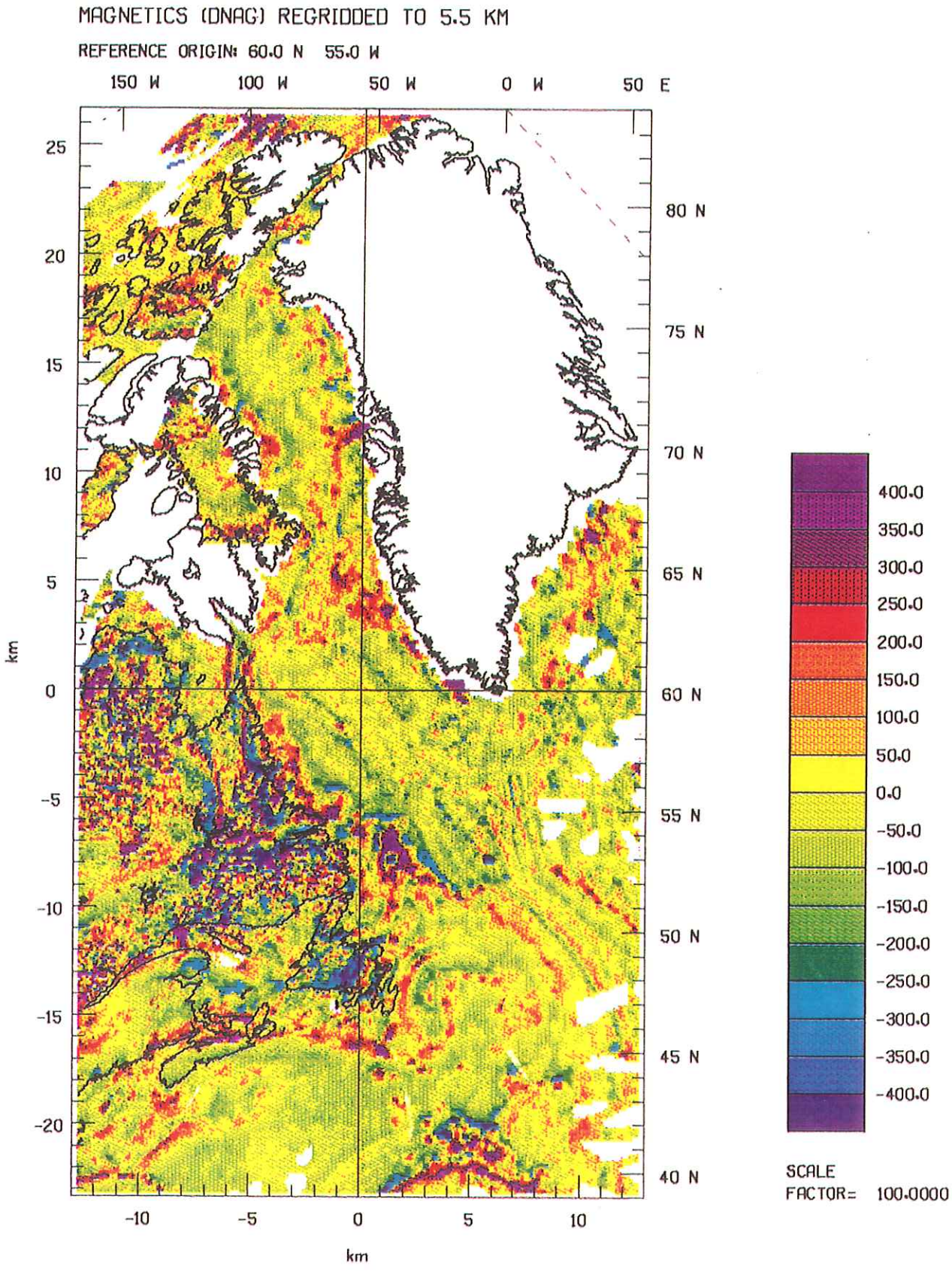
MAGNETICS (DNAG) REGRIDDED TO 5.5 KM
REFERENCE ORIGIN: 60.0 N 55.0 W
150 W
100 W
50 W
0 W
50 E
80 N
75 N
70 N
65 N
60 N
55 N
50 N
45 N
40 N
25
20
15
10
5
0
-5
-10
-15
-20
km
-10
-5
0
5
10
km
400.0
350.0
300.0
250.0
200.0
150.0
100.0
50.0
0.0
-50.0
-100.0
-150.0
-200.0
-250.0
-300.0
-350.0
-400.0
SCALE
FACTOR= 100.0000

ABSTRACT

This report describes the implementation of a data base containing marine and aeromagnetic data over eastern Canada and adjacent offshore areas.

The primary marine data set consisted of about 2.9 million observations collected over nearly one million line kilometres on 91 cruises during the period 1963-84. A small additional quantity of data was obtained from the National Geophysical Data Center (NGDC) at Boulder, Colorado.

The aeromagnetic data set consisted of:

a): numerous surveys carried out over land portions of eastern Canada since the late 40's by the Geophysics Division of the GSC, formerly the Resource Geophysics and Geochemistry Division;

b): three recently acquired data sets over Georges Bank, the Laurentian Channel, and the Northeast Newfoundland Shelf;

c): additional data sets obtained from the US Naval Research Laboratory and the US Geological Survey.

The aeromagnetic data were obtained in gridded form or in flight line format, after prior checking elsewhere for internal consistency and accuracy. A large part of the data base implementation consisted of similar checks on the marine data set, and these are described in this report.

The collection of the marine magnetic data spanned a 21-year period, and temporal variations of the earth's magnetic field are therefore an important factor. The International Geomagnetic Reference Fields (IGRF) were applied to all the data in order to compensate for these variations, and to reduce the observed total field values to anomalies.

The reference fields are defined at 5 year intervals, and values in the intervening years are obtained by linear interpolation. In order to determine the performance of the reference fields in eliminating time variations, we grouped the calculated anomalies by 5-year periods, and gridded each group separately. We found that anomalies in overlapping areas did not have the same values in the different periods. Since anomalies are related to geological features that remain stable over the time periods involved, this suggested that there is still some time dependency left in the reference fields.

To gain some insight into the nature of the residual time dependency in the reference fields, we calculated the errors at nearly 60,000 track crossover points in the marine data, and undertook

an analysis of their statistical properties. After comparing histograms of the crossover errors for different time periods and latitude bounds, we concluded that the pre-1975 reference fields are too low in the southern part of the study area (i.e. between 35N and 50N), resulting in derived anomalies that are too high.

We used a shadowgram technique to identify bad points in the marine data, and eliminated some 3% of the data set on that basis. After this process, an analysis of the crossover errors in the remaining data gave a mean value of -0.9 nT and a standard deviation of 69.9 nT for 53361 crossovers, excluding errors greater than twice the standard deviation of the mean value.

Having cleaned up the marine data set to a practicable level, we then proceeded to combine it with the different aeromagnetic sets. Level differences occurred at several locations between the two types of data, and it was decided to make all adjustments with respect to the marine data. At all locations save one, we applied constant level corrections, and eliminated small differences at the seams with a cosine taper. The only exception was Georges Bank, where we used an inclined plane for the level correction.

The resulting data set, at a geographical grid of 0.05 degrees latitude and longitude, was then used to produce a map of the magnetic anomalies over the continental margin of eastern Canada, bounded by latitudes 40N and 84N, to accompany the volume prepared by the AGC staff as their contribution to the commemorative series for the Decade of North American Geology (DNAG). The map was produced in a Lambert projection at a scale of 1:5 million.

TABLE OF CONTENTS

LIST OF FIGURES

1. INTRODUCTION

This report discusses three topics:

1) The implementation of a data base containing marine and aeromagnetic data over eastern Canada and adjacent offshore areas.

2) The procedures for manipulating, editing, processing, and displaying the contents of the data base.

3) The use of that data in the construction of a regional magnetic anomaly map.

Marine magnetic data have been collected off the coast of eastern Canada since the early 1960's; aeromagnetic data have been collected over land and sea areas of the same region as part of a national program dating back to the late 1940's. The data sets collected during these mapping operations were assembled recently at the Atlantic Geoscience Centre in order to create a unified and cohesive data base for eastern Canada and its offshore regions. After merging, adjustment, and extensive editing, the data are now in a 'clean' form that readily lends itself to analysis and interpretation with modern investigative tools.

During the process, we developed and implemented several procedures to facilitate the handling and processing of large sets of magnetic data: editing, gridding, merging, filtering, IGRF calculation, cross over analysis, and colour graphics display. Most of these procedures can be similarly applied to other data types available in gridded form, e.g. bathymetry and gravity.

An important end product of the above tasks is a 1:5 million colour map of the magnetic anomaly over the continental margin of eastern Canada. In providing a regional overview of the land and sea areas adjacent to the entire east coast, this map facilitates the identification and comparison of features associated with large and medium scale geological structures that are characteristic of oceanic and continental regions.

2. MARINE MAGNETIC OPERATIONS IN THE GSC

2.1. Historical background

Measurements of the marine magnetic field have been carried out off the east coast of Canada in two distinct types of operation: problem-oriented research cruises, and systematic mapping expeditions.

Research cruises began in 1963 shortly after the opening of the

Bedford Institute of Oceanography (BIO), and were generally mobilized in a given locale to study specific geologic problems by a variety of techniques; they were characterized in many cases by irregular orientations and spacings of ships' tracks, and in some cases (particularly in northern regions or in early years) by navigation that was not highly accurate.

Mapping expeditions, on the other hand, emphasized the systematic blanketing of oceanic regions with a regular network of ship tracks, using the most accurate navigational aids that could be afforded.

In spite of the differences between research and mapping operations, the different data sets often complemented one another, and were combined whenever practicable.

Systematic mapping was carried out through the years as a cooperative project involving components that now form part of two Federal Government departments: Energy, Mines and Resources (DEMR), and Fisheries and Oceanography (DFO). In the following sections, most of the discussion refers to mapping operations, as this is how the bulk of the data were collected.

Mapping began in 1964, when BIO geophysicists operated a magnetometer and gravimeter aboard the Canadian Scientific Ship BAFFIN during a hydrographic survey in the Bay of Fundy. This proved to be an efficient and cost-effective technique for acquiring potential field data, capitalizing on a systematic mapping program that required a large ship to operate under precise navigational control.

From that beginning developed the concept of multiparameter surveys, which combined the efforts of hydrographers and geophysicists in the collection and field processing of bathymetric, magnetic, and gravity data. (Macnab, 1974; Macnab and Srivastava, 1975; Macnab, 1983A; Miller et al, 1983; Macnab et al, 1985B)

By 1984, the combined output of the research and mapping operations resulted in a network of observations extending from the Gulf of Maine in the south to Davis Strait in the north, and in numerous reconnaissance tracks in Baffin Bay. Figure 1 shows the distribution of ships' tracks where marine magnetic data were collected throughout the region, while Figure 2 indicates the density of observations.

In total, nearly one million line kilometres of data were collected (see Figure 3 for a breakdown into yearly totals), yielding about 2.9 million observation points. Table 1 lists the year, area of operations, number of data points, and total line kilometres for each cruise.

FIGURE 1. Ships' track chart showing where magnetic data were collected by AGC between 1963 and 1984.

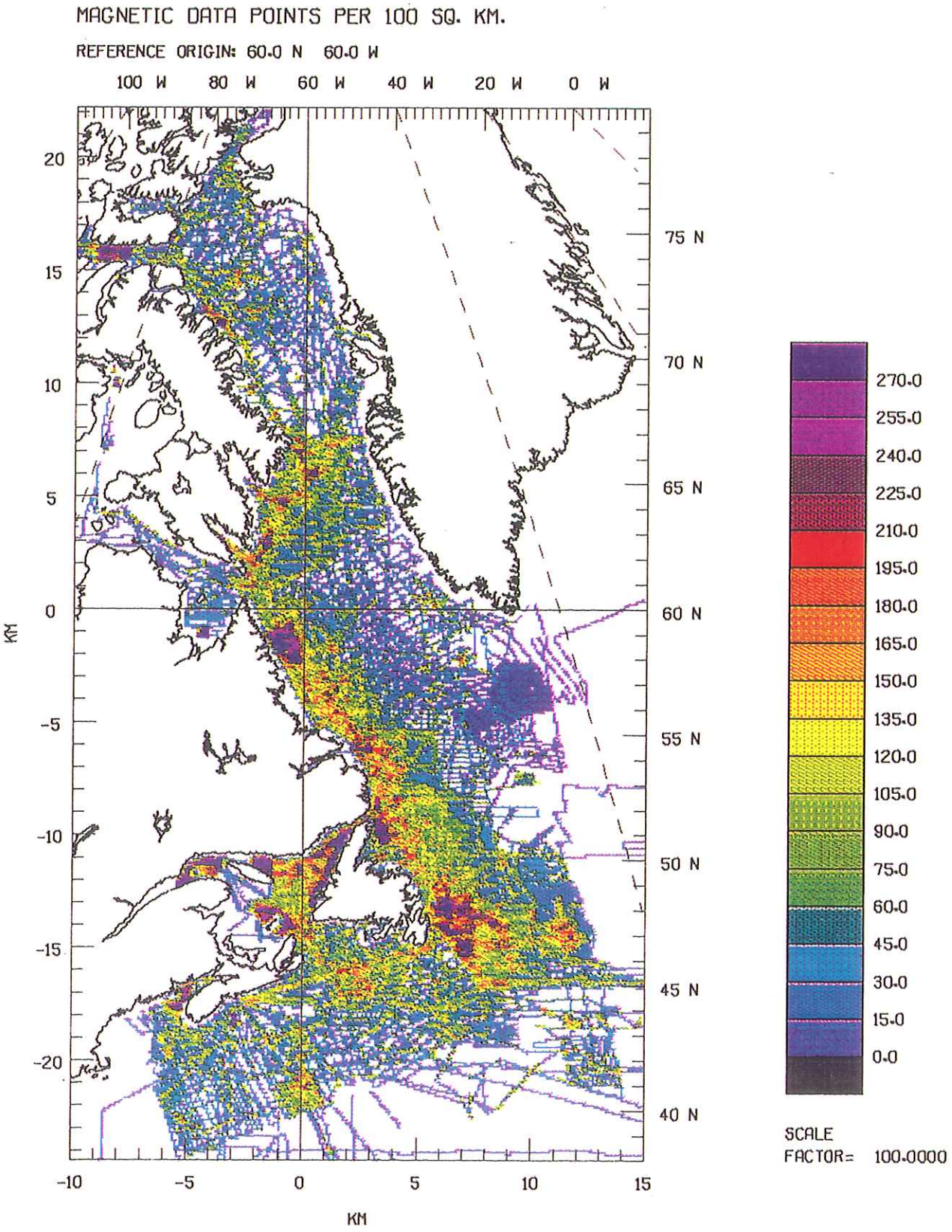

FIGURE 2. Density of magnetic observations in the period 1963-84, as measured by the number of data points per 100 sq km.

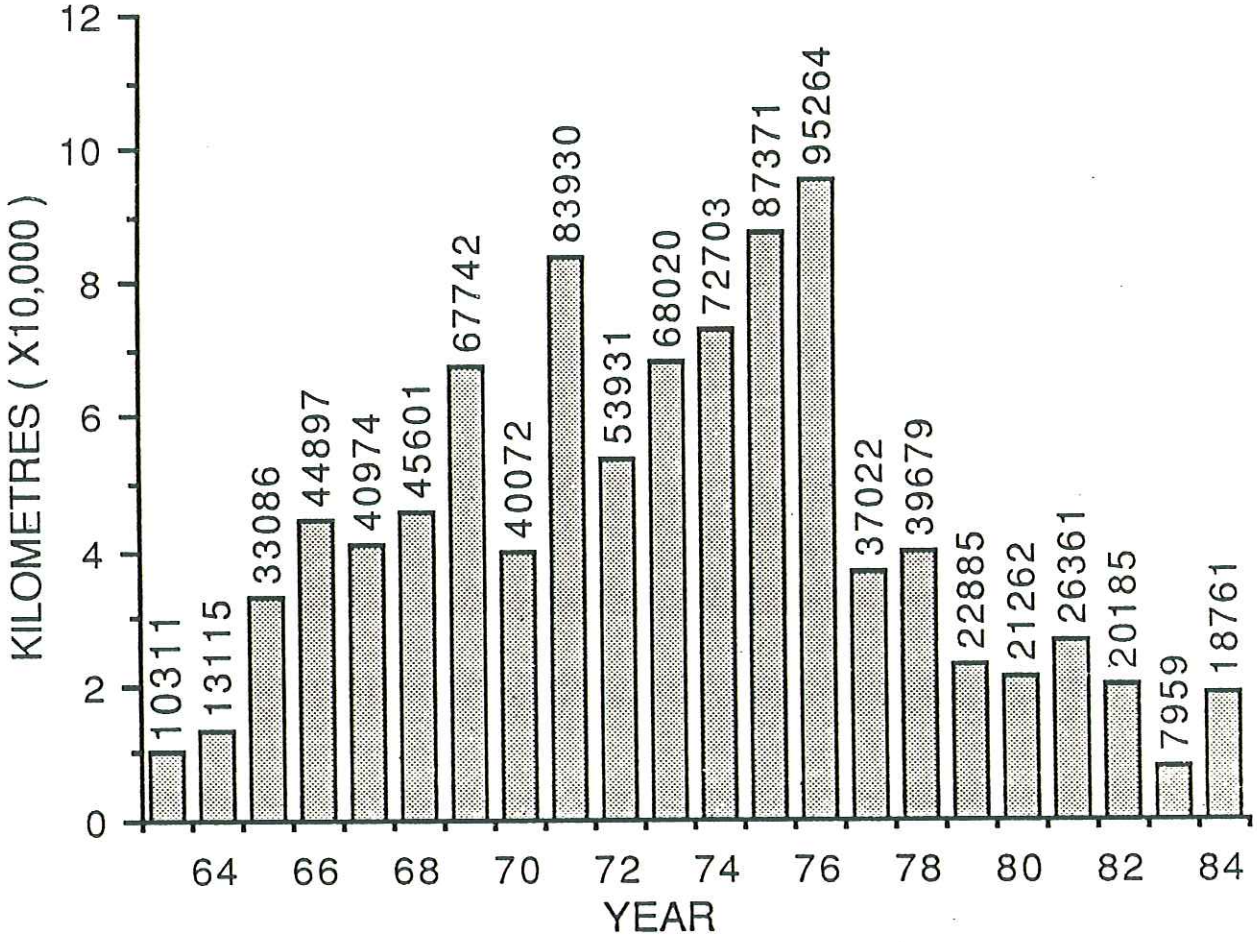

FIGURE 3. Yearly totals of line kilometres of marine magnetic data. Grand total: 951,131 km.

In the mid-1960's, the multiparameter survey program concentrated on detailed mapping of the south and central portions of the Grand Banks of Newfoundland. The late 1960's saw a shift to the eastern Gulf of St. Lawrence, while activities in the years 1971 to 1981 were concentrated mostly in the Labrador Sea and Davis Strait.

Without special and costly navigation systems, further advances northward into Baffin Bay were not possible, and so mapping operations in this region were deferred until the advent of the Global Positioning System (GPS). Survey operations in 1982-1984 were restricted to the continental shelves and margins adjacent to Nova Scotia and Newfoundland.

Some idea of the progress and rate of data collecting may be obtained from a study of Figure 4, which illustrates the density of data points over a succession of five-year periods spanning the interval of operations.

The most recent large scale systematic survey was in 1984; operations were suspended at that time for an indefinite period, pending the availability of GPS, and to allow an opportunity to put the data in order.

2.2. Survey design and philosophy

Surveys were usually designed and conducted in order to meet stringent hydrographic requirements for bathymetric data. A primary objective of these requirements was to map shallow areas as thoroughly as possible. Parallel survey lines therefore tended to be oriented at right angles to known bathymetric trends, and spaced according to water depth: two kilometres or less in the shallow areas of the continental shelf, opening gradually to thirty kilometres or so in deep ocean basins.

Check lines were executed on most surveys. On later operations, most of these had a regular orientation and spacing, in order to create a set of crossover points that were well distributed in both space and time. On earlier operations, check lines often suffered from a less regular layout, because a common tendency was to consider them as supplementary data gathering opportunities that could be pursued while the ship was on its way to or from port, or to perform buoy checks.

2.3. Ships

A mix of Government-owned and chartered vessels were deployed as survey platforms. Of the BIO fleet, the two ships that were most used were CSS BAFFIN and CSS HUDSON. Both were icebreakers with displacements approaching 5000 t, and could carry a scientific party of up to 25 (though in practice the usual survey team rarely approached that size). A smaller BIO vessel, the CSS

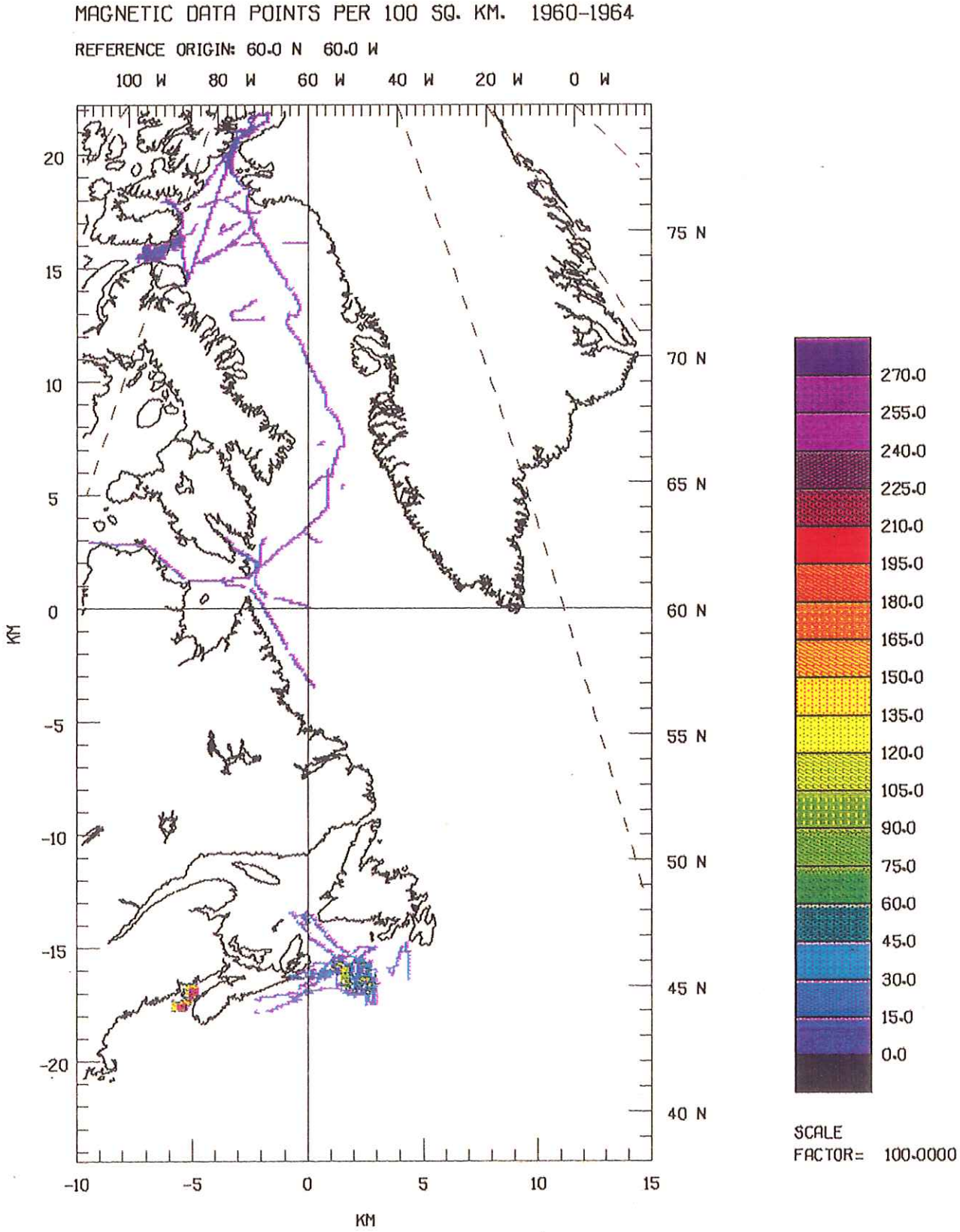

FIGURE 4A. Density of magnetic observations in the five year period shown at the top. Density is measured by th number of observations per 100 sq. km.

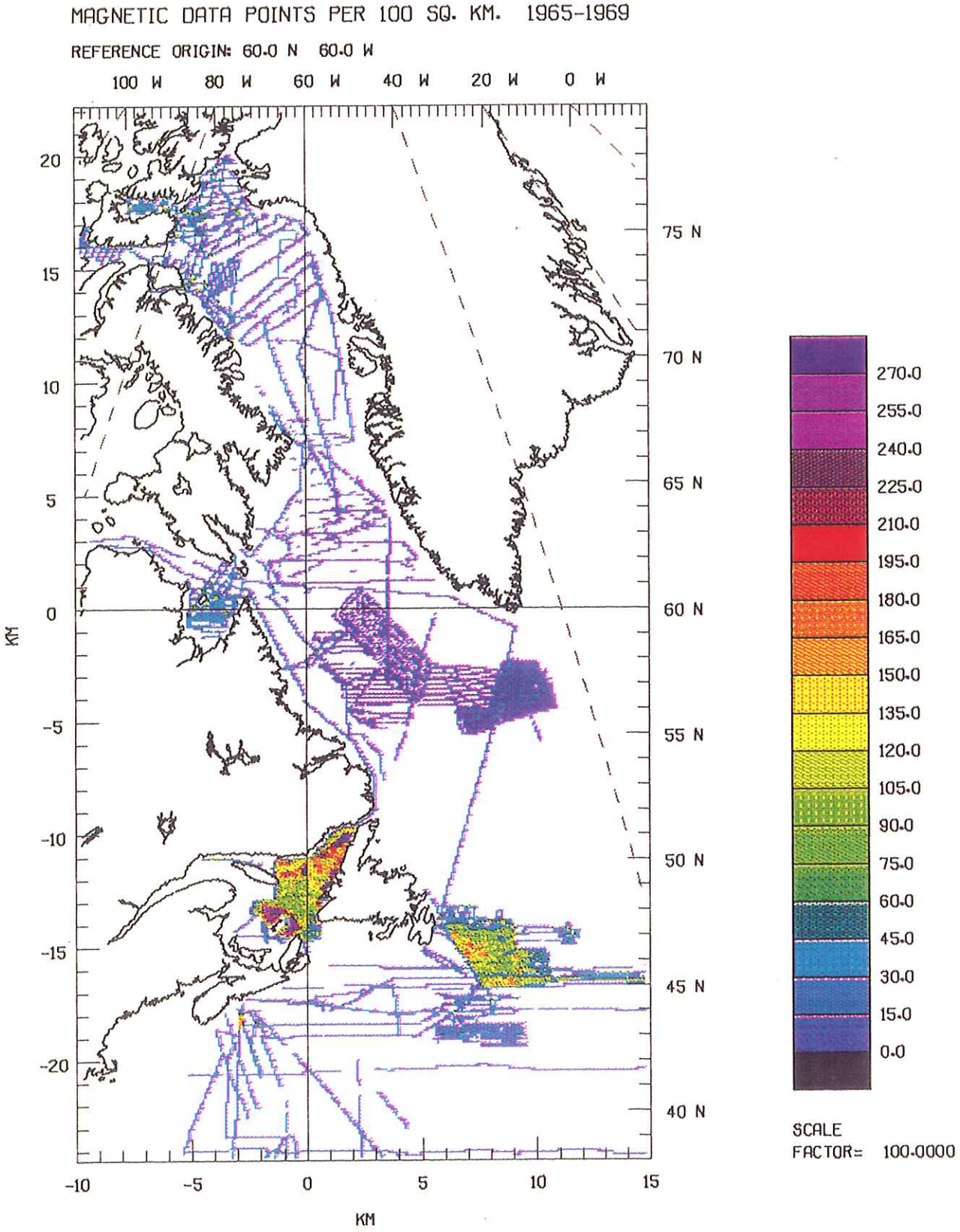

FIGURE 4B. Density of magnetic observations in the five year period shown at the top. Density is measured by the number of observations per 100 sq. km.

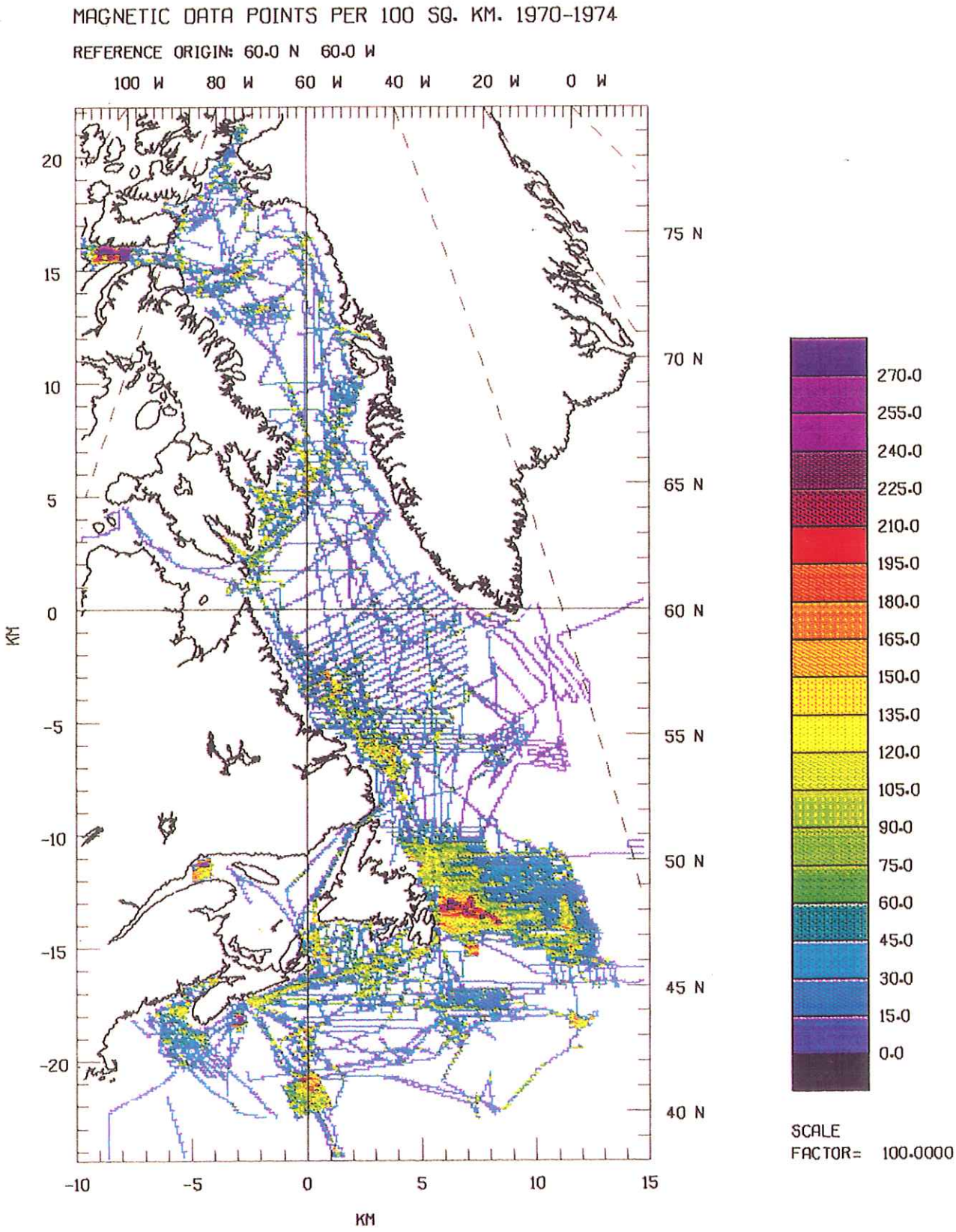

FIGURE 4C. Density of magnetic observations in the five year period shown at the top. Density is measured by the number of observations per 100 sq. km.

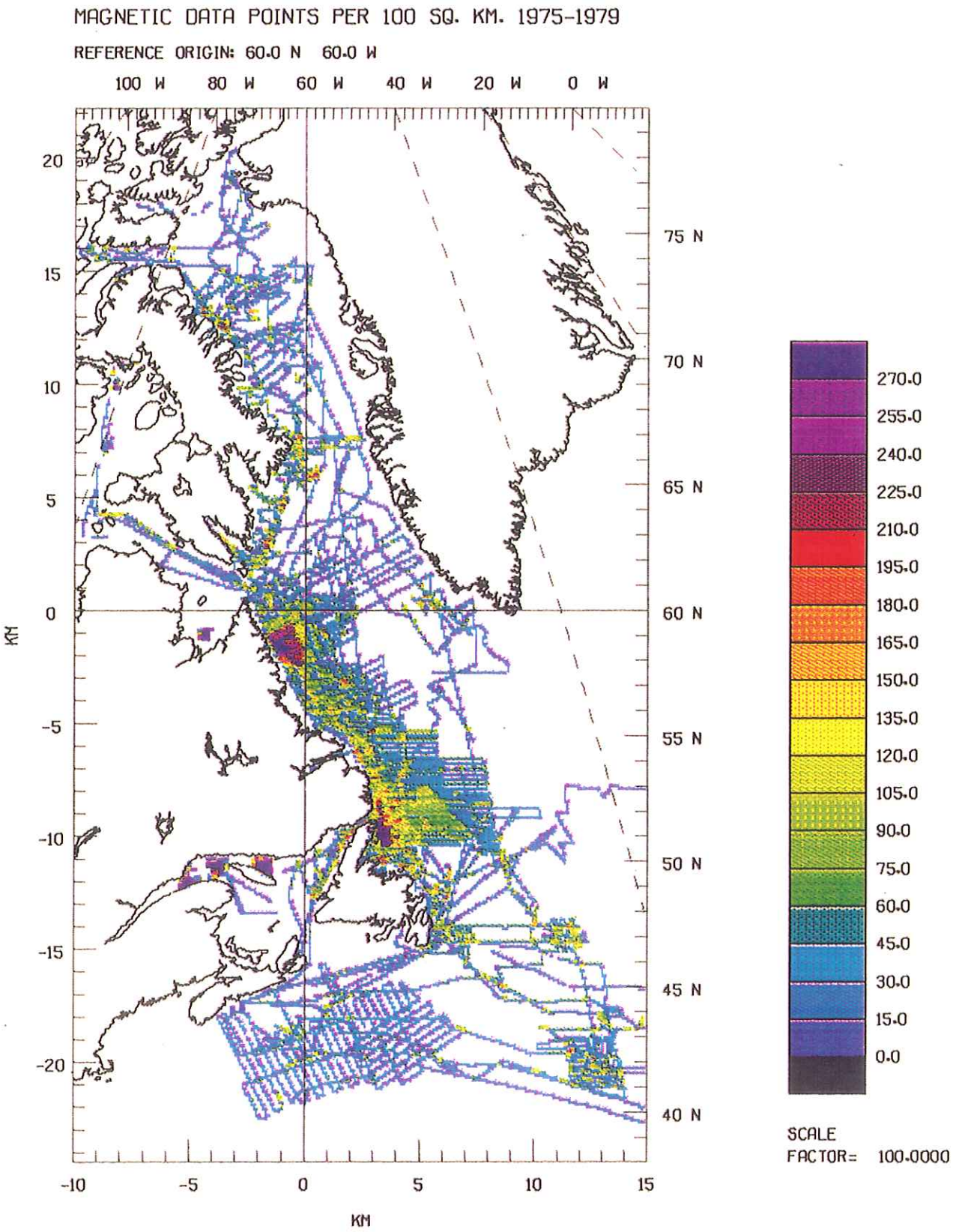

FIGURE 4D. Density of magnetic observations in the five year period shown at the top. Density is measured by the number of observations per 100 sq. km.

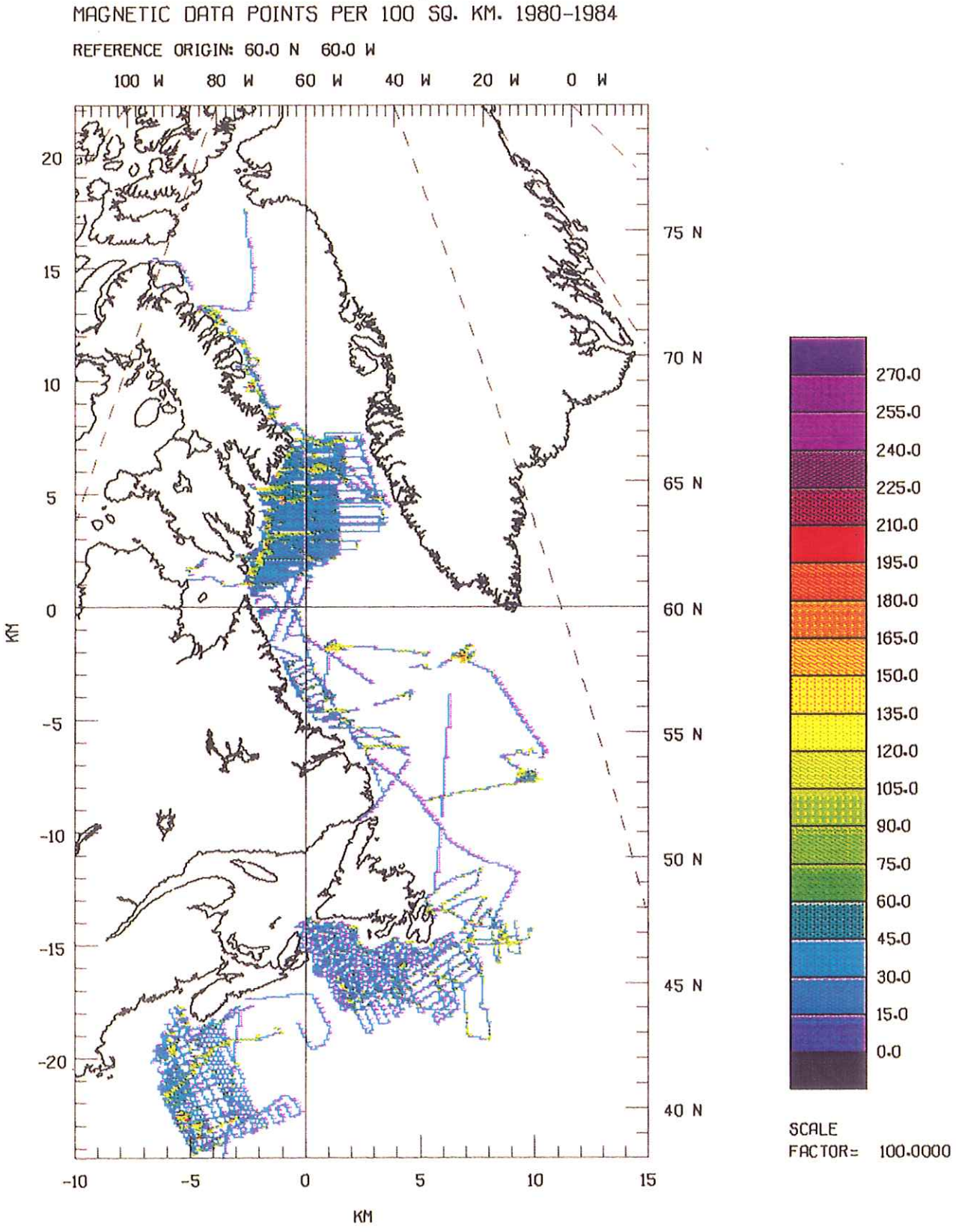

FIGURE 4E. Density of magnetic observations in the five year period shown at the top. Density is measured by the number of observations per 100 sq. km.

DAWSON, was also used on occasion; it displaced 2700 t, and had room for a scientific complement of 13.

During the 1972-78 survey seasons, two charter vessels were engaged: M/V MINNA and M/V MARTIN KARLSEN. Both were in the 2500-3000 t displacement range, with room for 12 to 15 scientific personnel.

2.4. Navigation

In the early years of the mapping program, ship positioning was accomplished largely through the use of Low Ambiguity Decca (Lambda) operating in the range-range mode. This system consisted of a ship-mounted master station and two shore-based slave stations. Ship positions were derived by triangulation, using the measured times of master-slave transmissions.

With a well-calibrated chain, Lambda yielded positional accuracies in the order of 50-150 m. Under good conditions, ranges of up to 300 nautical miles were possible.

In the range-range mode, Lambda suffered from a number of operational and logistical drawbacks. Most of these were eliminated with the introduction of rho-rho Loran-C as a primary positioning system in 1972. Rho-rho positioning is also a triangular technique based on measured transmission times from two or more shore stations to the ship. Where it differs from Decca Lambda is in the use of a precise shipboard clock to maintain synchronization between shore transmitters and the shipboard receiver. This clock tends to drift, but drift rates can be derived through an analysis of positions obtained from the U.S. Navy Navigation Satellite System (NNSS).

Consisting of a series of comparisons between Loran C and NNSS fixes, this analysis was at first performed manually. In 1976, navigation specialists at BIO developed BIONAV, an integrated navigation system that did the analysis automatically by combining the input from a variety of sensors to yield the best possible fix (Grant and Wells, 1982). With data from NNSS and the North Atlantic Loran-C chain, it was estimated that BIONAV yielded ship's positions to an accuracy of 200 m or better in most parts of the offshore area extending from the Bay of Fundy to Hudson Strait.

However, in the northern part of the Labrador Sea and in Davis Strait, positioning accuracy was drastically reduced by a variety of factors. In 1980 and 1981, this was offset by the temporary installation of Accufix stations (auxiliary Loran-C transmitters) at selected locations along the coast. The expense and difficulty of this approach dictated a deferral of further work in northern regions, pending the full operational implementation of GPS.

2.5. Instrumentation and data logging

Marine magnetic measurements are made with a sensor towed astern to reduce the disturbing effect of the vessel's hull. This effect is a function, among other things, of the vessel's magnetic heading and of the towing distance of the magnetometer sensor (Bullard and Mason, 1961). Towing the sensor a minimum of two ship lengths astern is generally believed to reduce the hull effect to about ten nT, and this was used as a rule of thumb throughout the East Coast survey program. Recent tests (Macnab et al, 1985B) indicated that at two ship lengths, the effect for an icebreaker hull such as CSS BAFFIN could be as much as fifteen nT.

In the early years of the survey program, total magnetic field data were collected by a proton precession magnetometer developed and built in-house. In the late 60's, this device was replaced by a succession of instruments manufactured by Barringer, Varian, and Geometrics. In all cases, the field sensor itself was encapsulated in a streamlined tow body.

Total magnetic field readings were logged ten times per minute. Data were saved on punched paper tape until the early 70's, when IBM-compatible magnetic tape was introduced in 7-track format. This was followed eventually by a conversion to 9-track format. As a backup in case of failure of the digital logging system, magnetometer output was also recorded on an analog strip chart recorder. Auxiliary information relating to the conduct of the survey was recorded regularly in watchkeeping and navigation notebooks.

On early surveys, temporary base magnetometers were deployed at nearby land stations whenever practicable, in order to monitor diurnal variations during survey operations. Moored magnetometer buoys were deployed for the same purpose at least twice, but the costs and logistical problems of this approach effectively ruled out its application in routine surveys.

2.6. Shipboard processing operations

Prior to 1972, data processing in the field was accomplished on PDP-8 computers, using programs written in Assembler or FOCAL. HP2100 computers were introduced on BIO ships in 1972, and FORTRAN software then in use on BIO's mainframe computer was adapted for use at sea.

In 1981, the functions and procedures for handling geophysical data aboard ship were consolidated into a suite of integrated computer programs known collectively as SHIPAC, which operated in the Hewlett Packard 1000 computing environment (Macnab, 1983B).

The procedures described in the remainder of this section were performed with SHIPAC software.

Within 24 hours of acquisition, data were written to a backup magnetic tape to safeguard against accidental erasure or damage. The data were checked for obvious recorder or equipment malfunctions, and were then displayed in preliminary form (usually in a video graphic display with subsequent hardcopy) to obtain an assessment of data quality. Most problems consisted of random spikes, noise bursts associated with ship's radio or electrical interference, or 'flat' data recorded when the magnetometer was switched off while the logger was left running.

De-spiking was a largely automatic process that got rid of isolated bad values by a simple statistical procedure: the ten readings logged for each minute of the magnetic record were averaged, and individual observations within that minute were eliminated if their standard deviations exceeded a preset threshold value. Continuous noise bursts and flat spots were removed manually by means of an interactive editing program operating on the data files.

When data for a given day were cleaned up as thoroughly as possible, each one-minute value was assigned a quality factor to indicate the reliability of that reading. In the case of magnetic data, this was usually reduced to a choice between two labels: usable data, and unusable data.

Concurrently with the magnetic data, other forms of data were usually being processed, e.g. navigation, gravity, and bathymetry. At some stage these were merged into one master file. Time and position information were used to evaluate the appropriate IGRF model in order to yield the magnetic anomaly. As a final check for errors and to verify the internal consistency of the cruise data set, an automatic crossover analysis was undertaken to compare measured values at points of survey track intersections.

This usually terminated the shipboard processing phase. Reduced data were double-archived and retained for further treatment after cruise end. All descriptive notes, working plots, etc., relative to shipboard processing operations were saved in a logbook as a record of what was done to the data, and why.

2.7. Post processing of marine data

Data processing methods evolved continually over the life of the survey progam. Progressively more powerful computer technology and improved software permitted increasing portions of the processing to be undertaken at sea, while developments in data base management systems affected the way data were handled both at sea and ashore.

Following a cruise, the data were processed to generate a variety of plots and statistical analyses that served as basic descriptions of the operation: stacked profiles, track plots, location diagrams, crossover discrepancies, etc. These were retained for quick reference at a later date.

If magnetic observatory records were available, some correction for diurnal variation was attempted at this point. This was usually carried out in conjunction with a review of the results of the crossover analyses: it consisted simply of deleting data segments that showed high discrepancies along a succession of crossover points, coincident with significant diurnal excursions.

The cruise data set was then combined with data collected on previous cruises, and more crossover analyses were performed. Depending on the nature of the discrepancies and the available diurnal records, further data deletions took place at this point to improve the overall agreement between all cruise data sets. Given the nature of the primary sources of error, it was difficult if not impossible to improve the data beyond a certain level. If crossover discrepancies could be reduced to a range of 10 to 20 nanotesla, this was deemed to be an acceptable figure of accuracy for the data set.

A more complete discussion of the methods employed in the post-processing phase is contained in a later section.

3. MARINE MAGNETIC DATA COLLECTED BY OTHER INSTITUTIONS

Other groups associated with foreign academic institutions and government agencies have collected marine magnetic data in the Canadian east coast offshore. Some of these observations were supplied directly to AGC and incorporated in the data base, e.g. those collected by the U.S. Naval Oceanographic Office aboard the SHOUP in 1966, the MARIPOSA in 1967, and the LYNCH in 1971.

The bulk of the external data came come from the archives of the National Geophysical Data Centre (NGDC) in Boulder, Colorado. Through the Ottawa offices of the GSC, we acquired North Atlantic data from NGDC in the area bounded by north latitudes 40 and 70, and west longitudes 25 and 60. This provided supplementary information over part of the east coast offshore, as well as the region southeast of Greenland (Figure 5).

4. AEROMAGNETIC DATA

Aeromagnetic data sets that form part of the data base are listed in Table 2.

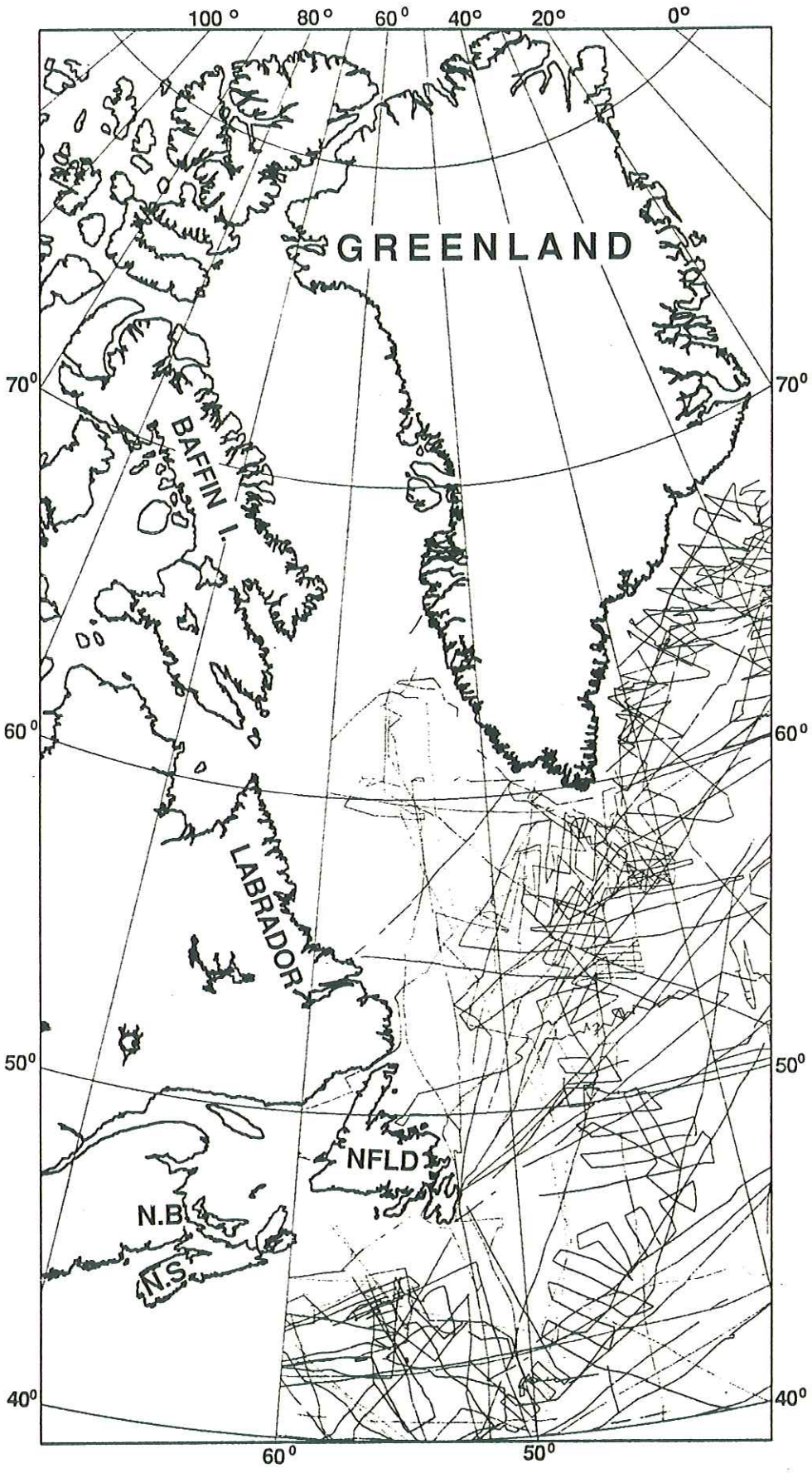

FIGURE 5. Locations of marine magnetic data acquired from the US National Geophysical Data Centre, Boulder, Colorado, and incorporated in the data base.

4.1. Aeromagnetic operations in the GSC

Aeromagnetic surveys have been carried out over the land portions of eastern Canada in a number of operations using an essentially common set of specifications, namely a half mile (805 m) flight line spacing at a mean terrain clearance of 1000 ft (305 m). Most of these surveys were carried out by private operators working under contract to the Federal Government; responsibility for contract management rested with components of the Resource Geophysics and Geochemistry Division (now re-organized into the Geophysics Division) of the GSC (Hood and Ready, 1976; Hood et al., 1985).

Prior to 1972, survey observations were recorded in analog form. Before metrication in the late 1970's, the primary output products were printed maps at scales of one inch to one mile, and one inch to four miles; after metrication, scales were changed to 1:50,000 and 1:250,000.

In 1972, routine digital recording techniques were introduced, clearing not only the way for computerized data handling and management, but also for distribution of data products in computer readable form. The pre-1972 analog data were then recaptured by digitizing published maps (Teskey et al, 1982).

Handling and compilation of aeromagnetic data collected during the national mapping program were carried out largely in the Ottawa offices of the GSC (Dods et al 1985). Digital data sets were corrected for secular variation effects by application of the IGRF, then gridded over a 812.8 m mesh using an inverse distance-weighted average technique (that particular mesh size was chosen because it corresponded to one pixel on the GSC's Applicon plotter at the primary publication scale of one to one million).

In some cases, private data that satisfied basic specifications were incorporated in the data base. Observations recorded at altitudes different from the standard survey elevations were upward or downward continued. Discontinuities between survey boundaries were eliminated or at least minimized, in order to produce the smoothest possible transition between contiguous data sets.

For merging with marine data at AGC, data from the Arctic Islands, Quebec, Newfoundland, and the Atlantic Provinces were extracted from the aeromagnetic data base (see Section 8 for details on how this was done). The areas covered by these data sets are indicated in Figure 6.

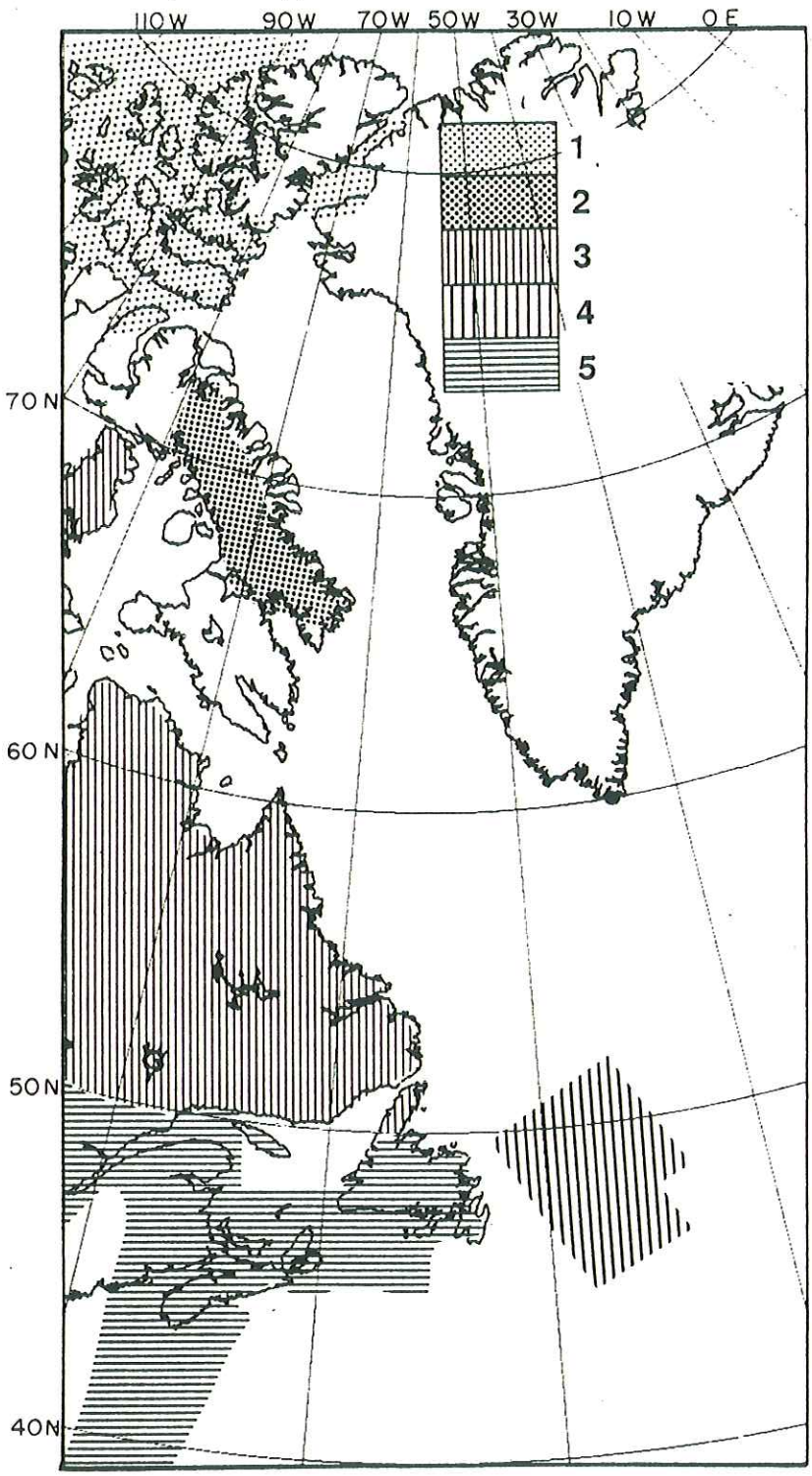

FIGURE 6. Coverage of various GSC aeromagnetic data sets compiled for eastern Canada. Data sets were provided at grid intervals and in projections as follows: 1) Arctic Ocean and Kane Basin - 2km, Transverse Mercator; 2) Baffin Island - 625 m, Universal Transverse Mercator; 3) Areas north of 50N - 4 km, Lambert; 4) Orphan Basin - 625 m, Universal Transverse Mercator; 5) Areas south of 50N - 2 km, Transverse Mercator.

4.2. Recent GSC aeromagnetic surveys in the offshore

In recent years, the GSC has sponsored or co-sponsored three major surveys in the Canadian east coast offshore.

Georges Bank and parts of the Scotian Shelf were mapped in 1982 by Kenting Earth Sciences Limited. Flight line spacings, generally, were 2 km over the continental shelf, 6 km over the continental slope. (Figure 7)

The Laurentian Channel was mapped in 1985 by Kenting Earth Sciences Limited. Flight line spacings were 1 km in nearshore areas, increasing to 2 and 4 km in deeper water. (Figure 8)

The Northeast Newfoundland Shelf was mapped in 1985 by Geoterrex Limited with Kenting Earth Sciences Limited as major sub-contractor. The survey was carried out on behalf of the GSC and a consortium of five oil companies (Amoco, Canterra, Chevron, Columbia and Petro Canada). A flight line spacing of 3 X 9 km was chosen in order to map the distribution, shape, and size of sedimentary basins (see Figure 9A). In conjunction with this high resolution operation, the GSC acting alone sponsored a supplementary regional survey in an adjacent area in order to map evidence of tectonic activity on the deep sea floor. The flight line spacing in this latter operation was 30 km (Figure 9B).

Technical details relating to field and data handling procedures in the above survey operations are recorded in various contractors' reports (Kenting Earth Sciences, Ltd., 1982, 1987; Geoterrex Ltd, 1986).

4.3. Other aeromagnetic data sets

Additional data sets originating from operations sponsored by US or industry agencies were acquired for incorporation in the AGC data base.

The US Naval Research Laboratory (NRL) has collected magnetic data over two areas pertinent to this project: the Arctic Ocean, and a region off Nova Scotia and Newfoundland containing the so-called J-Anomaly.

Arctic data were collected from 1974 to 1978 in the areas shown in Figure 10 (Vogt et al, 1979; Taylor et al, 1981), and were supplied to us in two kilometre grids by Dennis Teskey of GSC Ottawa. The J Anomaly was mapped in 1977 by a series of long profiles at 20 km spacing and 300 m altitude (Figure 11). The data were provided by Skip Kovacs of NRL in flight line form, i.e. as a time series of observations distributed along aircraft flight lines.

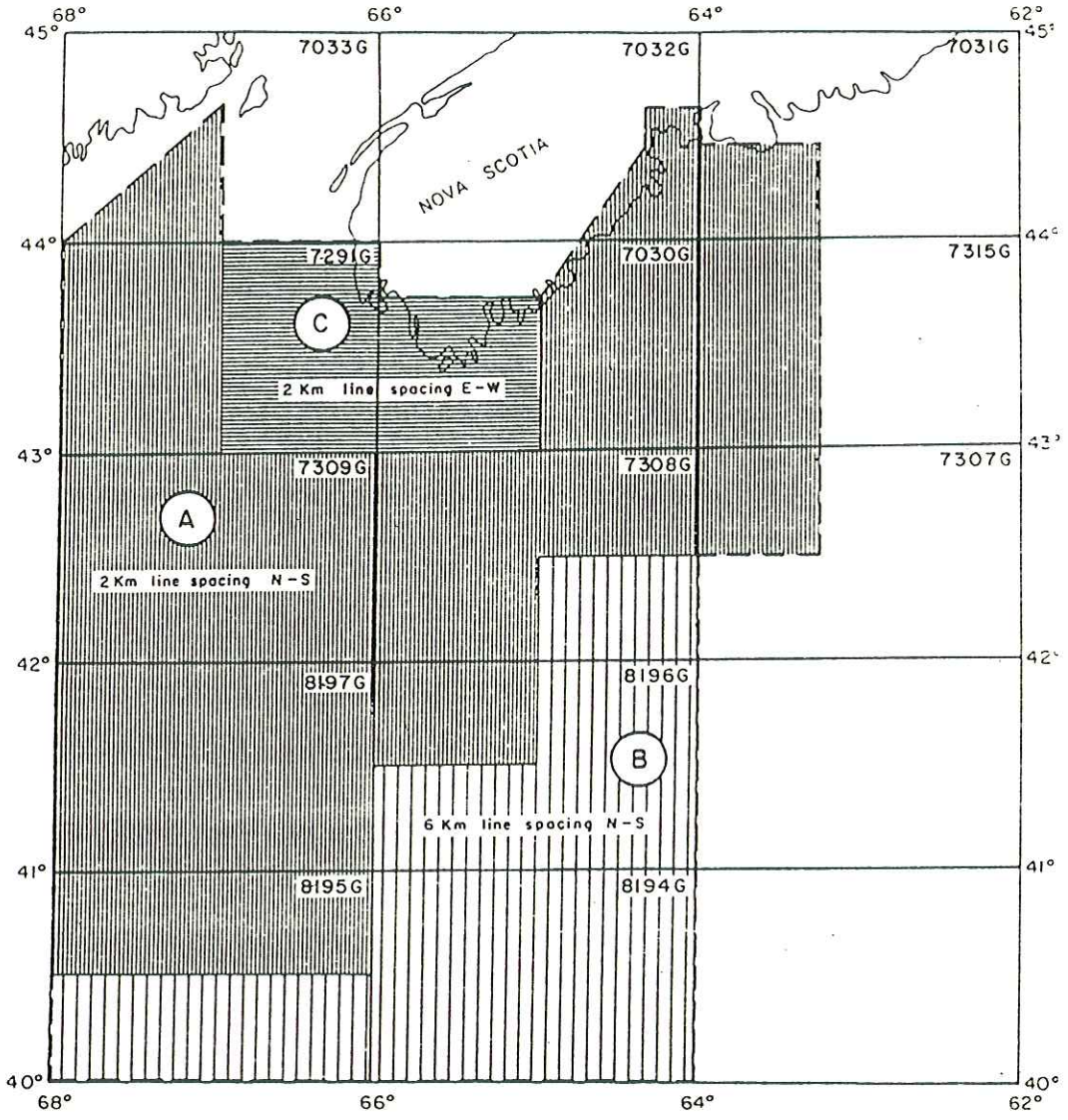

FIGURE 7. Proposed flight line layout for Georges Bank aeromagnetic survey (tie lines not shown). Actual flight lines deviated only slightly from this scheme.

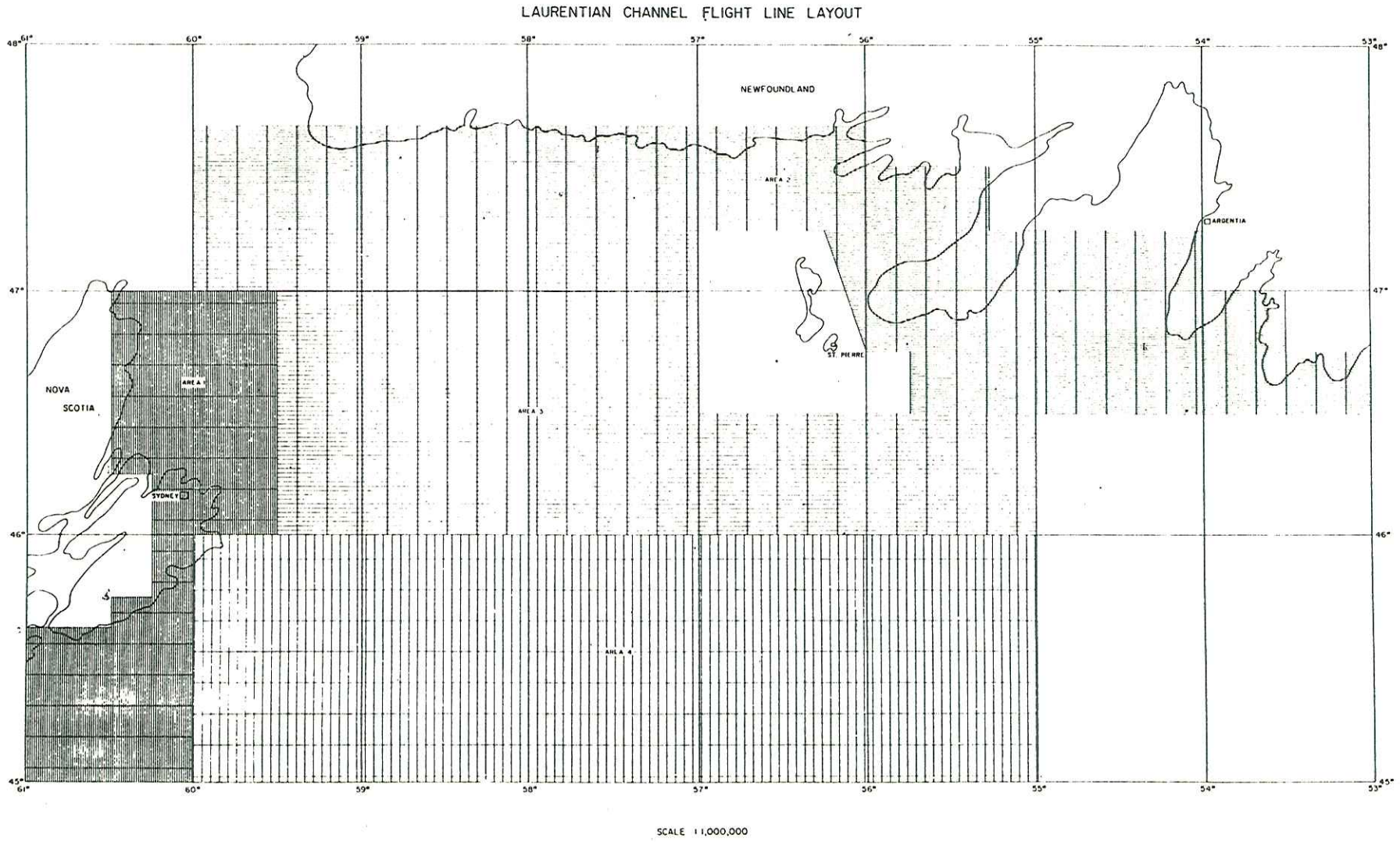

FIGURE 8. Proposed flight line layout for Laurentian Channel aeromagnetic survey. Actual flight lines deviated only slightly from this scheme.

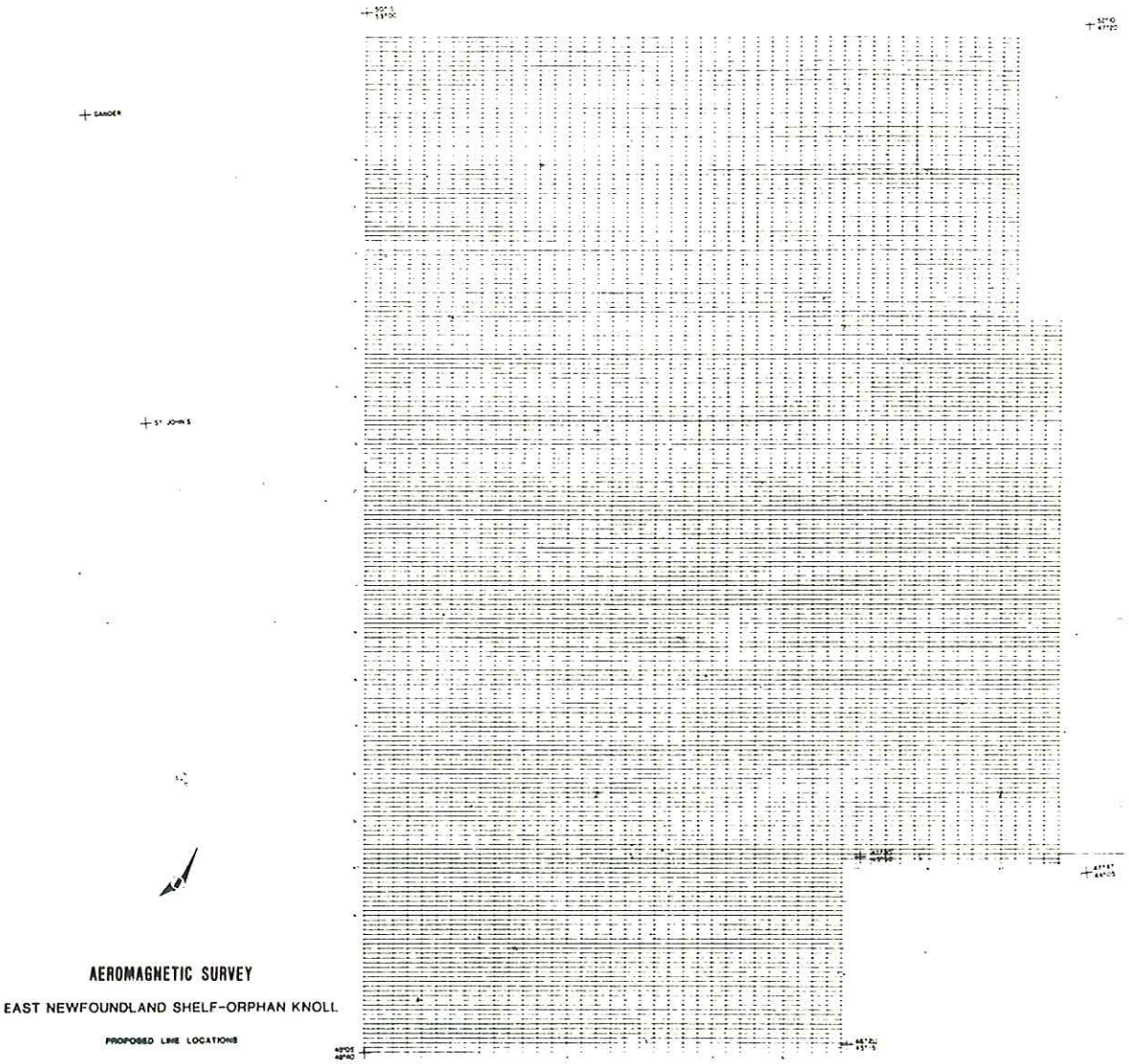

FIGURE 9A. Northeast Newfoundland Shelf aeromagnetic survey: Proposed high resolution flight lines(location see figure 38C).

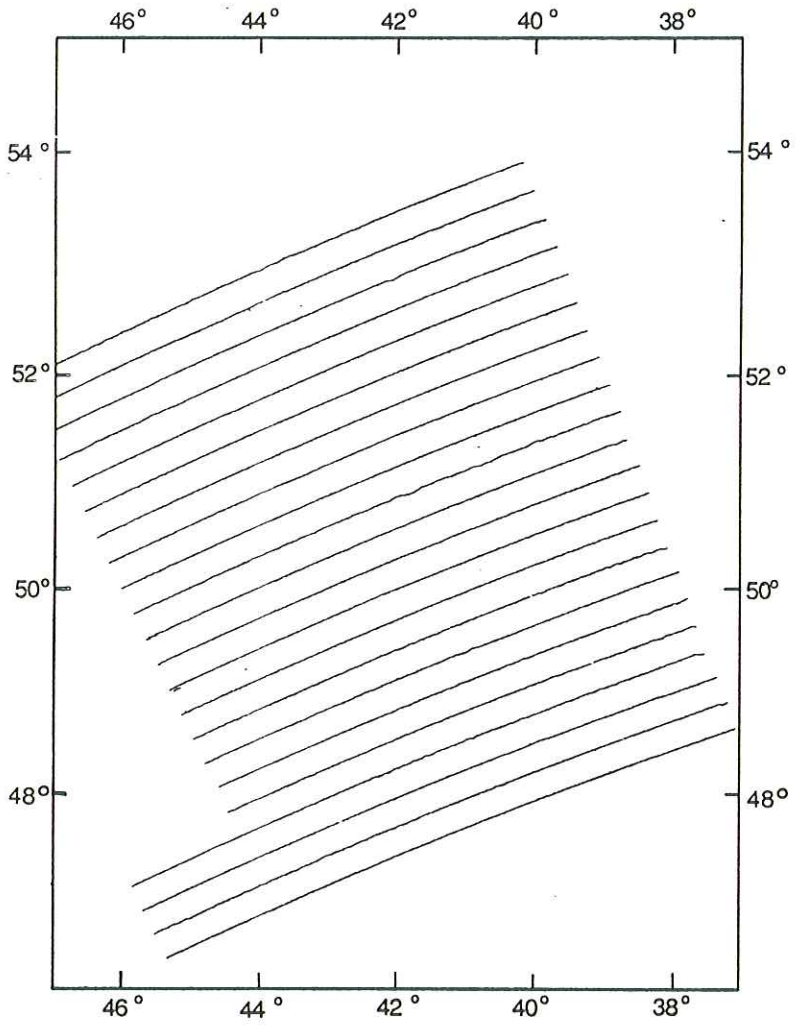

FIGURE 9B. Northeast Newfoundland Shelf aeromagnetic survey: regional flight lines(location see figure 38D).

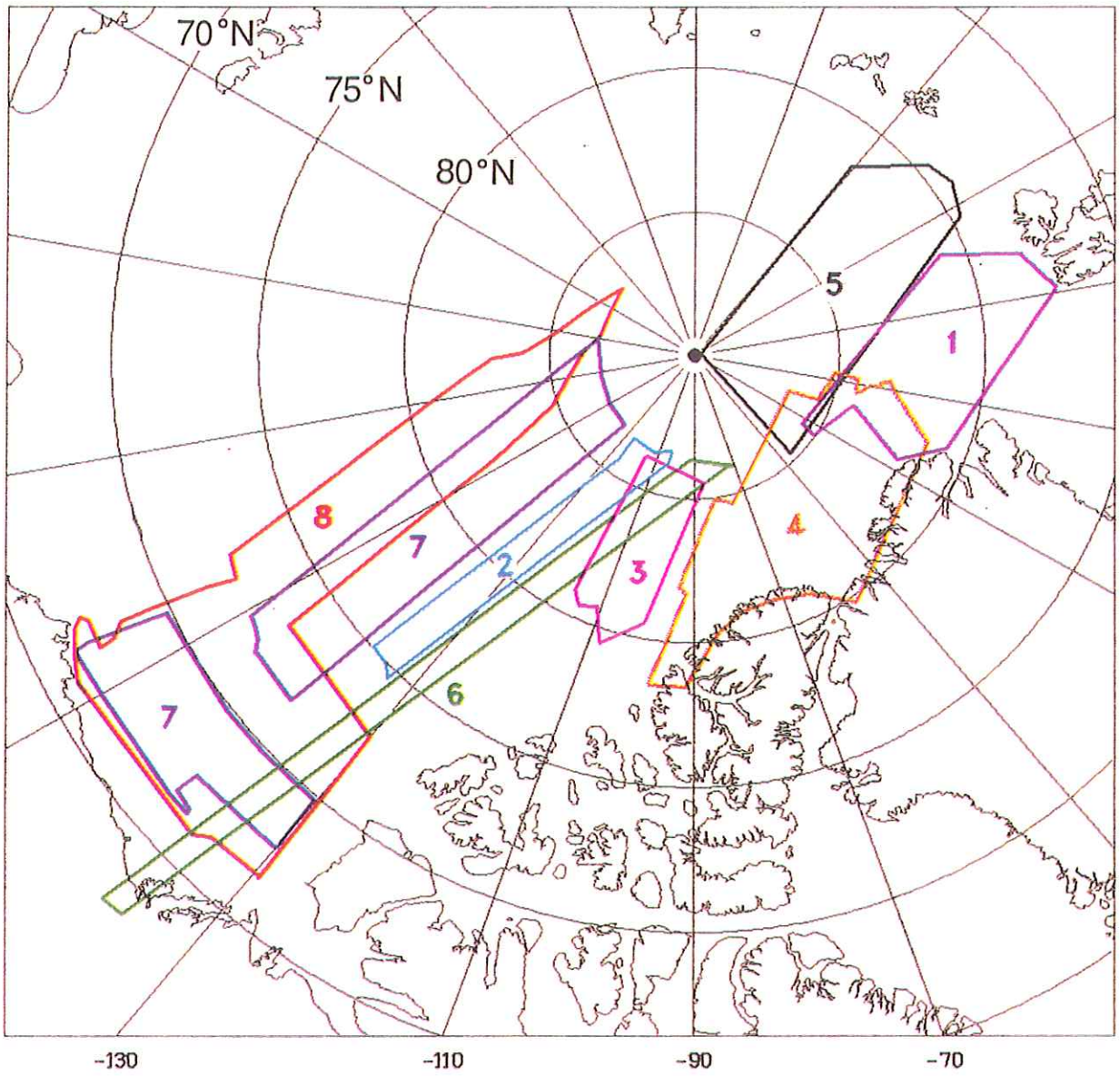

FIGURE 10. US Naval Research Laboratory aeromagnetic data in the Arctic. 1: Nansen Ridge, 1974. 2: Alpha Ridge, 1975. 3: Alpha/Nansen Ridge, 1975. 4: Lincoln Sea, 1975. 5: Nansen Ridge, 1975. 6: Alpha Ridge, 1976. 7: Canada Basin, 1977. 8: Canada Basin, 1978.

MERCATOR 1/10000000 AT 36

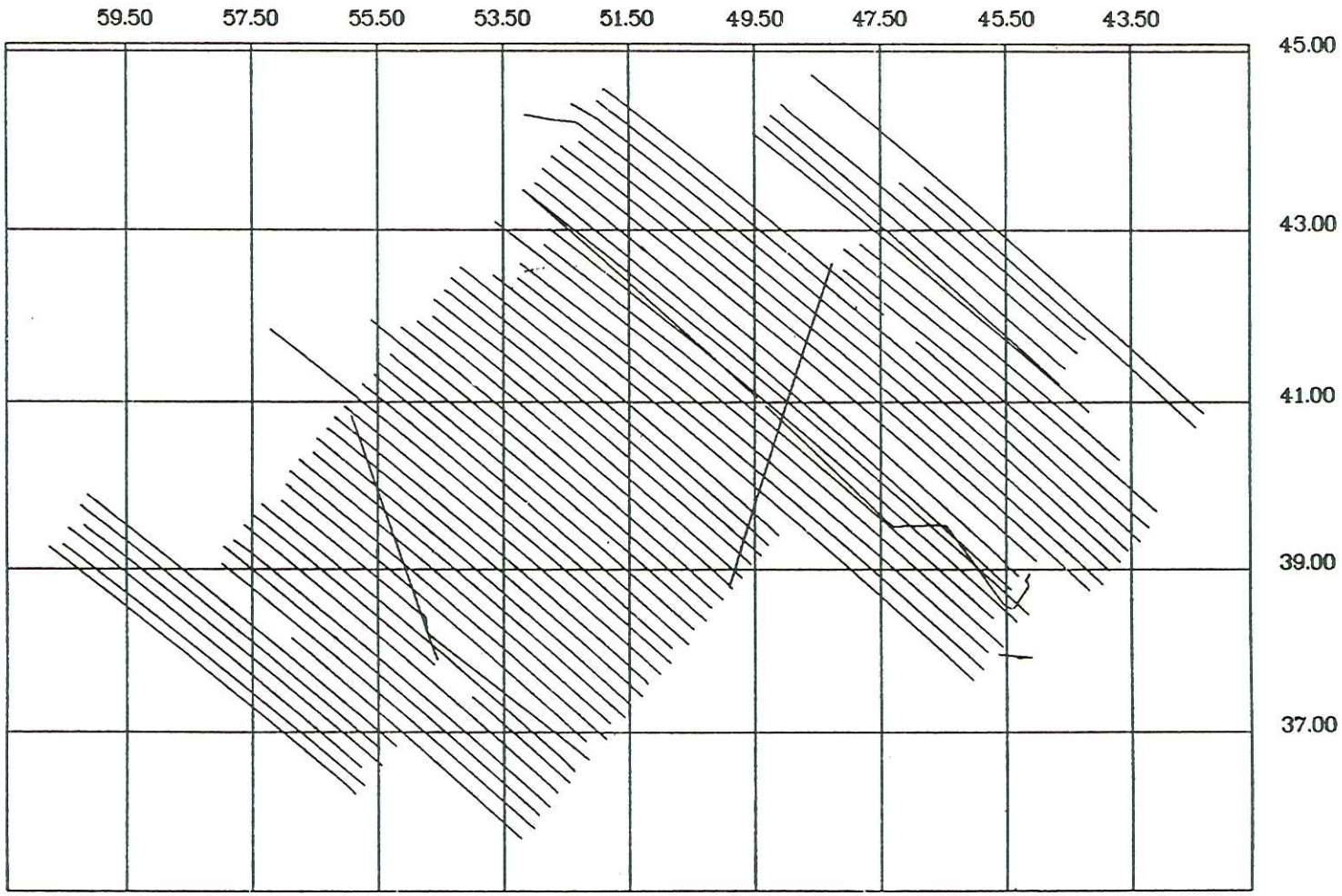

FIGURE 11. US Naval Research Laboratory J-Anomaly flight lines, flown in 1977.

In 1968, the USGS flew a high-resolution survey in the central part of the Gulf of Maine at a flight line spacing of 2 km and an altitude of 500 m (Figure 12). As part of Project MAGNET, a series of profiles was flown in 1964 over the entire Gulf of Maine at a flight line spacing of 10-20 km and an altitude of 500 m (Figure 13). Both data sets were provided to us in flight line form by Kim Klitgord of USGS Woods Hole.

In a compilation preparatory to production of the Magnetic Anomaly Map of North America, the Geophysics Division of the GSC had assembled most of the available aeromagnetic data from the continental USA and its offshore. Data were gridded at 2 km intervals. Subsets of this data were provided to help fill blank areas in the US Northeast that still remained in the AGC compilation.

5. VARIATIONS OF THE MAGNETIC FIELD

The aeromagnetic data cover a span of about 40 years, and the marine magnetic data, about a quarter century. When combining data collected over such intervals, it is very important to account for variations with time in the earth's magnetic field.

Usually an aeromagnetic survey is carried out in a relatively short time span of several weeks. This means that for the internal consistency of the data, the longer fluctuations of the magnetic field, such as secular variations, are not very important. However, the short term variations have an effect and must be corrected.

The marine data set often has tracks through the same area, but several years apart. In this situation, the secular variations of the earth's magnetic field have to be accounted for. These variations are modelled in a series of magnetic reference fields (IGRF) which were used to reduce all our observations to anomalies. The accuracy of the resulting anomalies, both in time and in location, can be estimated at the locations where two ship tracks intersect.

Clearly, the reference fields play a fundamental role in the process of combining different data sets. We shall begin by discussing the short term variations which are not accounted for by the reference fields, and then go on to discuss some characteristics of the reference fields themselves. In a later section, we describe the results of a crossover analysis performed on the marine magnetic data set, which provides some indication of the performance of the reference fields, in addition to demonstrating the accuracy and internal consistency of the data.

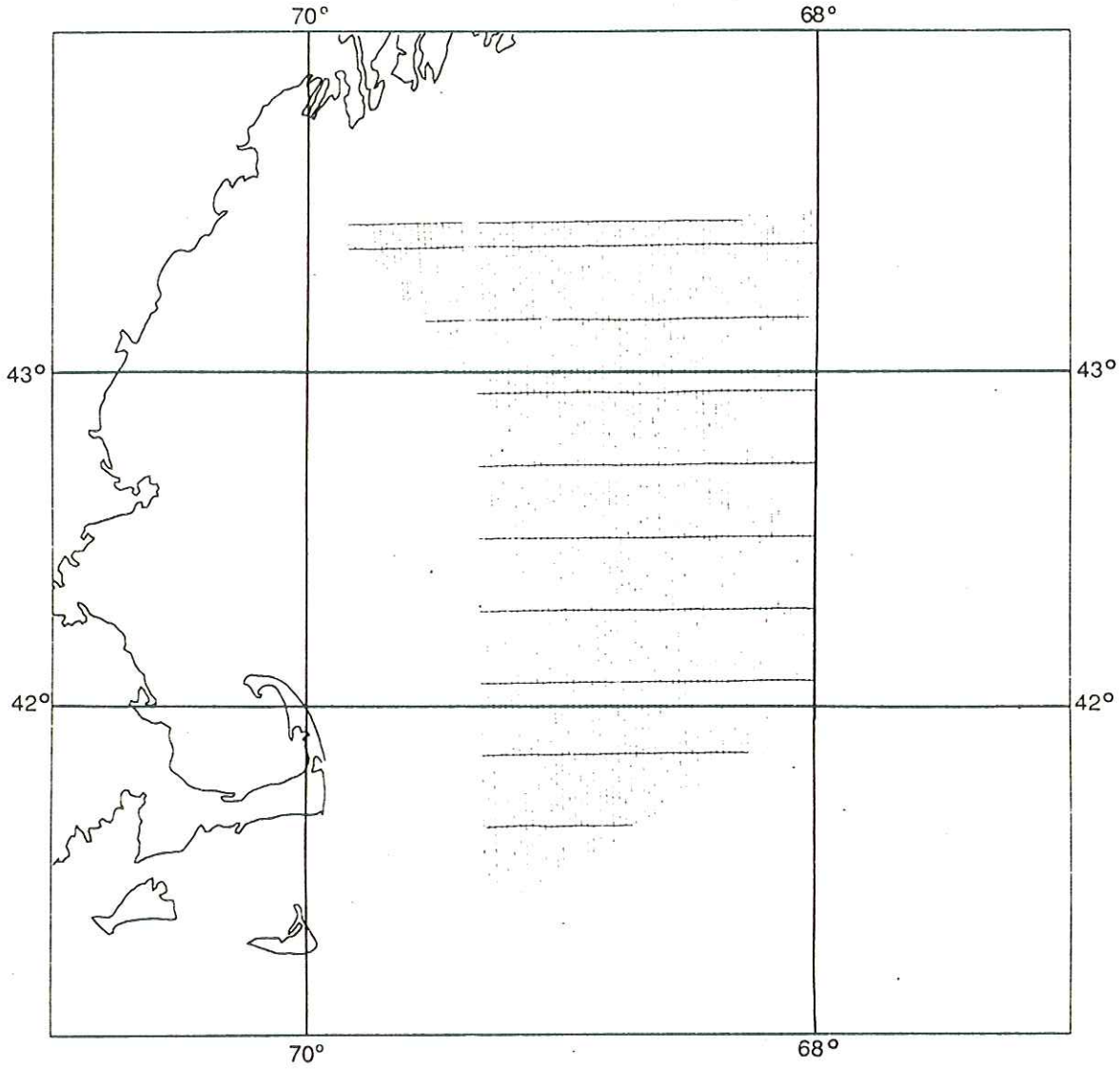

FIGURE 12. US Geological Survey Gulf of Maine aeromagnetic survey lines, flown in 1968.

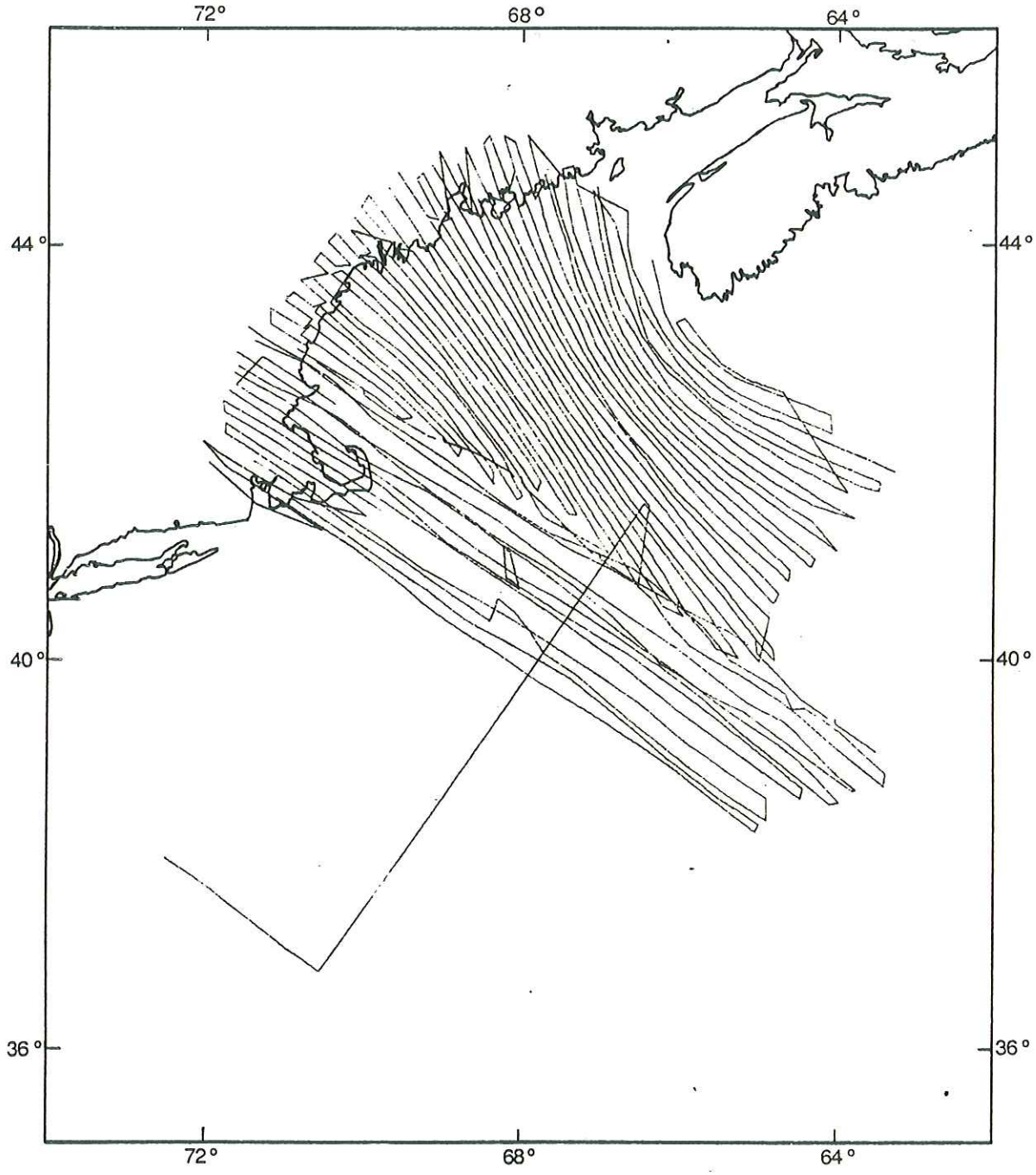

FIGURE 13. Project MAGNET flight lines, flown in 1964.

5.1. Short term variations

Short term variations originate in the earth's external magnetic field; they are caused for the most part by complex processes and interactions associated with the solar-terrestrial environment (e.g. Regan and Rodriguez, 1981).

Quiet variations are related to solar electromagnetic radiation and to the gravitational influence on the ionosphere; they occur daily and worldwide with typical amplitudes of tens of nanotesla, depending on latitude.

Disturbed variations are complex and highly variable. The variations range from low level high frequency micropulsations through single isolated disturbances in the polar regions to planet-wide intense magnetic variations lasting several days and termed magnetic storms. The ultimate cause of these variations is the direct interaction of solar energy and magnetic field lines with the magnetosphere, resulting in growth and decay of primary magnetospheric currents and in changes of energy balance within the magnetosphere.

The auroral zone is an area of extremely complex geomagnetic phenomena; processes in this region are major and nearly continuous sources of disturbed variations. The zone covers a circular area having a diameter of 4000-5000 km, centred roughly over northern Baffin Bay. The consequence of this is that magnetic observations over most of eastern Canada, down to the latitude of southern Labrador, are highly susceptible to auroral disturbances.

Quiet and disturbed variations can be monitored at shore locations, but the relationship of the monitored variations to those in the operating area of a given survey is often compounded by the effects of conductivity contrasts in the crust or upper mantle, and by the land-sea interface (Hill and Mason, 1962; Auld et al, 1979). As a result, variations in the land and sea environments may exhibit substantial relative differences in their phases and amplitudes; corrections are not straightforward to calculate or to apply.

The problems may be significantly minimized through deployment of moored magnetometer buoys near the centre of the operating area. AGC has sponsored at least two specialized operations that made use of such buoys: in the auroral zone in Baffin Bay, where variations can exceed 100 nanotesla, as illustrated in Figure 14 (Jackson et al, 1979); in the Quiet Magnetic Zone off the Scotian Shelf, where features in the magnetic field are highly subdued and easily masked by even minor variations (Barrett and Keen, 1976). As pointed out previously, however, this approach was not practicable for routine use on account of cost and logistical factors.

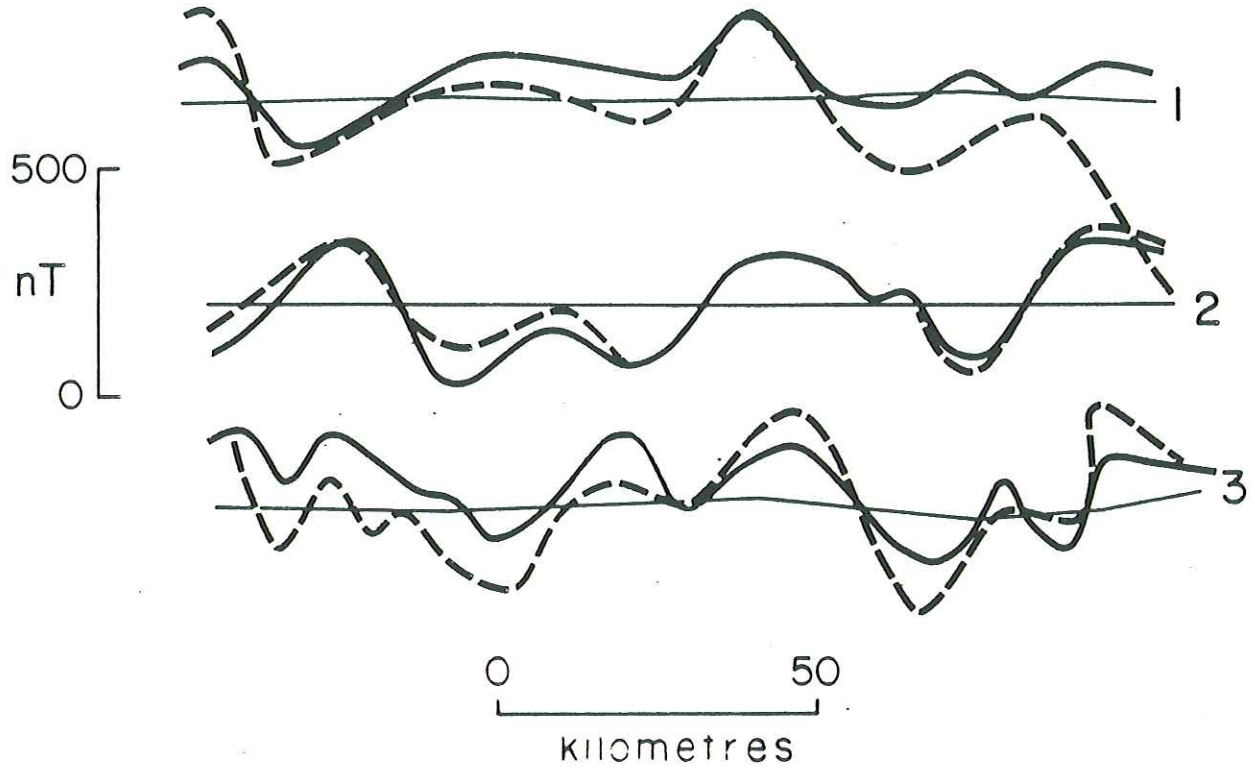

FIGURE 14. Magnetic variations observed from a moored magnetometer in Baffin Bay (from Jackson et al, 1979). Solid lines represent data corrected for magnetic variation, dashed lines represent uncorrected data.

5.2. Secular variations and reference fields

The International Association of Geomagnetism and Aeronomy (IAGA) has developed and published a series of models of the earth's main magnetic field, known collectively as IGRF - the International Geomagnetic Reference Field (IAGA Division I, Working Group 1, 1986). Each model is a mathematical representation of the magnetic field at five year intervals between 1945 and 1985; linear interpolation is applied to calculate the theoretical field for intervening years.

Applying the IGRF to a set of magnetic total field observations essentially removes the long wavelength, time varying components of the earth's main field, and leaves the short wavelength, unvarying magnetic anomalies that are associated with source rocks close to the earth's surface.

The original IGRF was adopted in 1968 (IAGA, Commission 2, Working Group 4, 1969) and consisted of a model for the main field at 1965.0 and a model for the secular variation of the main field (together called IGRF 1965). The secular variation model included in IGRF 1965 was a simple linear model specifying constant rates of change of the main field coefficients.

The first revision of the IGRF was adopted in 1975 (IAGA Division I, Study Group, 1976) and consisted of a model of the main field at 1975.0 and a forecast model of the secular variation during 1975-1980. The main field model was simply an extrapolation of the 1965 model to 1975. Inaccuracies in the secular variation model could lead to a main field model in 1975 that differed from the real main field.

By the late 1970's, uncertainties in the secular variation models led to unacceptable inaccuracies in the IGRF. The second revision of the IGRF (IAGA Division I, Working Group 1, 1981) consisted of spherical harmonic models of the main field at 1965.0, 1970.0, 1975.0, and 1980.0, along with a forecast secular variation for 1980-1985. The models for 1965.0, 1970.0, and 1975.0 were considered definitive because they were derived from sets of data that are unlikely ever to be significantly increased or improved (Peddie, 1982).

The latest modification was adopted in 1986 (IAGA, Division I, Working Group 1, 1986) and consisted of the extension of the definitive field to 1980.0 and the addition of a model for the secular variation during 1985-1990. Also, main field models were added for 1945.0, 1950.0, 1955.0, and 1960.0.

Recent tests on large marine data sets collected over time spans of decades have validated the general suitability of the

reference fields in reducing magnetic observations to a common datum level (Verhoef and Scholten, 1983; Macnab et al, 1985A).

5.3. IGRF implementation

The IGRF model consists of sets of spherical harmonic coefficients that describe the main geomagnetic field at five year intervals, as well as a predicted secular variation for the present quinquennium. The main field models for 1960-1985 have 120 coefficients each and extend to degree and order 10. The main field models for 1945 to 1955, and the predictive secular variation model, have 80 coefficients and extend to degree and order 8.

IGRF coefficients for synthesizing field values were acquired from World Data Centre A in Boulder, Colorado and incorporated into AGC software. As the full IGRF expression is highly compute-bound and is very time consuming when large numbers of observation points are involved, an approximation technique was developed to accelerate calculations with no appreciable sacrifice in accuracy (Macnab et al, 1985A). The method was verified during the course of these investigations by comparison against the full IGRF expression.

5.4. The time varying nature of the IGRF

Figure 15 illustrates the IGRF model at five year intervals to illustrate how it varies with time; the variation is neither monotonic nor uniform, i.e. it displays different behaviours in different regions and at different times.

Over Hudson Bay, the variation displays an oscillatory nature where large scale features of the model field appear to move east, then west. This can be easily observed by noting how the high amplitude area situated at the left hand edge of the diagram creeps to the right in 1960-75, then reverses its motion and creeps to the left in 1975-80.

In the vicinity of Nova Scotia, the features in the reference field remain relatively stable in 1960-75, but assume a westward motion in 1975-85 to produce a net decrease. In Baffin Bay and the Labrador Sea, the features migrate eastward in 1960-75 to produce a net increase, then stabilize in 1975-85.

Changes in the level of the reference fields may be summarized as follows:

Interval	Hudson Bay	Nova Scotia	Lab Sea/Baf Bay
1960-75	Increase	Constant	Increase
1975-85	Decrease	Decrease	Constant

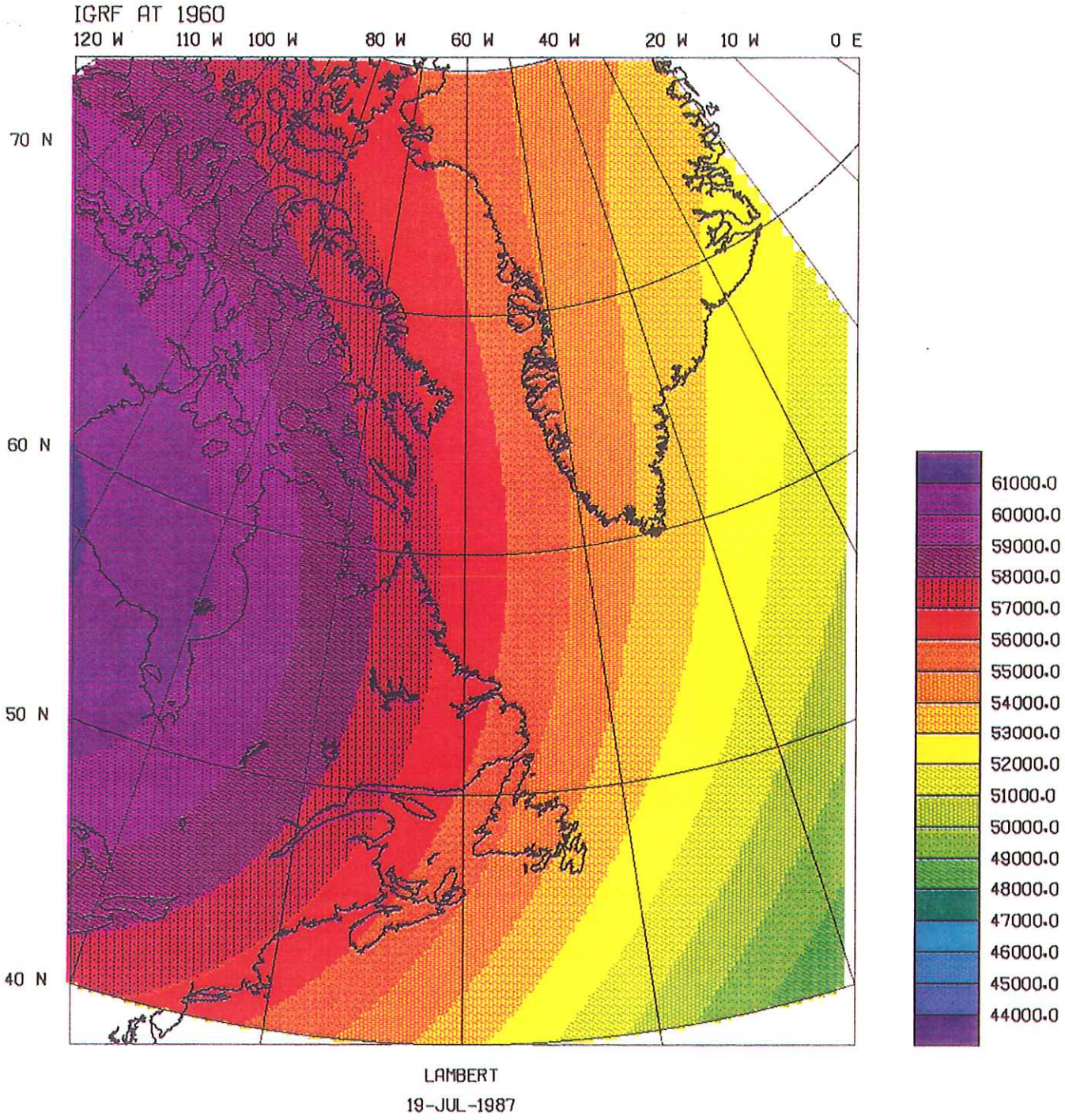

FIGURE 15A. Total magnetic fields simulated by the International Geomagnetic Reference Field at 1960.0, calculated from standard coefficients (IAGA, 1986).

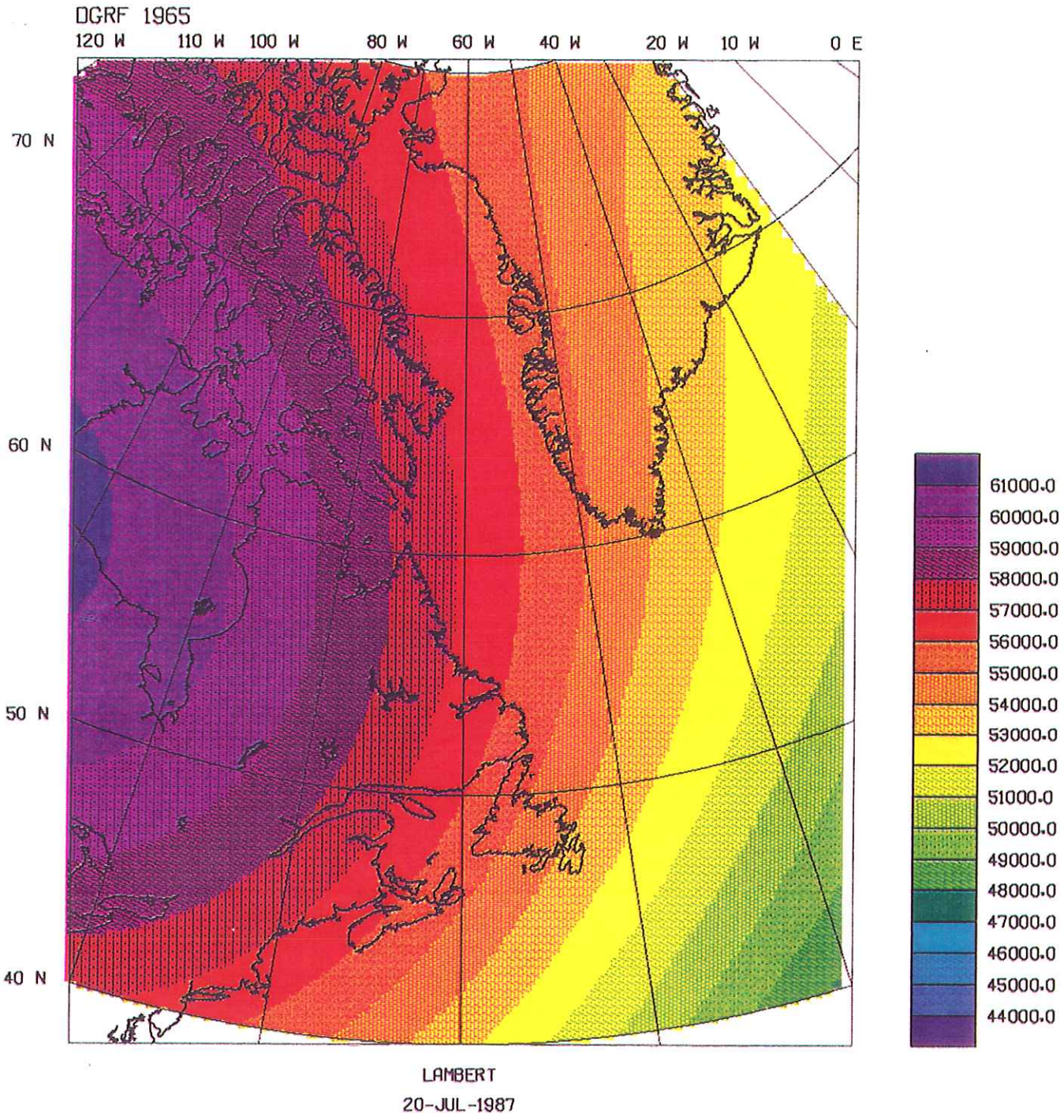

FIGURE 15B. Total magnetic fields simulated by the International Geomagnetic Reference Field at 1965.0, calculated from standard coefficients (IAGA, 1986).

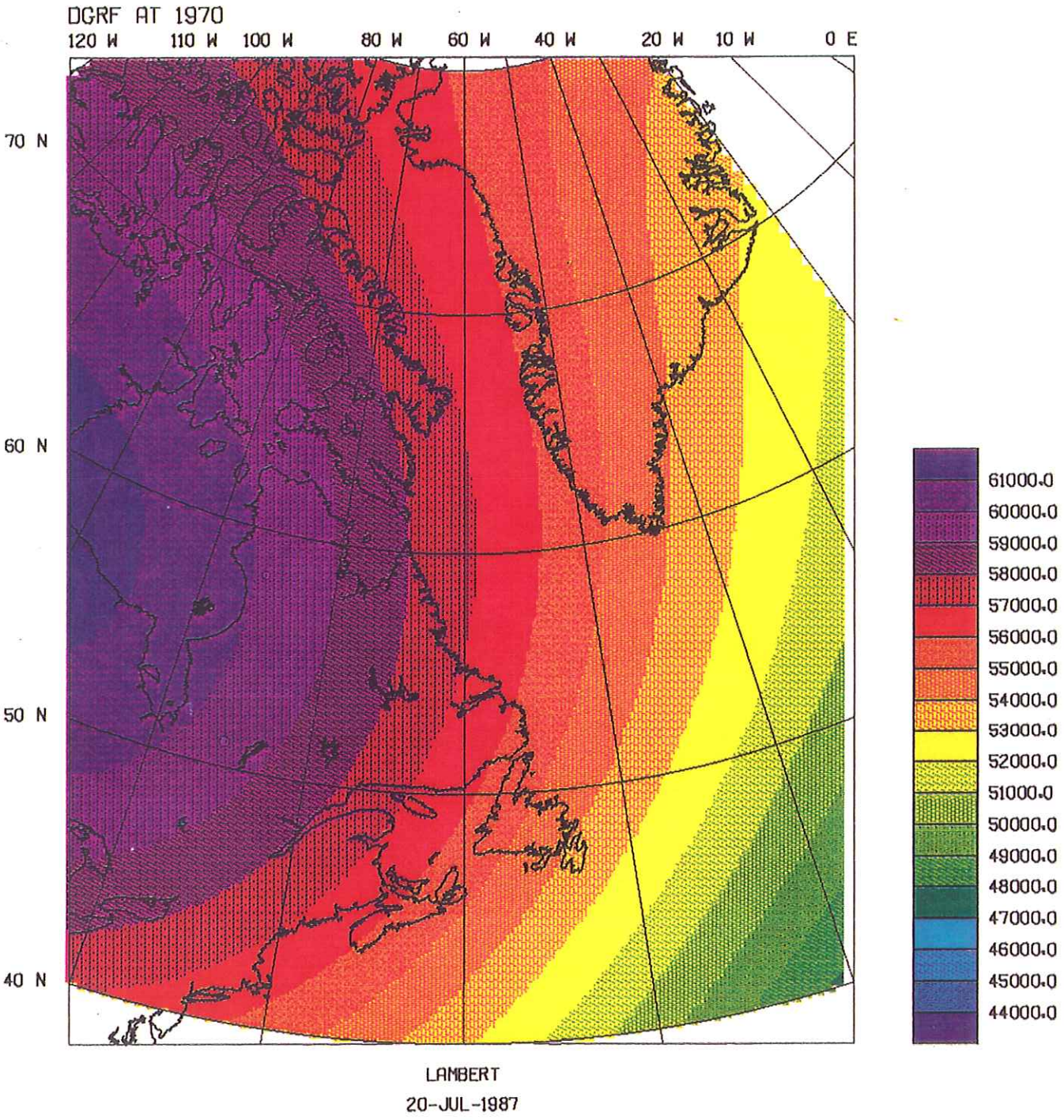

FIGURE 15C. Total magnetic fields simulated by the International Geomagnetic Reference Field at 1970.0, calculated from standard coefficients (IAGA, 1986).

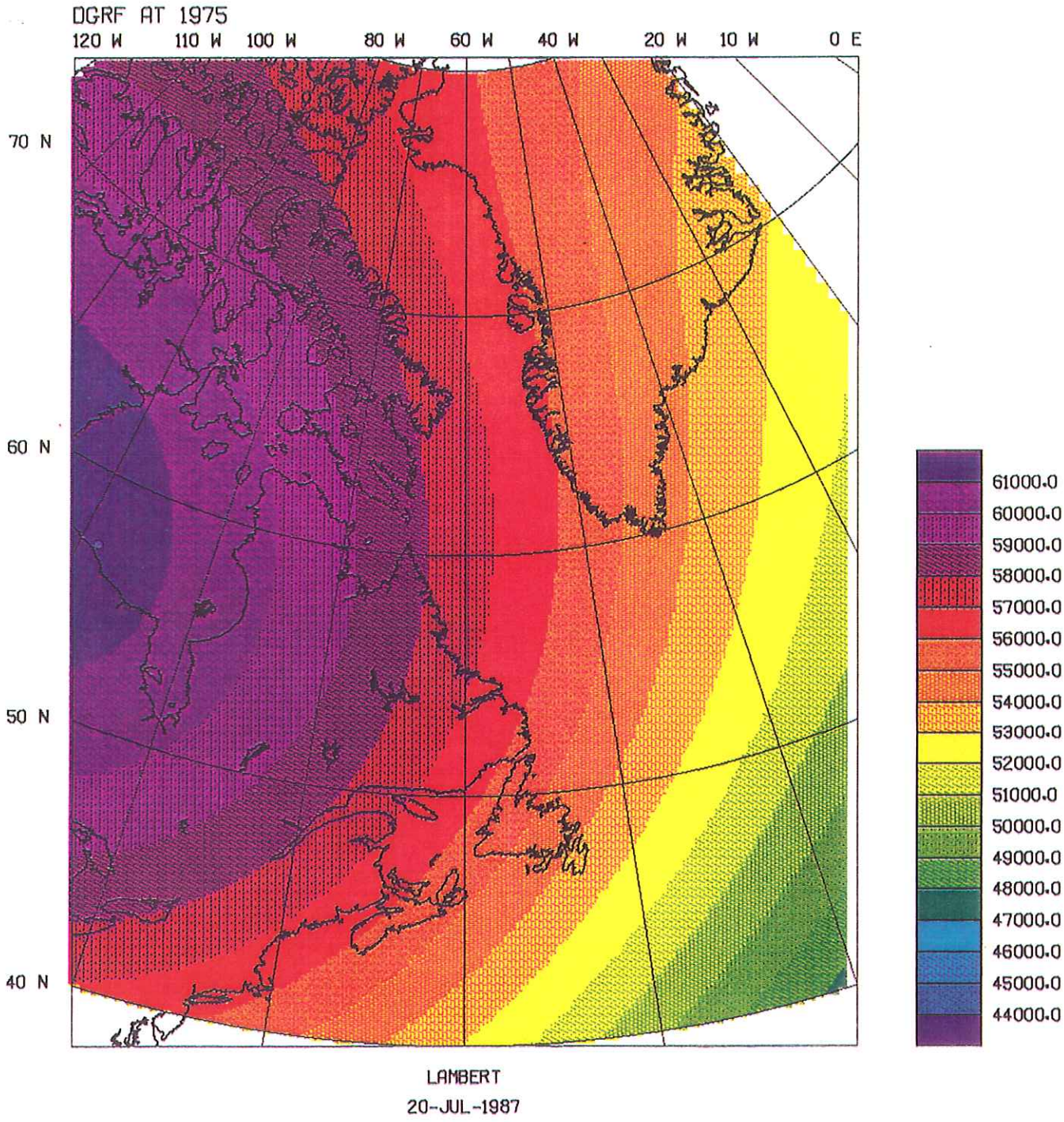

FIGURE 15D. Total magnetic fields simulated by the International Geomagnetic Reference Field at 1975.0, calculated from standard coefficients (IAGA, 1986).

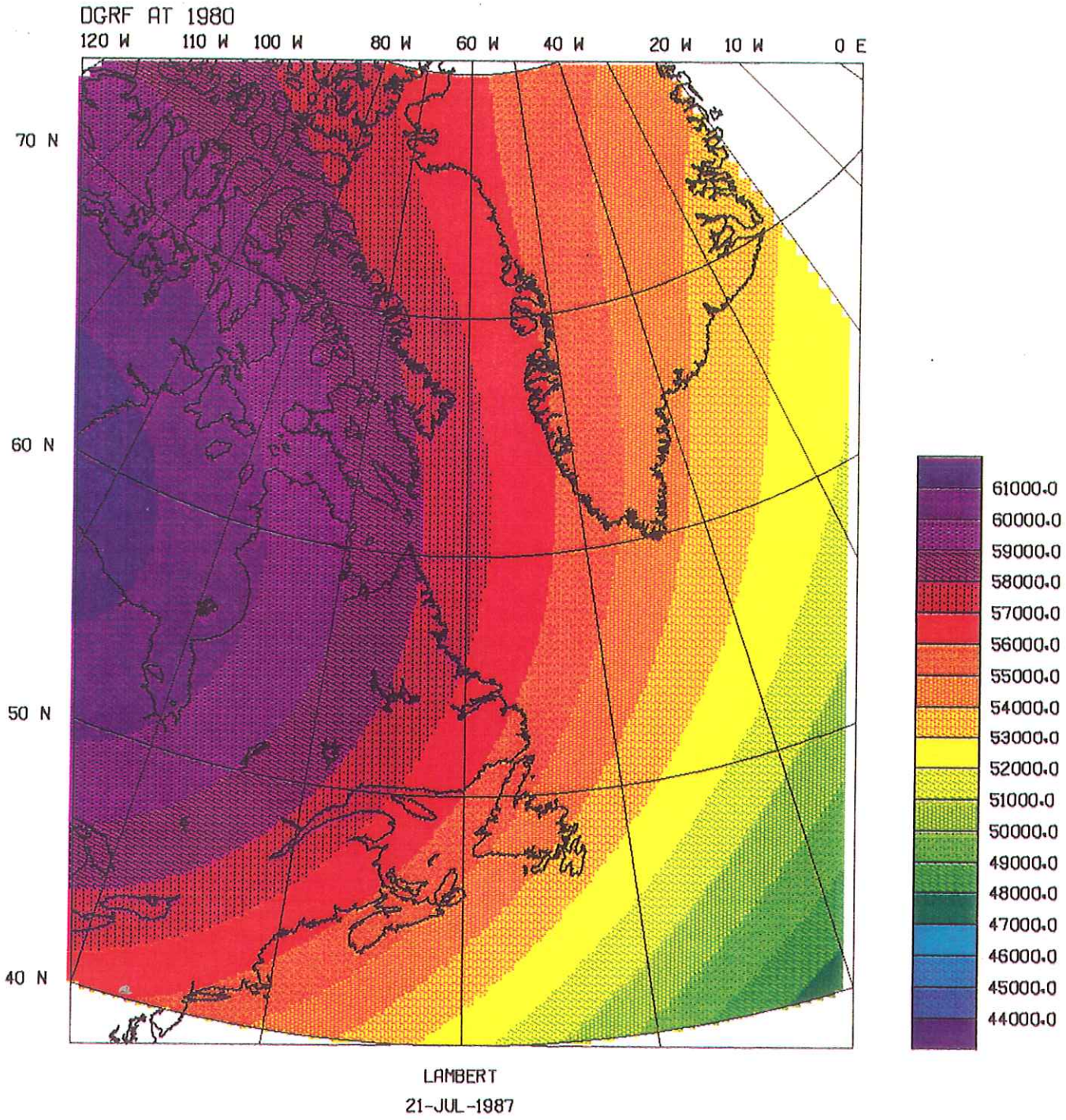

FIGURE 15E. Total magnetic fields simulated by the International Geomagnetic Reference Field at 1980.0, calculated from standard coefficients (IAGA, 1986).

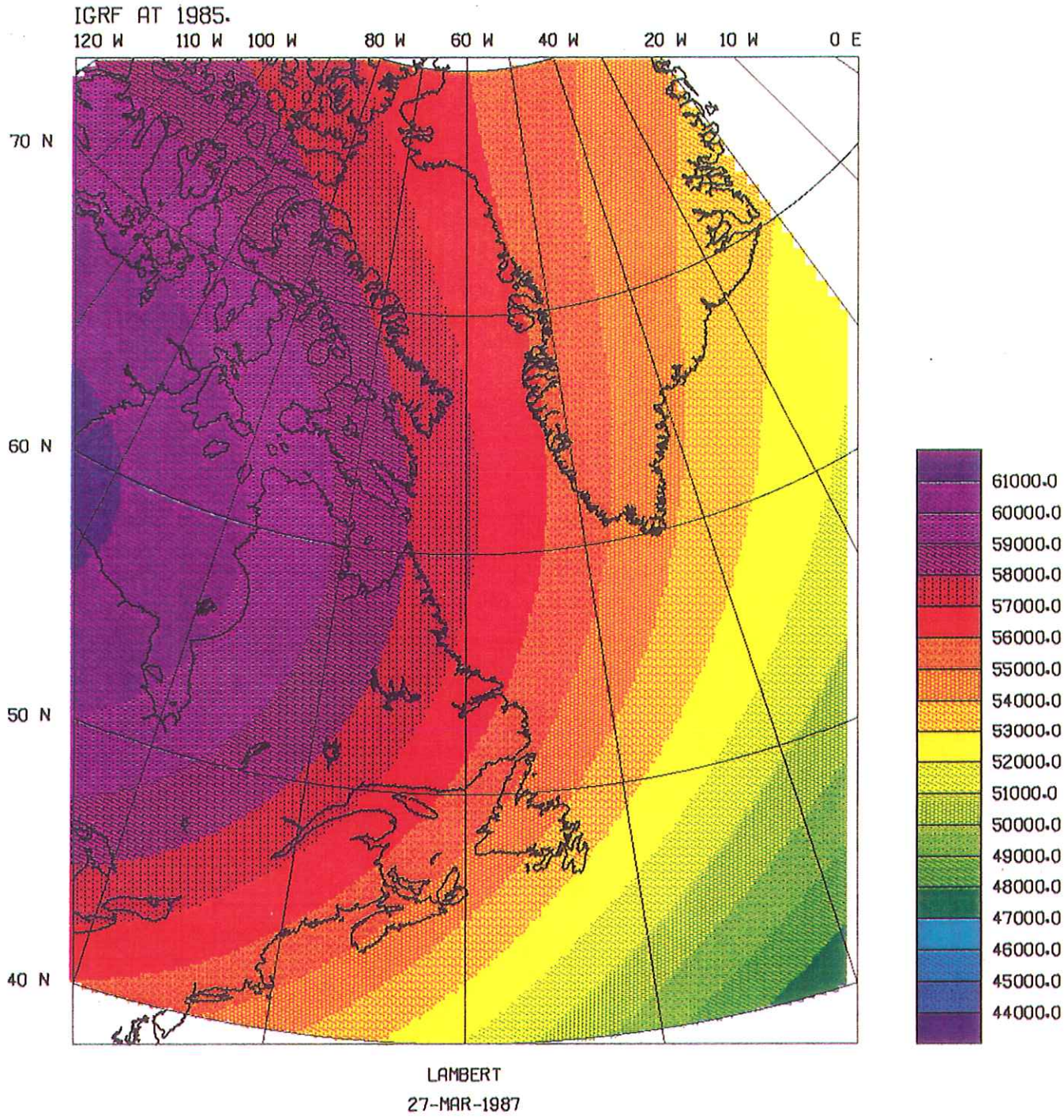

FIGURE 15F. Total magnetic fields simulated by the International Geomagnetic Reference Field at 1985.0, calculated from standard coefficients (IAGA, 1986).

The plots of Figure 16 show the annual rates of change of the IGRF over succeeding five-year epochs from 1960 to 1985. The plots were generated by taking the differences between the values used to produce the previous figure, and dividing by five.

The rates of change over 1960-75 are reasonably consistent, in that their broad patterns are more or less carried forward from epoch to epoch. This could be taken to indicate some stability in the rate of change. On the other hand, the rates of change for 1975-85 show a pronounced departure from the previous patterns, indicating a major alteration in the nature of the rate of change. The reason for this change is not immediately obvious, but it seems reasonable to query whether it is an artifact associated with the data and the methods employed for deriving the model coefficients.

A key point to note at this time is the pivotal nature of the year 1975, when important changes occur in the nature of the variation. This is clearly demonstrated in the plots of Figure 17, which display the reference field and its secular variation for the period 1960-85 at three widely-spaced locations. In all three plots, the slope of the reference field exhibits in 1975 a significant discontinuity in the negative direction, while the secular variation displays a major negative alteration at the same time. The significance of this will be discussed later.

5.5. Residual time dependencies in the IGRF model

The above observations prompted an analysis to determine whether and to what extent the major model changes in 1975 got propagated into the derived anomaly field.

First, we divided the total data base into subsets corresponding to the five-year IGRF epochs, i.e. 1960-65, 1965-70, etc. Each five-year subset was then gridded individually, using the same gridding routine and filter parameters as for the total data base (described below under Data processing and manipulation). Grid size was increased from .05 degree to .1 degree, however, in order to decrease the volume of the resulting grid files, and to reduce computing time. Tracks found to be out of level with their neighbours were eliminated from each grid file (discussed below under Removal of bad data points).

Figure 4 (A to E) illustrates the geographical density of data in each five-year subset, indicating the number of original observations per 100 sqare kilometres. Data distribution in the first epoch (1960-65) was too sparse to use in further calculations.

The magnetic anomalies exhibited considerable differences between five-year subsets. For ease of visual comparison, the gridded data were given two additional treatments prior to the production of plots:

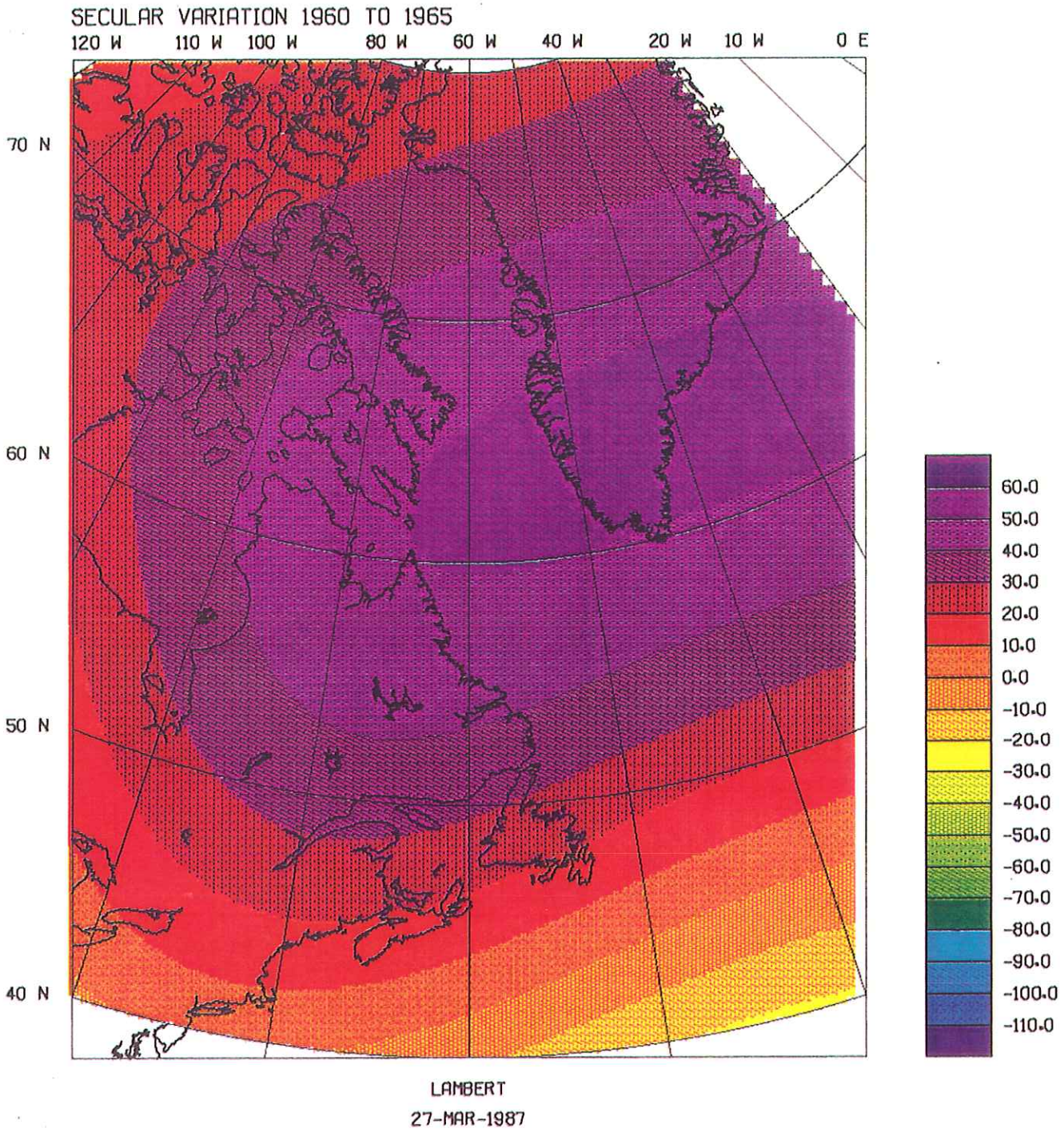

FIGURE 16A. Annual rates of change of the International Geomagnetic Reference Field in the five-year epoch shown at the top. This figure was generated by plotting one fifth of the difference between total field plots at the beginning and end of the epoch (as shown in the previous figure).

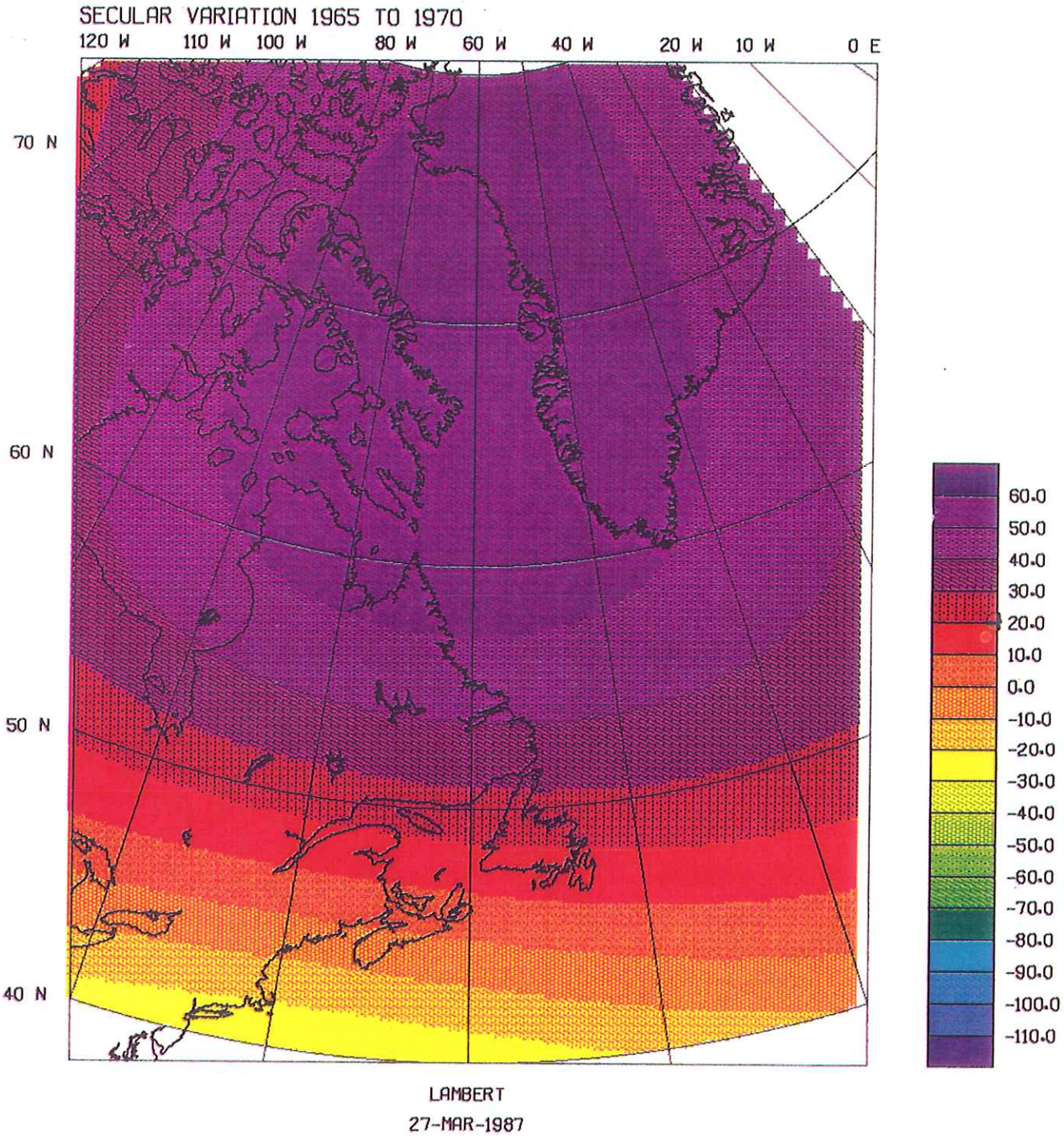

FIGURE 16B. Annual rates of change of the International Geomagnetic Reference Field in the five-year epoch shown at the top. This figure was generated by plotting one fifth of the difference between total field plots at the beginning and end of the epoch (as shown in the previous figure).

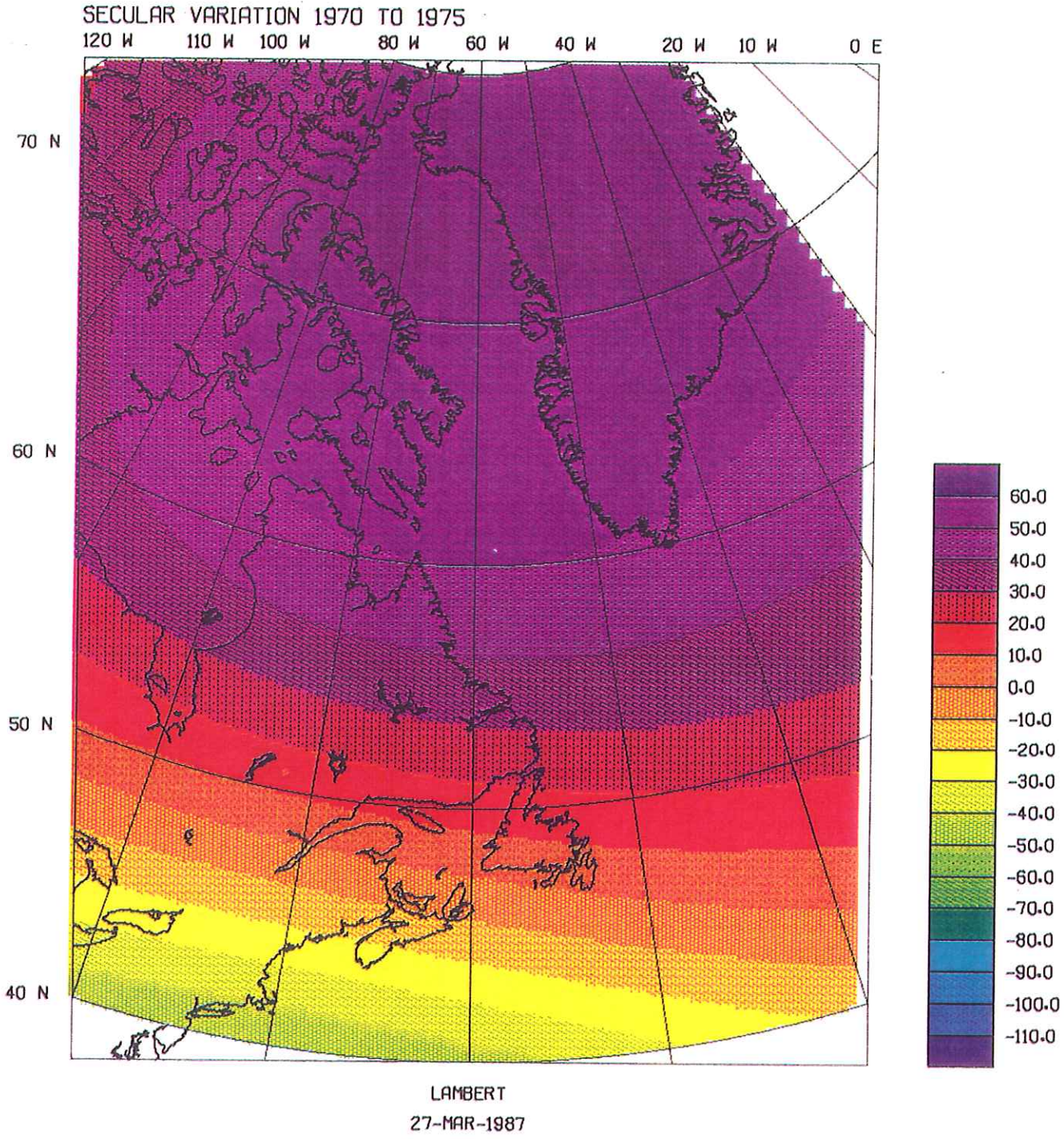

FIGURE 16C. Annual rates of change of the International Geomagnetic Reference Field in the five-year epoch shown at the top. This figure was generated by plotting one fifth of the difference between total field plots at the beginning and end of the epoch (as shown in the previous figure).

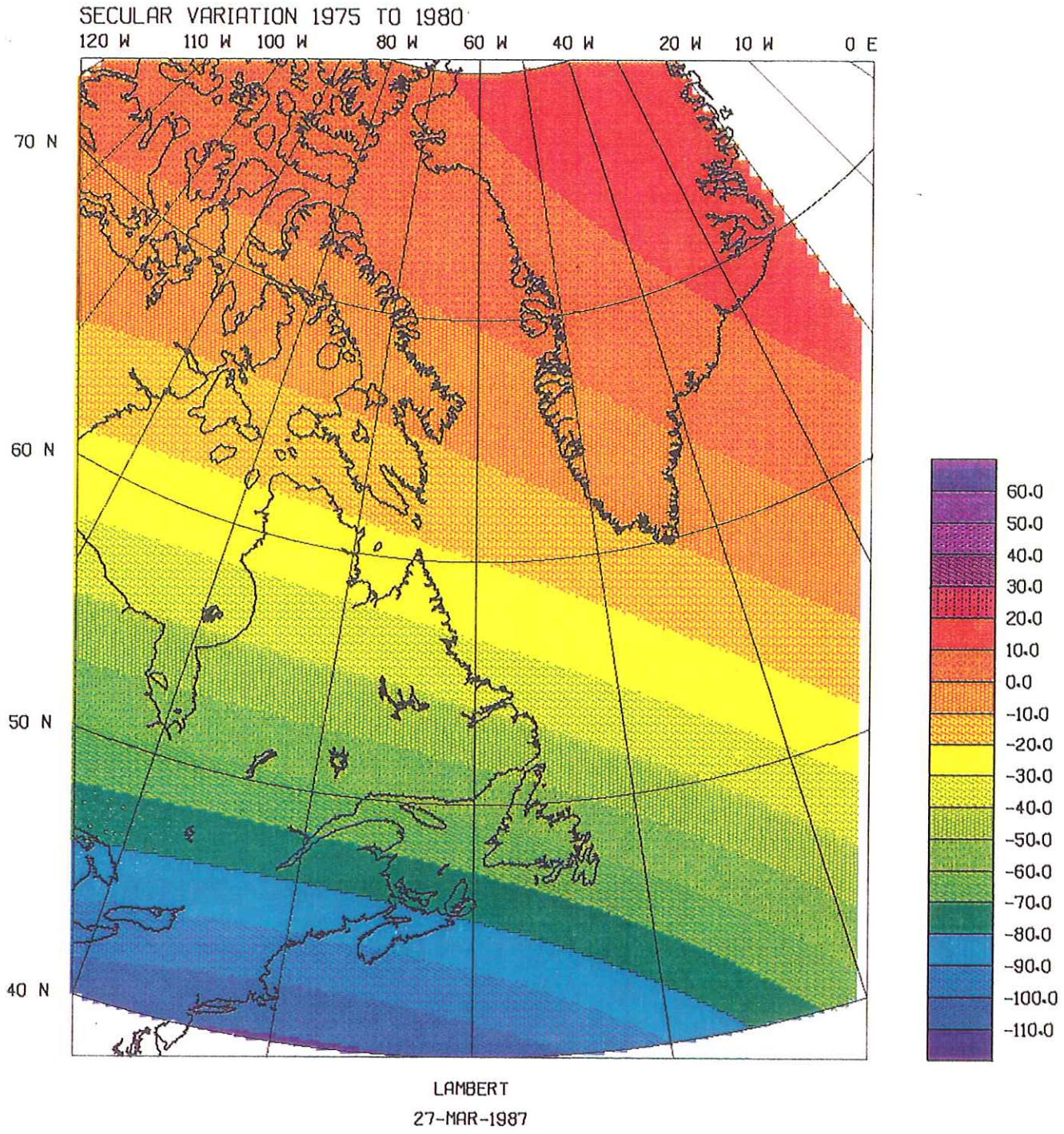

FIGURE 16D. Annual rates of change of the International Geomagnetic Reference Field in the five-year epoch shown at the top. This figure was generated by plotting one fifth of the difference between total field plots at the beginning and end of the epoch (as shown in the previous figure).

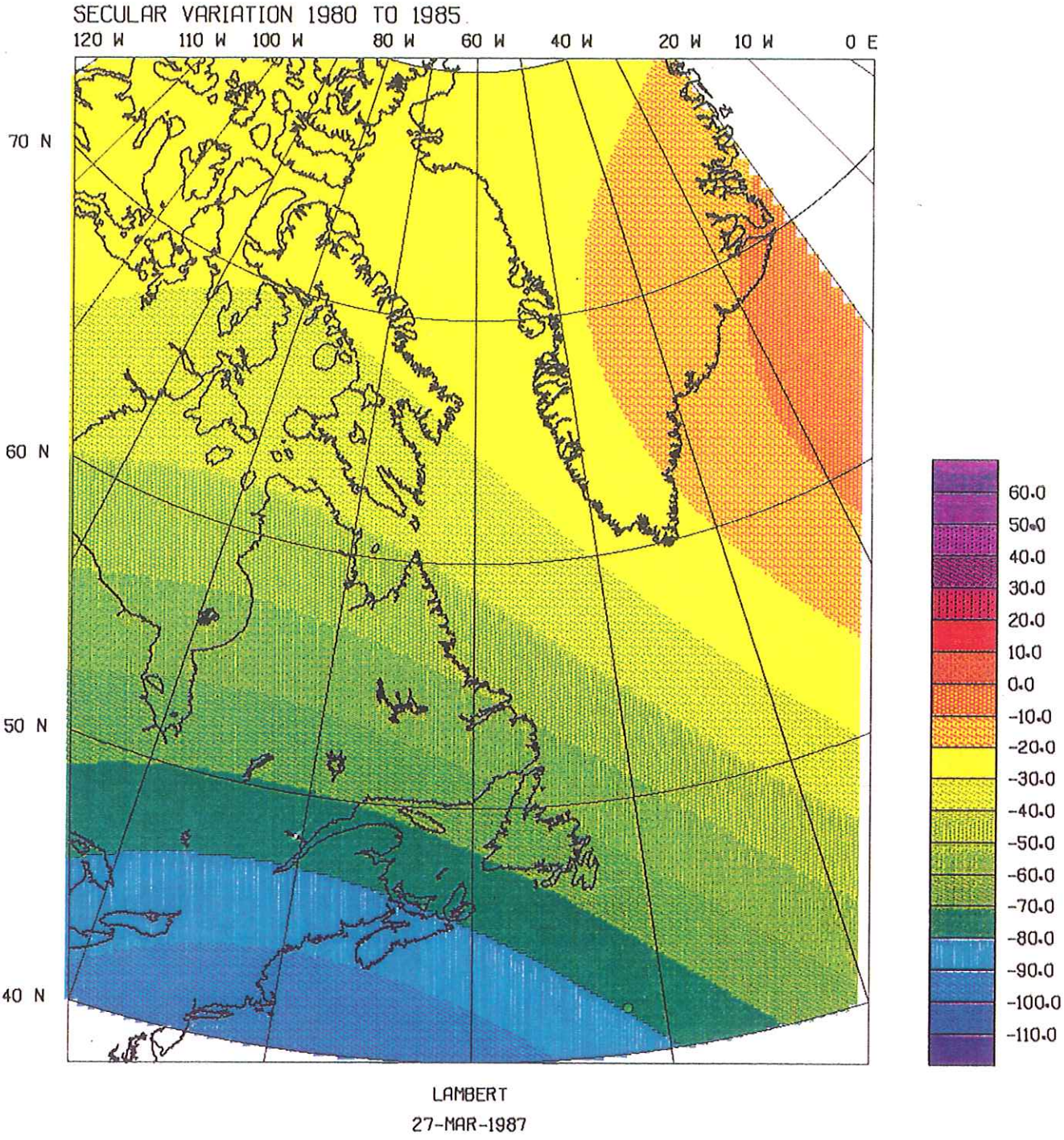

FIGURE 16E. Annual rates of change of the International Geomagnetic Reference Field in the five-year epoch shown at the top. This figure was generated by plotting one fifth of the difference between total field plots at the beginning and end of the epoch (as shown in the previous figure).

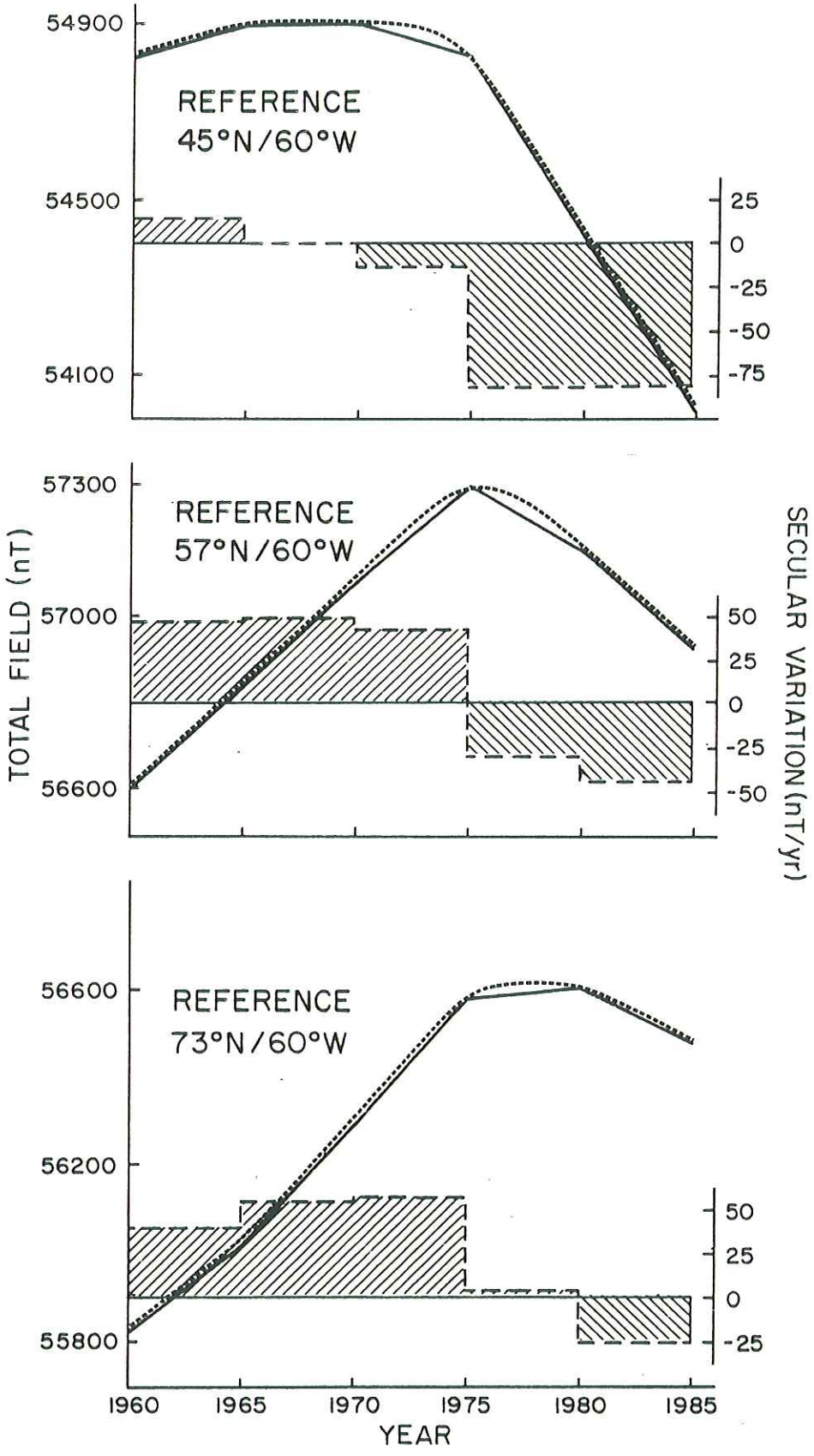

FIGURE 17. Reference fields (continuous and dashed lines) and secular variation (shaded areas) for the period 1960-85 at three widely-spaced locations. The dashed lines result when intermediate changes in the field are modelled with a bicubic spline instead of a linear interpolation; see text for explanation.

1) Extrapolations generated by the gridding routine were eliminated through the enlargement of all gaps, and by extending null regions by two grid points in the E-W and N-S directions.

2) Short-wavelength features were attenuated by filtering the data with a two-dimensional Gaussian weighting function (described in a later section).

Results are plotted in Figure 18, which clearly illustrates how the five-year anomaly subsets have distributions that are irregular and only partly overlapping.

To facilitate visual comparisons wherever observation areas coincided, differences were then computed between anomaly values in the 1970-75 and the remaining epochs, and plotted in Figure 19.

The primary conclusion one can draw from an inspection of this figure is that the anomaly field does not behave in a uniform manner throughout the entire region. This behaviour is summarized in the following table, which describes the nature of the level changes in the anomaly field (Increase, Decrease, or Constant) over three epochs in three widely-separated areas: the Scotian Margin, Labrador Sea, and Baffin Bay.

Epoch	NS Margin	Labrador Sea	Baffin Bay
1965-70	Incr	Decr-Cons	Decr-Cons
1975-80	Decr	Incr	Incr-Cons
1980-85	Decr	Incr	?

(Reference: 1970-75 epoch)

There is no known reason for anomaly values to vary in this fashion, as they are the manifestation of geologic structures that remain stable in both composition and placement, at least during the time intervals that we are concerned with here. We observe that the behaviour of the field variation appears to change in 1970-75, which coincides with the previously-noted epoch of change in the IGRF model.

We are thus led to conclude that the changes in the anomaly field are only apparent, and that they are introduced as a result of the residual variations that the IGRF model fails to account for. With the information on hand so far, we cannot yet specify the nature of those variations. We return to this question in the section dealing with the analysis of crossover errors.

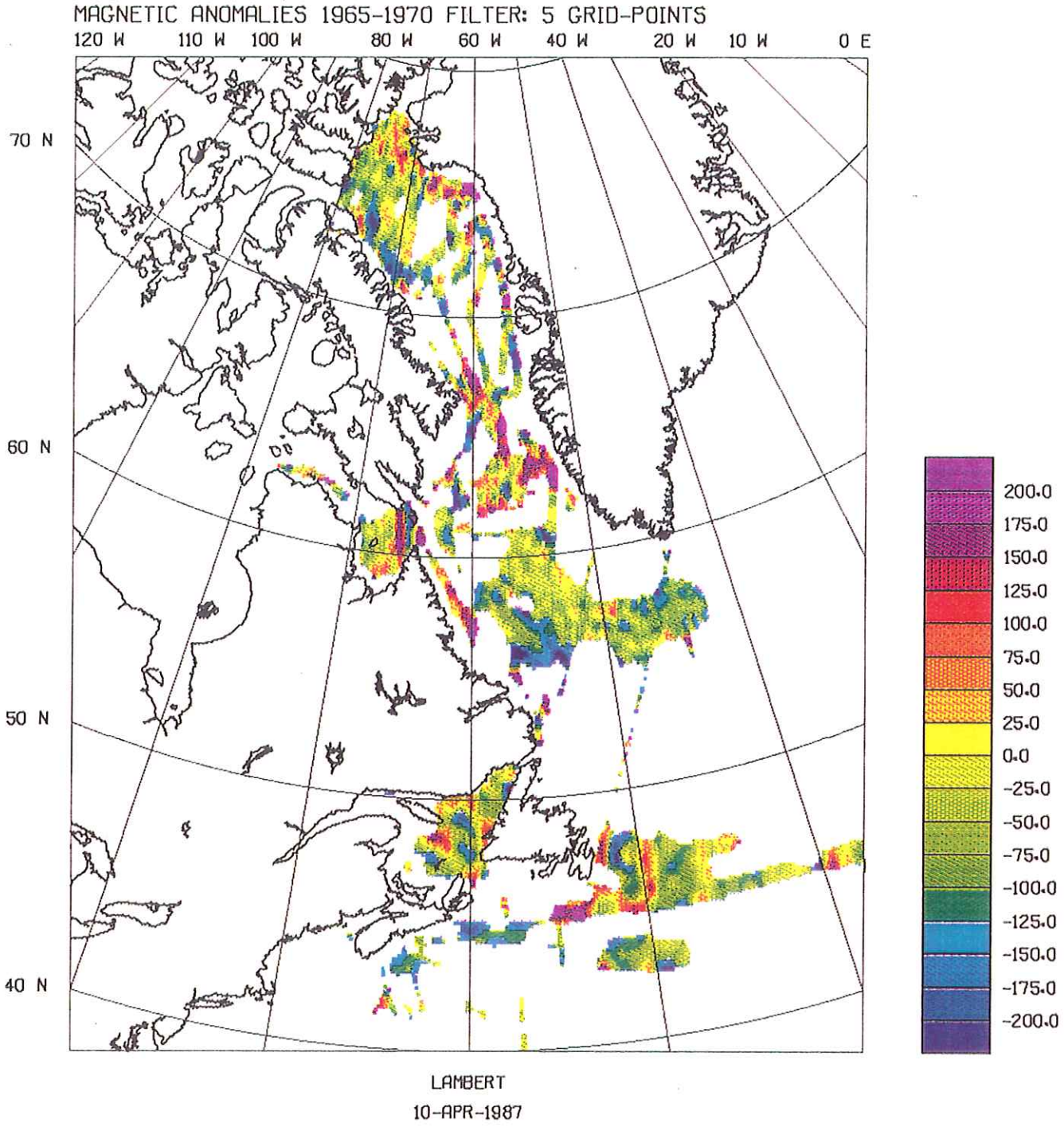

FIGURE 18A. Plots of the gridded and filtered anomaly values derived from observations in the five-year epoch shown at the top.

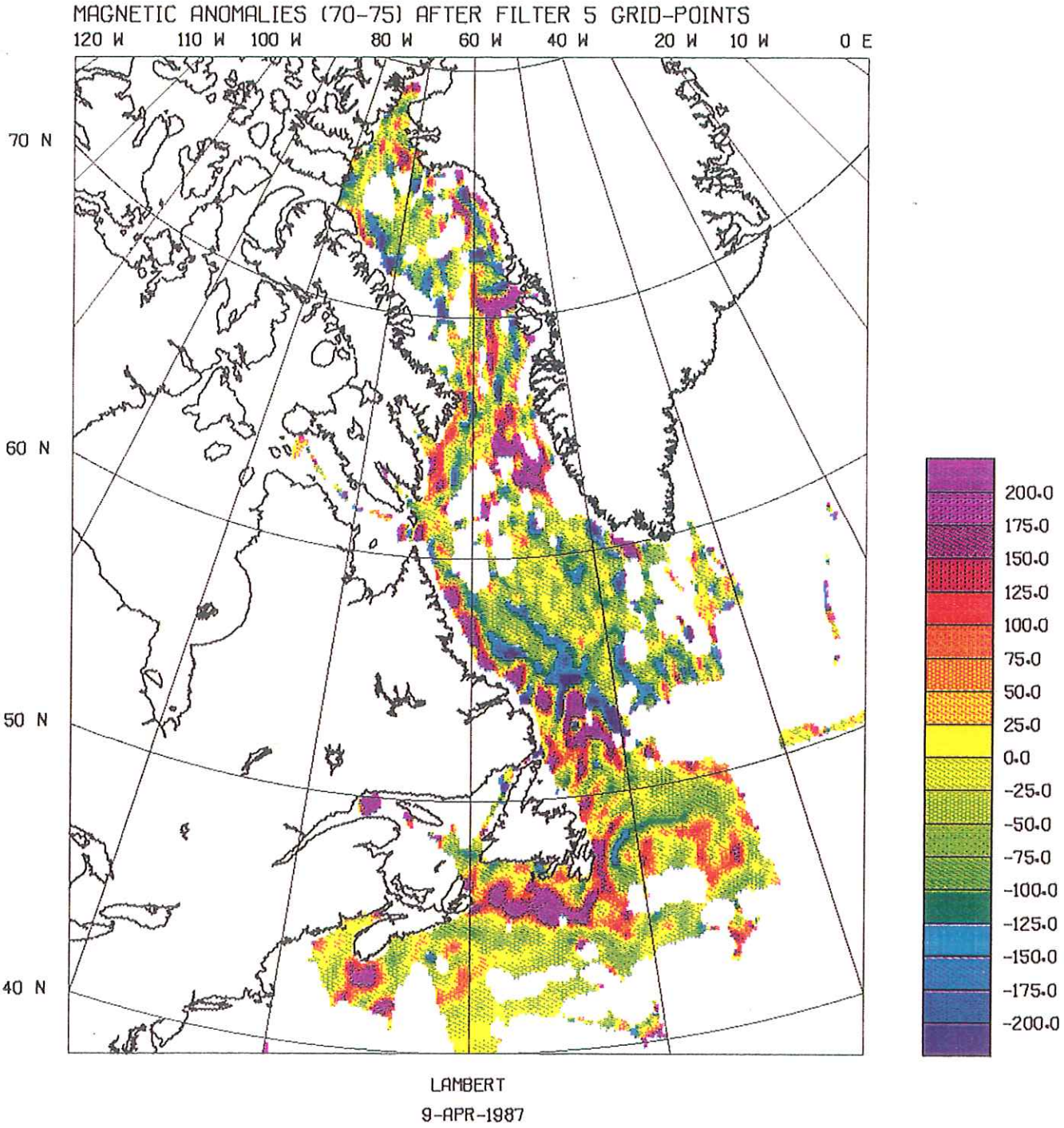

FIGURE 18B. Plots of the gridded and filtered anomaly values derived from observations in the five-year epoch shown at the top.

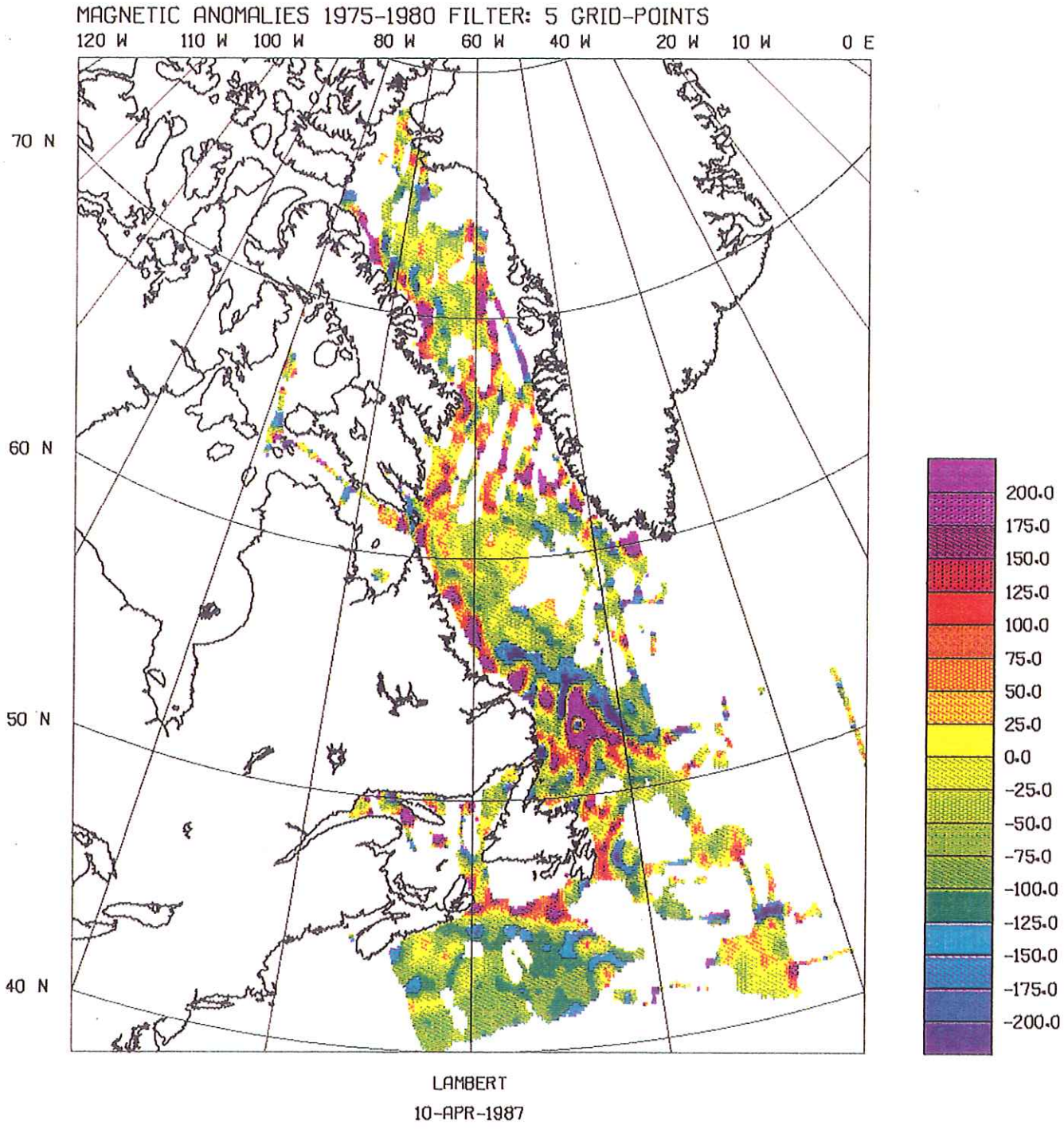

FIGURE 18C. Plots of the gridded and filtered anomaly values derived from observations in the five-year epoch shown at the top.

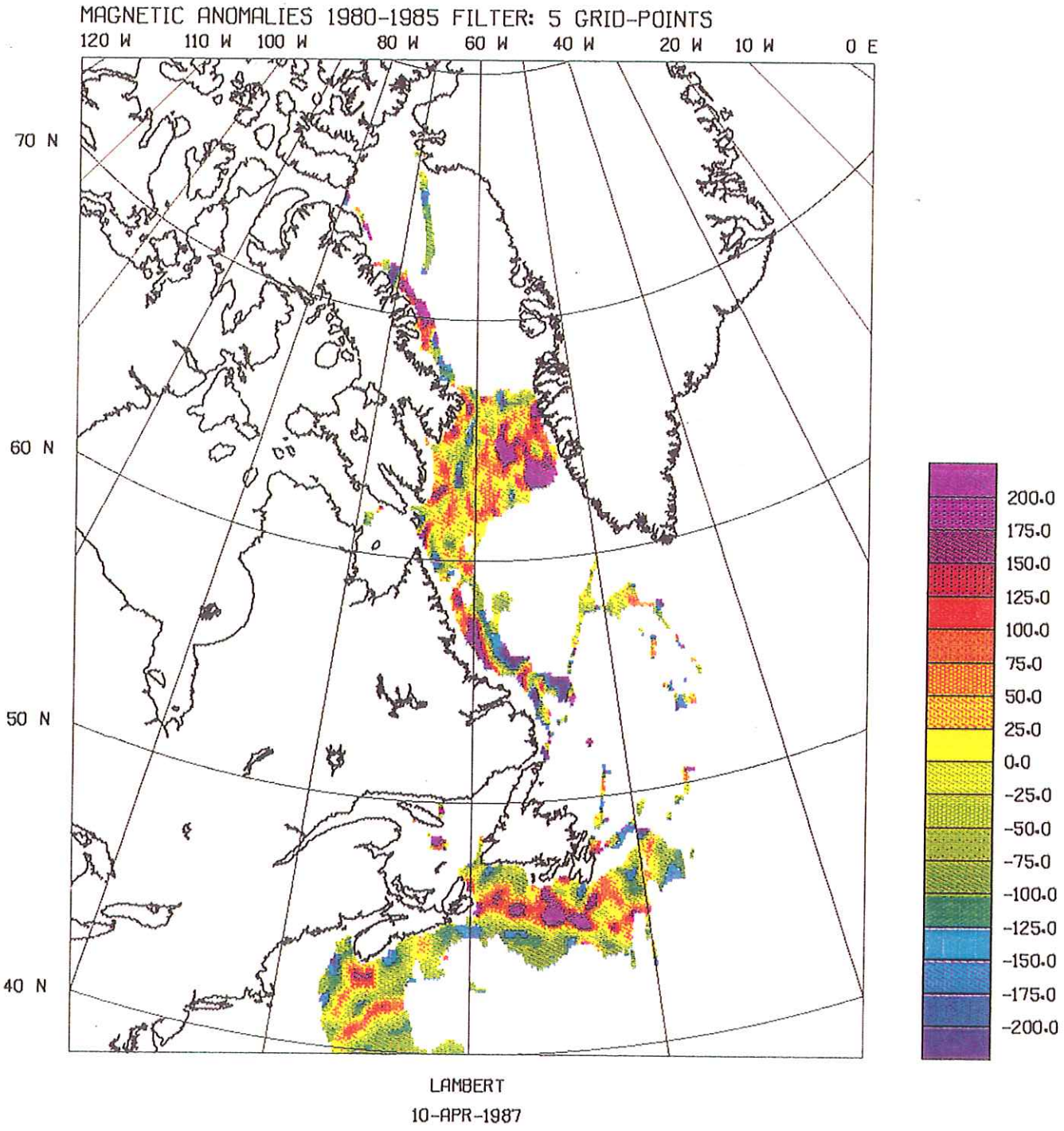

FIGURE 18D. Plots of the gridded and filtered anomaly values derived from observations in the five-year epoch shown at the top.

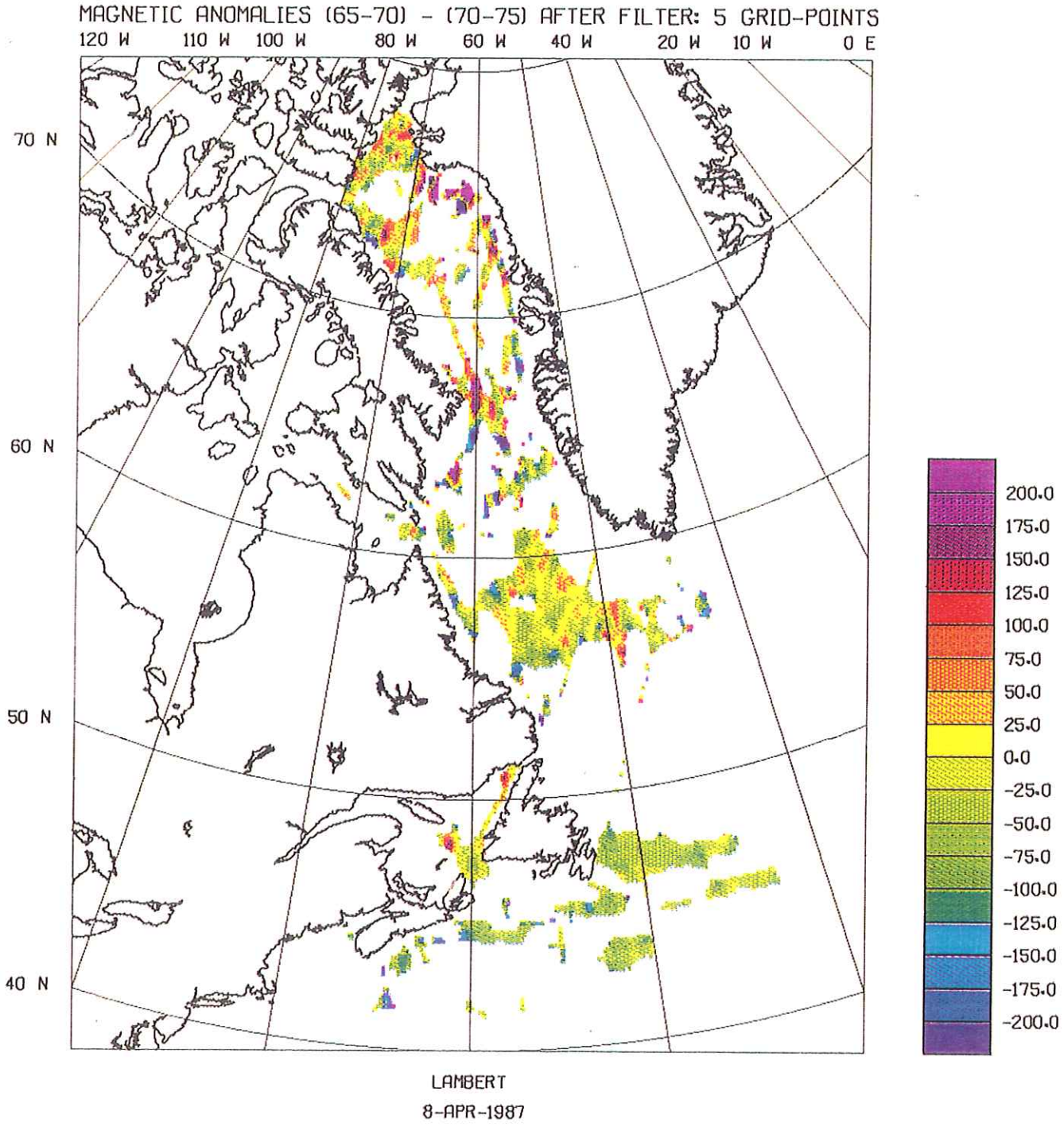

FIGURE 19A. Differences between the anomaly plots of the previous figure, with reference to the epoch 1970-75.

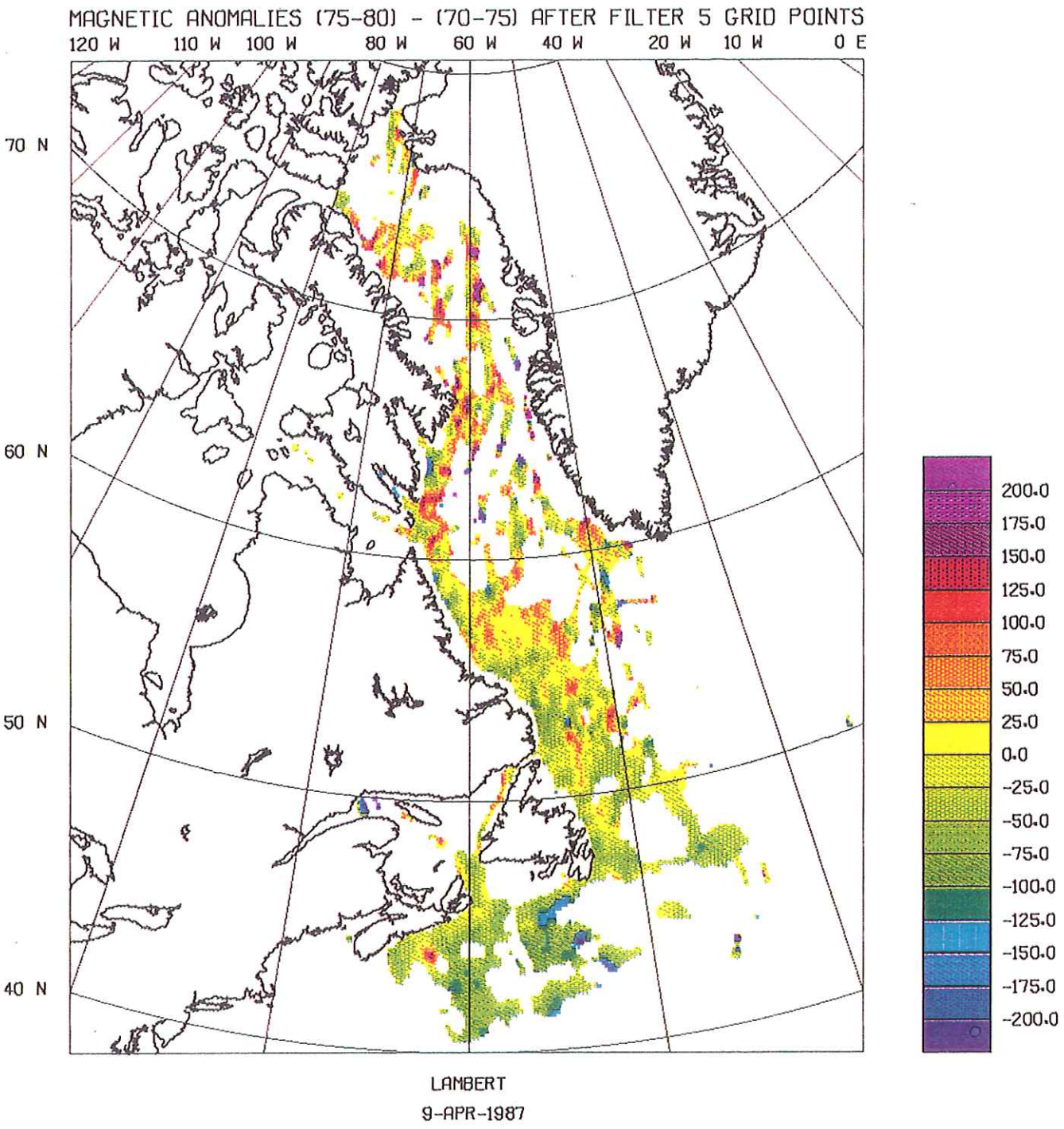

FIGURE 19B. Differences between the anomaly plots of the previous figure, with reference to the epoch 1970-75.

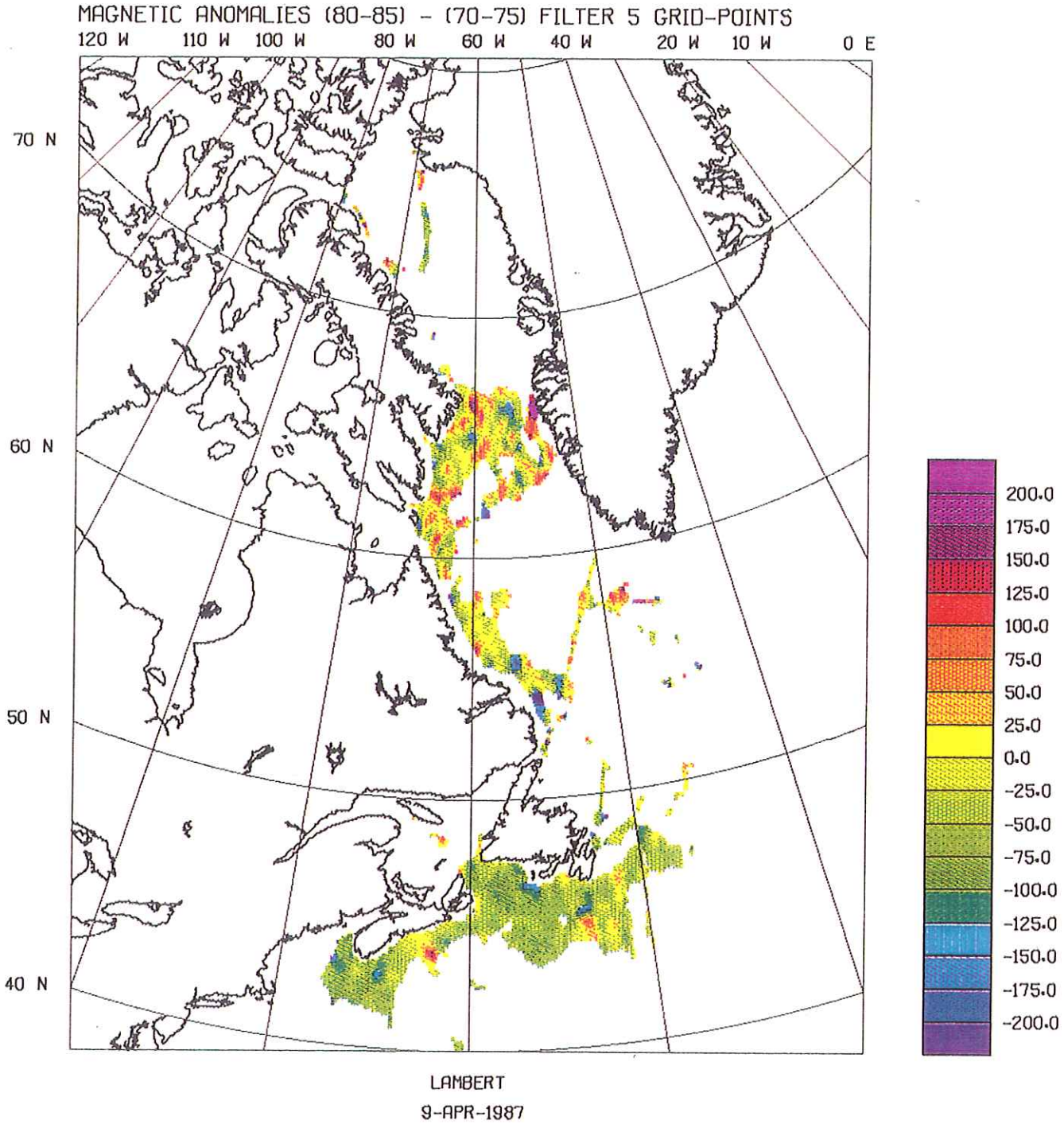

FIGURE 19C. Differences between the anomaly plots of the previous figure, with reference to the epoch 1970-75.

6. DATA PROCESSING AND MANIPULATION

A number of software tools were implemented to facilitate the inspection, manipulation, editing, and display of data during various phases of the data base implementation and the production of the regional map. Some of these processes were executed on networked MicroVAX computers; other operations involving large data sets and voluminous memory arrays were carried out on a VAX 750.

6.1. Gridding and contouring

An initial step was to convert irregularly-spaced ship track data into observations distributed over a regular grid. For this, an automated gridding routine was applied which combined an adjustable digital filter with a weighting method (Slootweg, 1978; Verhoef et al, 1986). The method produced grid values that were unbiased by track line geometry, and also diminished the influence of residual positioning errors. It had the disadvantage that along-track details with wavelengths shorter than the mean track spacing were lost.

Computer contouring was accomplished in three steps:

1) Generate a square grid over the area to be contoured.

2) Estimate the mesh point values for this grid from the data point values.

3) Draw contour lines using the mesh point values.

The spatial filter used in the calculation of mesh point values from unevenly spaced data was a low-pass Butterworth filter of the first order, which reduced the short wavelength components in the data. The choice of the cut-off wavelength of this filter depended on the data point distribution and the expected spectral content of the variable to be contoured.

In general, observation points were irregularly distributed: data points tended to be more closely spaced in along-track than in cross-track directions. Filter constants were carefully specified to minimize the effects of this sort of data distribution, while predicting how much filtering would occur for any given wavelength.

If too low a cut-off wavelength was selected for the filter, the coherent structure of the resulting contour lines was disturbed by irregularities in the data distribution. If on the other hand the cut-off wavelength was too high, short wavelength detail did not appear in the contours. Thus an optimum value had to be established which depended on the mean distance between tracks. If the mean distance varied largely over an area, the gridding

was done with different filter settings in different subareas, and the resulting grid files merged by means of a simple averaging technique. In this case, however, the resulting grid was spectrally inhomogeneous.

For routine handling of track data, the gridding procedure used the original time-sequential field observations as input, each observation being tagged with latitude and longitude coordinates. The output consisted of a grid file representing a matrix of mesh points separated by equal increments of latitude and longitude.

The grid file contained three quantities for each mesh point:

1) The summation of the values of the contributing data points multiplied by the weighting function.

2) The summation of the weight function.

3) The number of contributing data points.

Data points contributed to a grid value whenever the weight function, which depended on the distance between the data point and the grid point, was higher than 0.3 per cent of its maximum value. This maximum value occurred when data point and grid point coincided.

The gridding operation consisted first of scanning and multiplying all data points by the appropriate weighting function for each grid point, with summations stored in the grid file as quantities 1), 2), and 3) defined above. The value at each grid point was then calculated by dividing summation 1) for that location by the corresponding total weight function 2). If the number of data points contributing to one grid point was less than a set limit, a flag value was stored to indicate 'no value'.

Storing quantities 1), 2), and 3) separately for each grid point made it easy to update the grid file whenever new data were available, or to enter corrections for bad data. For instance, suppose that after contouring, one observed several contour lines which were obviously disturbed by a series of erroneous values along a particular track. Eliminating these bad values was easily accomplished by re-running the gridding program on a synthetic track that matched the location of the bad track, but with signs reversed on all the offending data points. The weight summations were then adjusted accordingly in the appropriate grid locations. Note that it was not necessary to regrid the entire set of data to enter corrections for any given track segment.

Contour maps were produced by drawing line segments within the elementary grid squares. The end points of these segments were found by linear interpolation between the mesh points. Other options were to display contours as changes in colour or line

pattern. In this case, the locations of the changes were also found by linear interpolation between the mesh points.

6.2. Filter effect of gridding

A cutoff wavelength of 20 nautical miles appeared to be the optimum for the total set of observations collected by AGC. This meant that at 20 nautical miles from a mesh point, the weights were 6 dB or approximately 70% down, decreasing further with increasing distance. In areas of smaller than average track spacing, this filter setting resulted in the loss of some detail. The wider distribution of data in Baffin Bay (see Figure 1) necessitated an increase in the cutoff wavelength to 30 nautical miles.

The filter effect of the gridding procedure is illustrated in Figure 20. Note that the dotted profile displays a slight level shift. This might be the result of biases in the observed data, or it might be introduced from adjacent lines; the grid file contains influences from both sources.

The technique of comparing values observed along track with reconstituted grid values was also applied to locate track segments that agreed poorly with their neighbours. The average differences between observed and reconstituted values should have yielded random residuals for short wavelength anomalies over a number of points with no bias. However, where a track segment agreed poorly with its neighbours, the residuals could be expected to have a consistent sign.

6.3. Two-dimensional Gaussian weighting function

There were occasions when the gridded data had gaps that needed to be filled, or required additional filtering (as when examining long-wavelength features of the anomaly field). For the most part, these operations were carried out by means of a two-dimensional Gaussian weighting function. This particular function was chosen because it was easy to implement in software, and had good execution times.

In practice, the operator moved from point to point in the grid, applying Gaussian weights to the values in grid points situated within a predefined radius. Choice of radius and weight parameter depended on the size of features one wanted to filter, or the size of the gap to fill. Note however that in the case of filtering it was not directly evident which wavelengths were reduced, due to the spectral character of the Gaussian weight function.

Depending on the application, the function also checked for a minimum acceptable number of valid data points within its radius

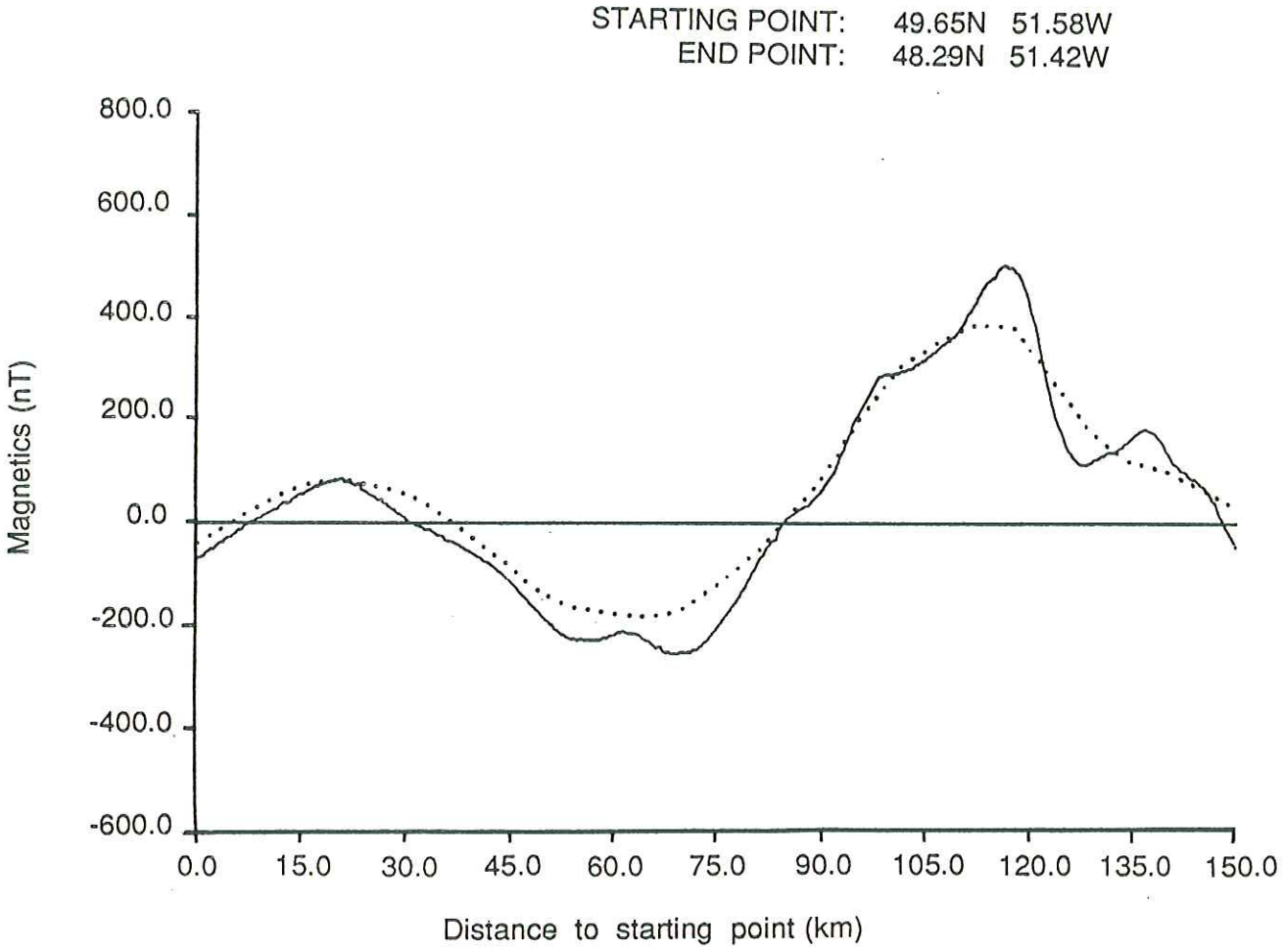

FIGURE 20. Filtering effect of the gridding routine. The solid line represents the observed magnetic anomalies along a track of a 1979 cruise to the east of Newfoundland. The dotted line shows the anomalies along the same track, but now recalculated from a set of gridded values. The filter effect of the gridding, for which a Butterworth filter with a 20 nautical mile cut-off wavelength was used, is clearly seen as the attenuation of the short wavelength anomalies.

of operation, and moved on to the next grid point if this criterion was not satisfied.

6.4. Shadowgrams and the detection of bad data points

Data presentation by way of a contour map has the disadvantage that features with amplitudes smaller than the contour interval may get lost. One solution is to present a three-dimensional view of the grid values. Another solution is to display slopes instead of values. The latter approach is easy to implement by calculating and plotting the directional derivative of the grid values. The direction of this derivative is user selectable, and depends on the slopes one wants to enhance.

The resulting plot suggests the shadows that would be obtained by shining light across the surface of the gridded data from a given direction. An advantage of this presentation is that one obtains a better resolution, due to the relative increase in power of the shorter wavelengths caused by the application of the directional derivative. Bad data points that stand out from their neighbours are therefore more easily detected.

As an illustration of the method, we describe below a specific application of the shadowgram method that was used to identify bad data in a subset of AGC data located northeast of Newfoundland.

Figure 21 is an anomaly map derived from marine magnetic observations. Clearly visible are the arcuate trends of the Avalon basement across the Grand Banks and continuing into Orphan Basin (e.g. Haworth, 1980), where they decrease in amplitude. This map contains an erroneous track segment, although even a careful inspection of the contours does not reveal anything seriously amiss.

Figure 22 is a shadowgram of the same area, with the source of illumination at 210 degrees (i.e. 30 degrees west of south). Even a cursory glance suffices to detect an irregular zigzag feature extending from the northern edge of the map to a point near the southern edge. An inspection of ship tracks in the area showed that this feature indeed corresponded to an identifiable track segment.

The gridded data set was then recalculated using a synthetic correction track as outlined above, to eliminate the effect of erroneous data. Figure 23 is the corrected magnetic anomaly field, and it exhibits little change from the uncorrected anomaly. The corrected shadowgram in Figure 24, however, clearly shows the improvement in the data set.

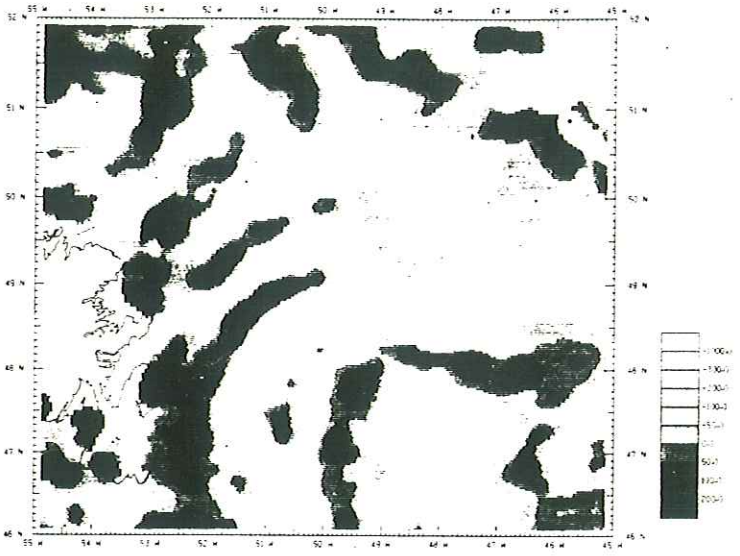

FIGURE 21. Magnetic anomalies in an area to the northeast of Newfoundland. Clearly visible are the arcuate trends of the strong positive anomalies of the Avalon basement across the Grand Banks. The data include a 'bad track' which is hardly visible.

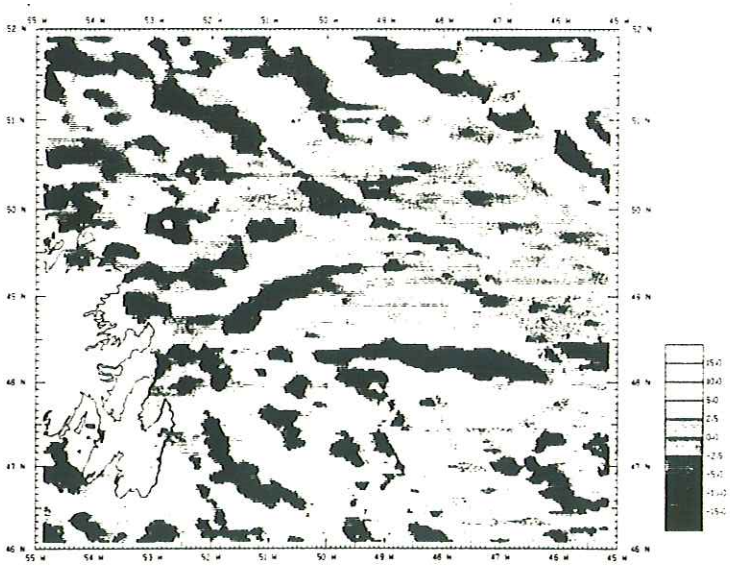

FIGURE 22. Shadowgram of the magnetic anomalies of the previous Figure, in the direction of 210 degrees, i.e. 30 degrees west of south. The values plotted are the slopes (unit is nT/km) of the anomalies. The 'bad track' shows the irregular zigzag feature extending from the northern edge of the map to a point near the southern edge.

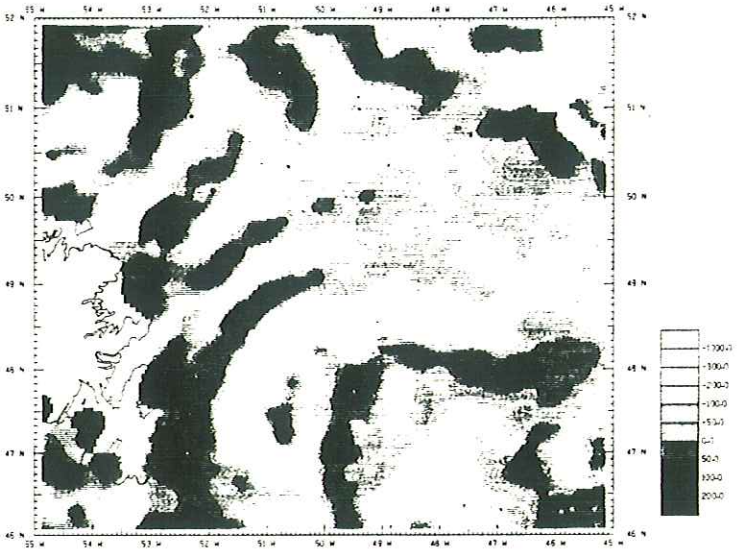

FIGURE 23. Magnetic anomalies after correcting for the 'bad track'. The correction resulted in some minor changes only in the anomaly pattern.

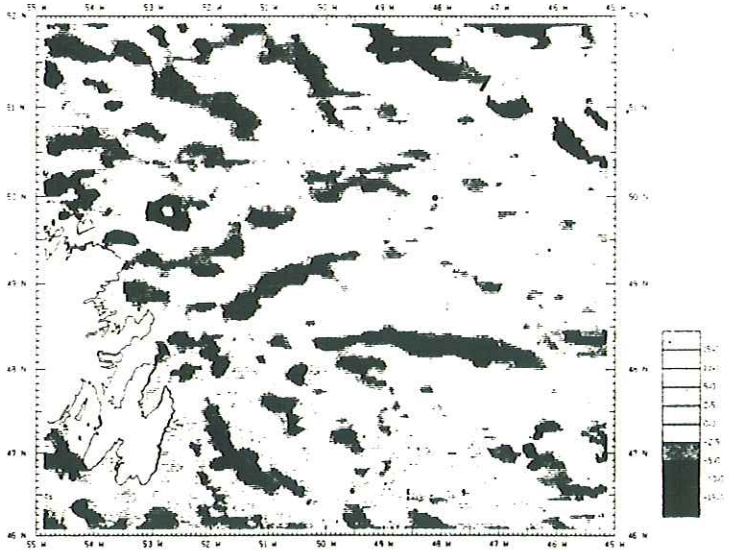

FIGURE 24. Shadowgram of the corrected anomalies in the direction of 210 degrees. The correction resulted in a significant change in the shadowgram. Note how the dominant lineation of the previous shadowgram has now disappeared.

6.5. Removal of bad points from the data base

The shadowgram technique was eventually applied to the entire data base using various directions of illumination, in order to locate and to identify erroneous track segments, and to flag them in the original cruise data sets. Synthetic correction tracks were then fed into the gridding process to eliminate the bad data. This resulted in the elimination within the grid of about 3% of the data set (flagged track segments are listed in Table 3), and led to a significant improvement in the statistical properties of the data base (discussed under calculation of crossover errors).

6.6. Directional filtering

Some parts of the magnetic data exhibited corrugations that were obviously due to level differences between adjacent and parallel ship tracks. A de-corrugating technique was developed for performing directional filtering on data sets so affected; it involved spectral analysis and Fourier Transform processing.

An example of corrugated data is shown in Figure 25, which illustrates the anomaly field to the east of Nova Scotia. The East Coast Magnetic Anomaly (ECMA) is clearly visible as a strong positive feature extending from about 41.5N/65W to 43.5N/59.5W, while a few subtle NNW-SSE lineations can be seen in the lower part of the map area. These lineations are more clearly visible in the shadowgram of Figure 26, which has been constructed with a direction of illumination of 90 degrees.

An inspection of the track lines in Figure 1 indicates several track segments in the area with a similar spacing and orientation; the lineations in the magnetic field are obviously related to these tracks, and are probably caused by levelling problems in the data. Clearly, the NNW-SSE lineations will produce relatively high values in that direction of the power spectrum, with a wavelength determined by the track spacing.

Figure 27 is the two-dimensional power spectrum of the data in this particular area, obtained by applying a 2D Fourier Transform to the gridded data.

In simple terms, the power spectrum shows the variation of the square of the amplitude of the magnetic anomalies with their wavelength. In addition to the general decay of the power going from longer to shorter wavelengths, there is some local increase in the power along the direction of 55 degrees. This shows up as a series of small spots in the figure, extending from the centre along the 055-235 axis (see line indicated by arrows in the two-dimensional power spectrum).

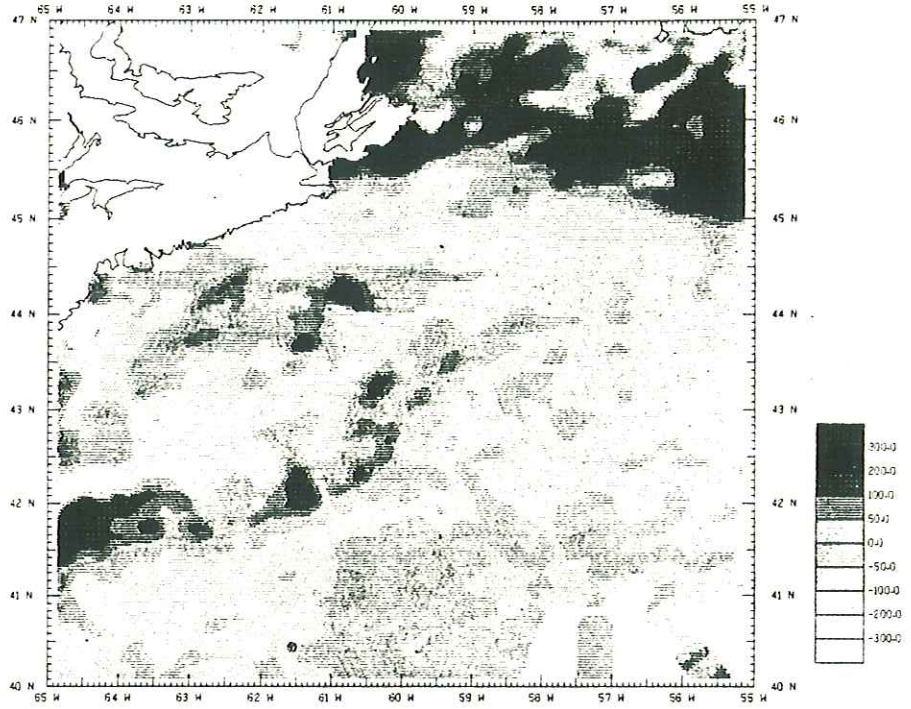

FIGURE 25. Magnetic anomalies to the east of Nova Scotia. Clearly visible is the East Coast Magnetic Anomaly (ECMA) as a strong positive feature running from about 41.5N/65W to 43N/59.5W. Some NNW-SSE lineations can also be seen in the magnetic anomalies.

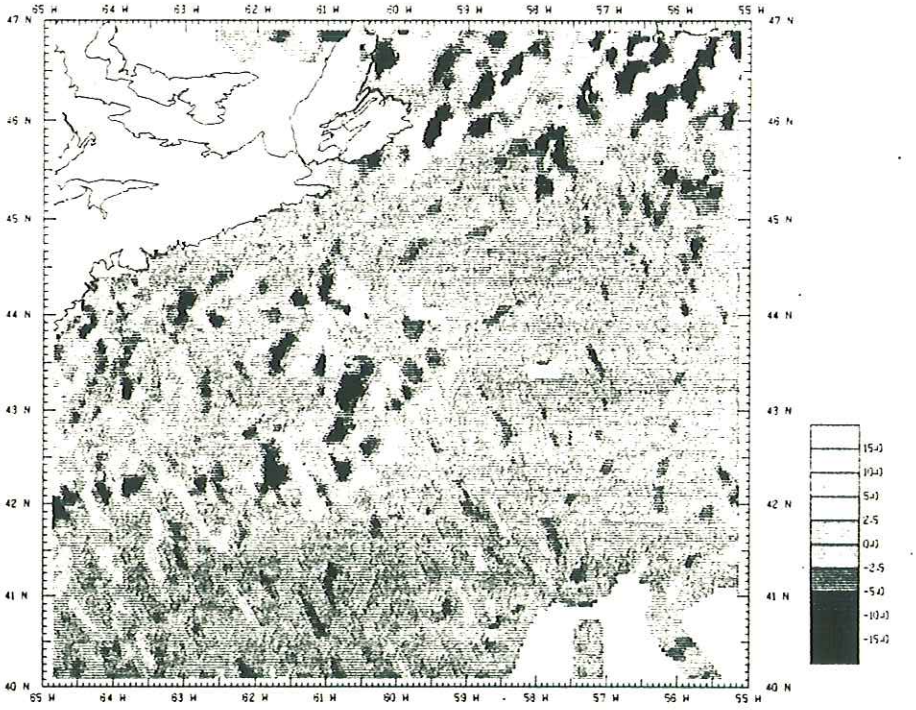

FIGURE 26. Shadowgram of the magnetic anomalies illuminated from 90 degrees, i.e. from the east. Note the dominant NNW-SSE lineations in the shadowgram.

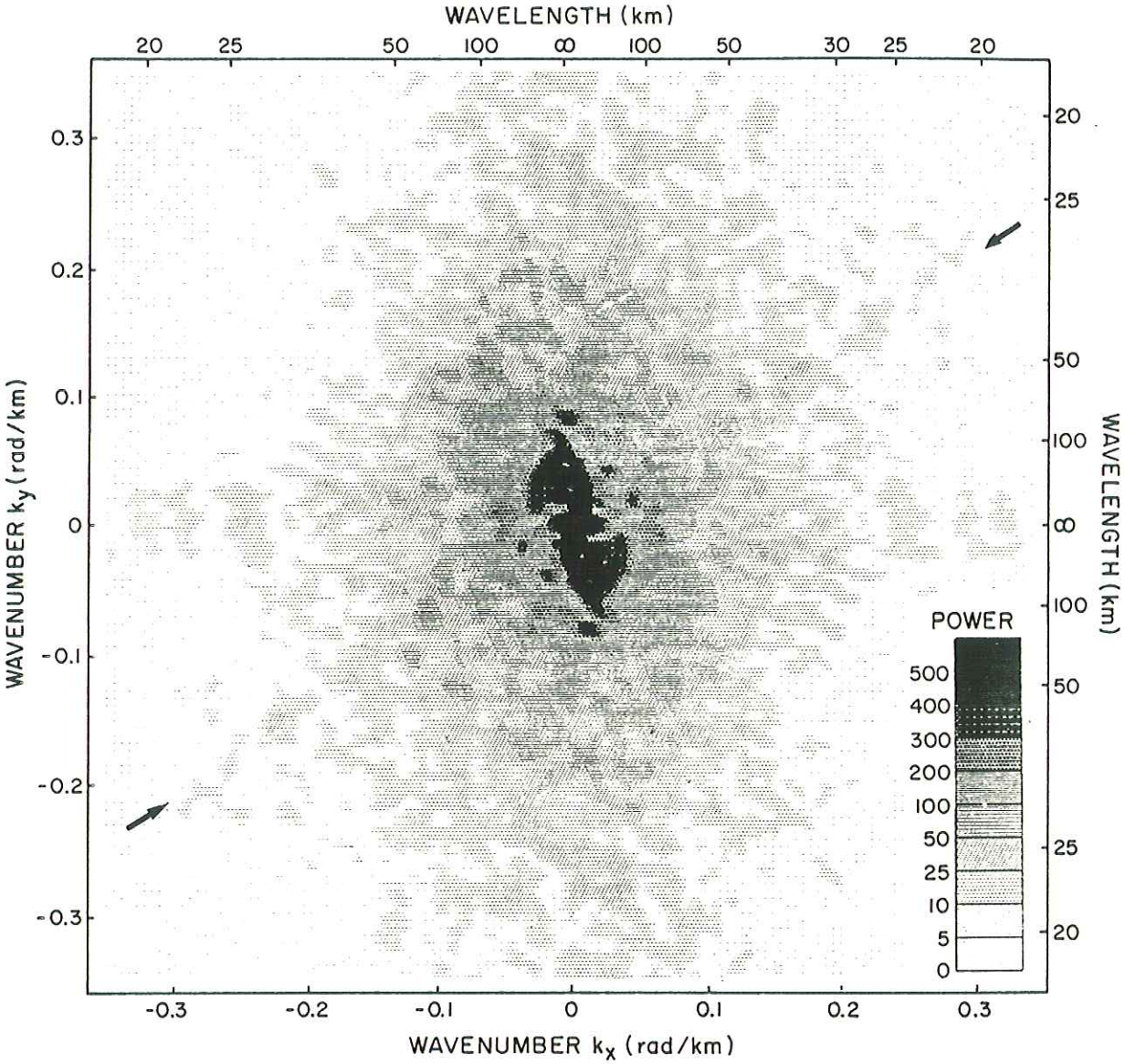

FIGURE 27. Two-dimensional power spectrum of the uncorrected magnetic anomaly field east of Nova Scotia. Before applying a 2D Fourier Transform to the data, a best fitting plane was subtracted from the data and a cosine taper was applied. The wavenumber in the X-direction is shown along the horizontal axis, while the wavenumber in the Y-direction runs along the vertical axis. As the input data were a real function, the spectrum shows some symmetry: the first and third quadrant are the same, as are the second and fourth. For presentation purposes, wavelengths of less than 18 km are not shown. The arrows indicate the 055 direction.

The picture becomes clearer if we calculate the power spectrum at an azimuth of 55 degrees (Figure 28). The power in this direction and between wavelengths of 18 and 65 km is greater than the corresponding power in other directions, as shown in Figure 27. This indicates a relationship between lineations in the field, and the spacing and orientation of the tracks.

In order to isolate anomalies in the power spectrum, it is possible to define a mean spectrum by averaging over the different directions, and then to look at the deviations from the averages (e.g. Simpson et al, 1986). However, the power spectrum of magnetic anomalies in general is not axially symmetric like that obtained from gravity anomalies; it has instead an elliptical shape due to the vectorial character of the magnetic anomalies.

To reduce the effect of mislevelling between tracks and hence to eliminate the lineations in the magnetic field, we reduced the power in the direction of 55 degrees by applying a directional filter. The procedure involved a filter with a Gaussian directional component and a halfwidth specification. In addition to its directional component, the filter included a Butterworth wavelength bandpass. We used cut-off wavelengths of 18 and 65 km for the bandpass filter, with a roll-off of 48 db/octave.

The dotted line in the azimuthal power spectrum (Figure 28) shows the power in the direction of 55 degrees after filtering. Figure 29 shows the filtered anomaly field, with the corresponding shadowgram in Figure 30. There has clearly been an improvement in the data set, especially with regard to the NNW-SSE lineations.

The method described here can eliminate levelling problems through use of a directional filter. However, the use of such a filter also eliminates genuine power in the specified direction. We are investigating different approaches to resolve this loss of information. One approach is to use the power in the direction of corrugation to define level corrections that are applied directly to observed data along selected tracks.

7. MARINE CROSSOVER ERRORS

A crossover is a point of intersection between two segments of ships' tracks. All factors being equal, observations along the two track segments should agree at their point of intersection. The fact is that magnetic observations rarely coincide at crossover points. However, assuming a random distribution of errors, the resulting discrepancies can serve as general indicators of the total error in the final anomaly field.

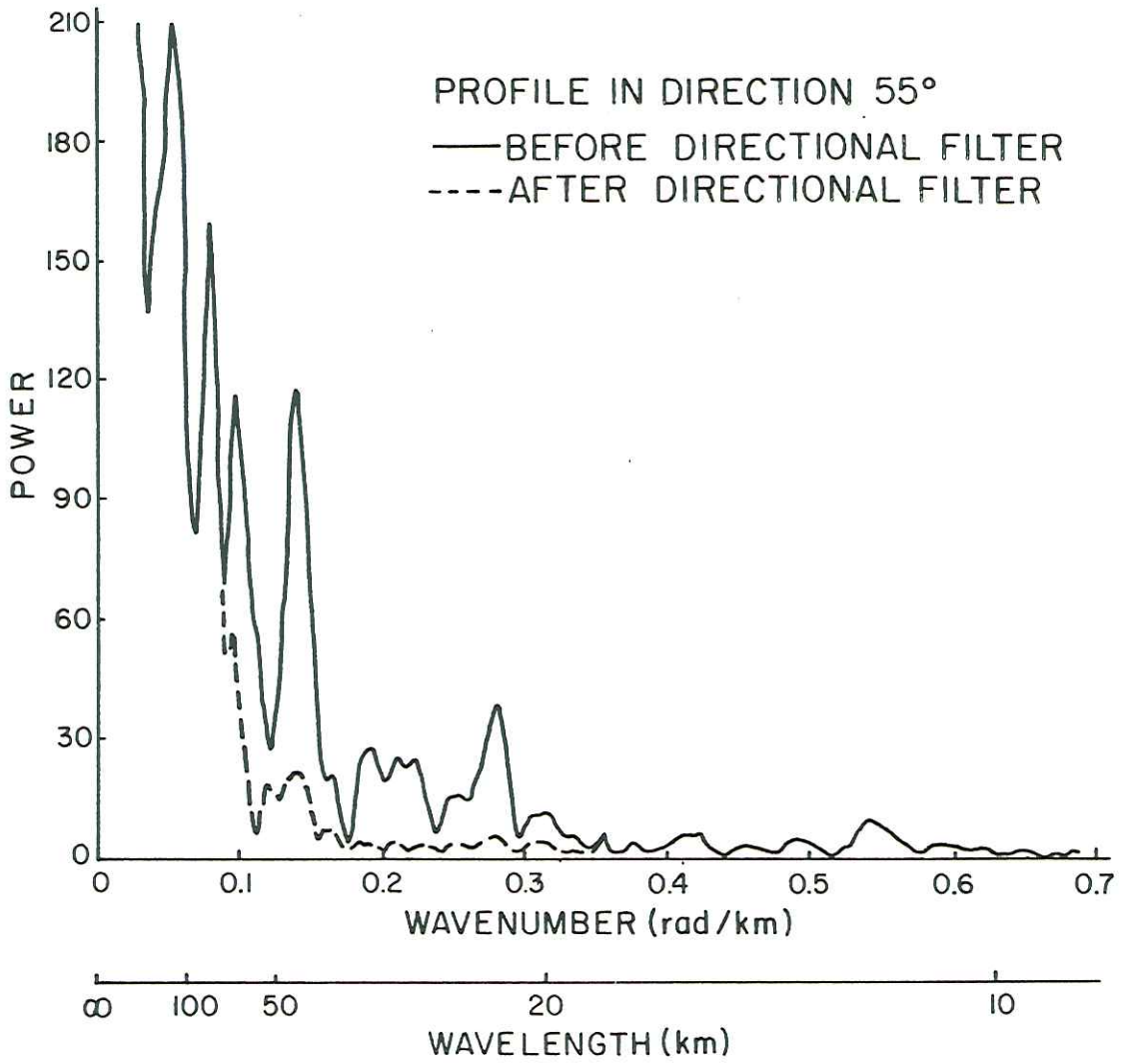

FIGURE 28. Power spectrum in the direction of 55 degrees. The continuous line shows the spectrum of the original anomalies, while the dashed line shows the spectrum after directional filtering. Note the relatively high power between wavenumbers 0.36 and 0.12 in the original power spectrum, which has been reduced by the filter.

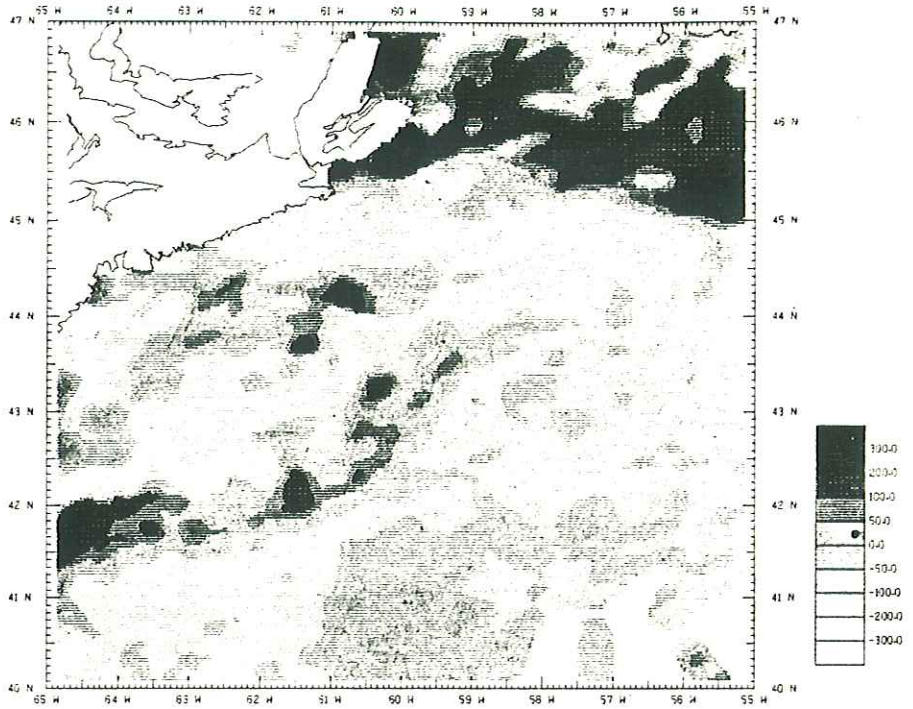

FIGURE 29. Magnetic anomalies after applying a directional filter. The directional part of the filter is Gaussian; we used a direction of 55 degrees and a halfwidth of 20 degrees. In addition, there is a bandpass Butterworth filter for which high and low cutoff wavelengths of respectively 18 and 65 km were used with a roll-off of 48 db/octave. Only small changes can be seen in the the anomaly pattern.

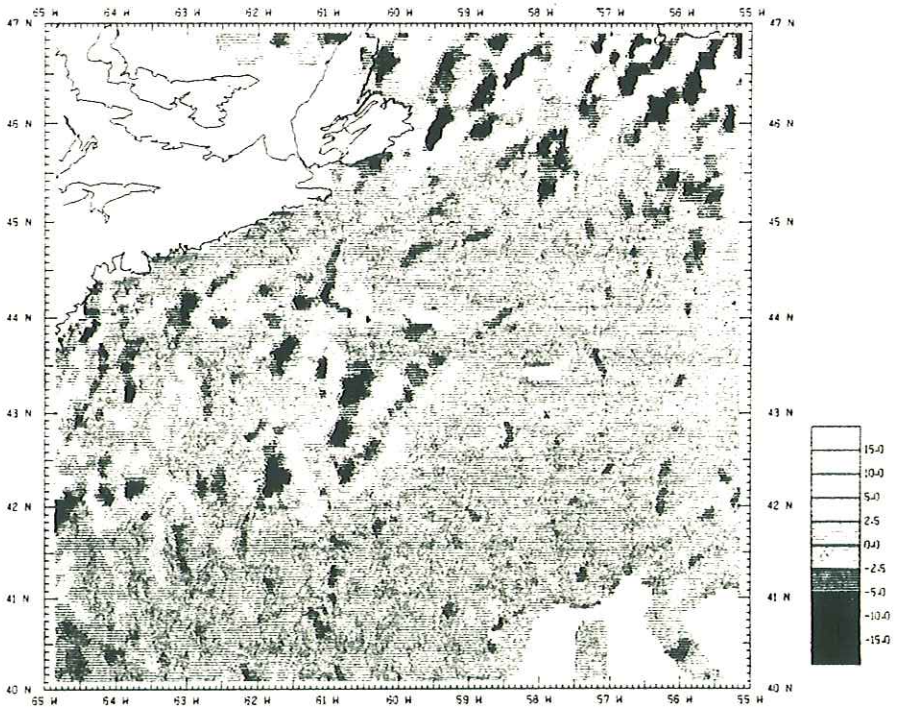

FIGURE 30. Shadowgram of the filtered magnetic anomalies, illuminated from 90 degrees. Note the absence of NNW-SSE lineations.

7.1. The calculation of crossover errors

For purposes of this analysis, a track segment is defined as a straight line joining two succeeding observations that are separated in time by 1 minute, or with an average ship's speed of 10 knots, by about 300 metres in distance. In case of data gaps we allowed the time interval to increase to a maximum of 16 minutes, provided that the distance was less than 5 kilometres. Two values are obtained at each crossover point by interpolating the observations at the ends of each line segment; the crossover error is the difference between these two values.

The detailed procedure for deriving crossover errors from the magnetic data set was adapted from the method used for gravity data (Earth Physics Branch, 1986):

1) A table of track segments was created by scanning the observation records in the total data base, and extracting relevant information for each observation point: time, latitude, longitude, and magnetic anomaly value. Track segments were discarded if they lacked a valid magnetic observation at either or both ends, or if they featured an anomaly value in excess of 2000 nT.

2) Segments were sorted by ascending longitude.

3) Sorted line segments were compared against each other to detect pairs that intersected. If they did, times and anomaly values were interpolated for the point of intersection on both track segments, and stored in another table along with the latitude and longitude of the crossover point.

4. Crossover errors were calculated as the differences between pairs of interpolated anomaly values, and stored for subsequent display and manipulation. The convention followed throughout was to subtract <u>older</u> values from <u>newer</u> values, i.e. the errors were <u>positive</u> when newer values were greater than older, and <u>negative</u> when less.

The total data set was too large to carry out the crossover analysis in a single pass, so the observations were divided into four latitude bands with a half degree of overlap. Crossovers were then determined in each of the four subareas, and combined in one table after elimination of duplicate crossover points in the overlap zones.

The four latitude bands are listed in the following table, along with the number of observation points in each, and the number of detected crossover points.

Limits	Observations	Crossovers
35.0 - 47.5	833,061	16,805
47.5 - 53.0	716,337	23,020
52.5 - 62.0	575,758	12,793
61.5 - 85.0	553,919	10,613

After merging and elimination of duplicates, we were left with 59,444 crossover errors which could be displayed and manipulated to investigate a variety of relationships.

Figure 31 was produced to demonstrate a possible location dependence, and shows positions of crossover errors larger than 500 nT. These larger errors show a clear tendency to localize in areas of shallow water where the magnetic anomalies have high amplitudes and short wavelengths e.g. Davis Strait, Flemish Cap; these could indicate navigation errors, where slight displacements in position can lead to significant disagreements between observations. A few large errors plot in deeper water where anomalies tend to be more subdued in both wavelength and amplitude; these could signal a problem in the IGRF model, or could result from high amplitude short term variations.

Numerous histograms were produced to display error distributions after various stages of editing and selection. The left side of Figure 32 shows the distribution of errors for the original, unedited data set. Mean error is 1.7 nanotesla, with a standard deviation of 111.9 nanotesla.

The right side of Figure 32 shows the error distribution after the following refinements were applied: bad data points were identified and excluded from further calculation (see discussion under Removal of bad data points); crossover points with anomaly values exceeding 1000 nanotesla were excluded; crossover errors exceeding twice the standard deviation were excluded. Mean error is now -0.9 nanotesla, with an improved standard deviation of 69.9 nanotesla.

7.2. An analysis of the crossover errors

The interpretation of the crossover errors was complicated by three factors:

1) The total set of magnetic observations had a very irregular distribution over a large geographic area, as well as over an extended interval of time.

2) Crossover points had a similar irregular distribution, but one which did not match that of the original data.

3) The IGRF model, which was used to derive the values from which crossover errors were calculated, exhibits non-uniform behaviour over both space and time.

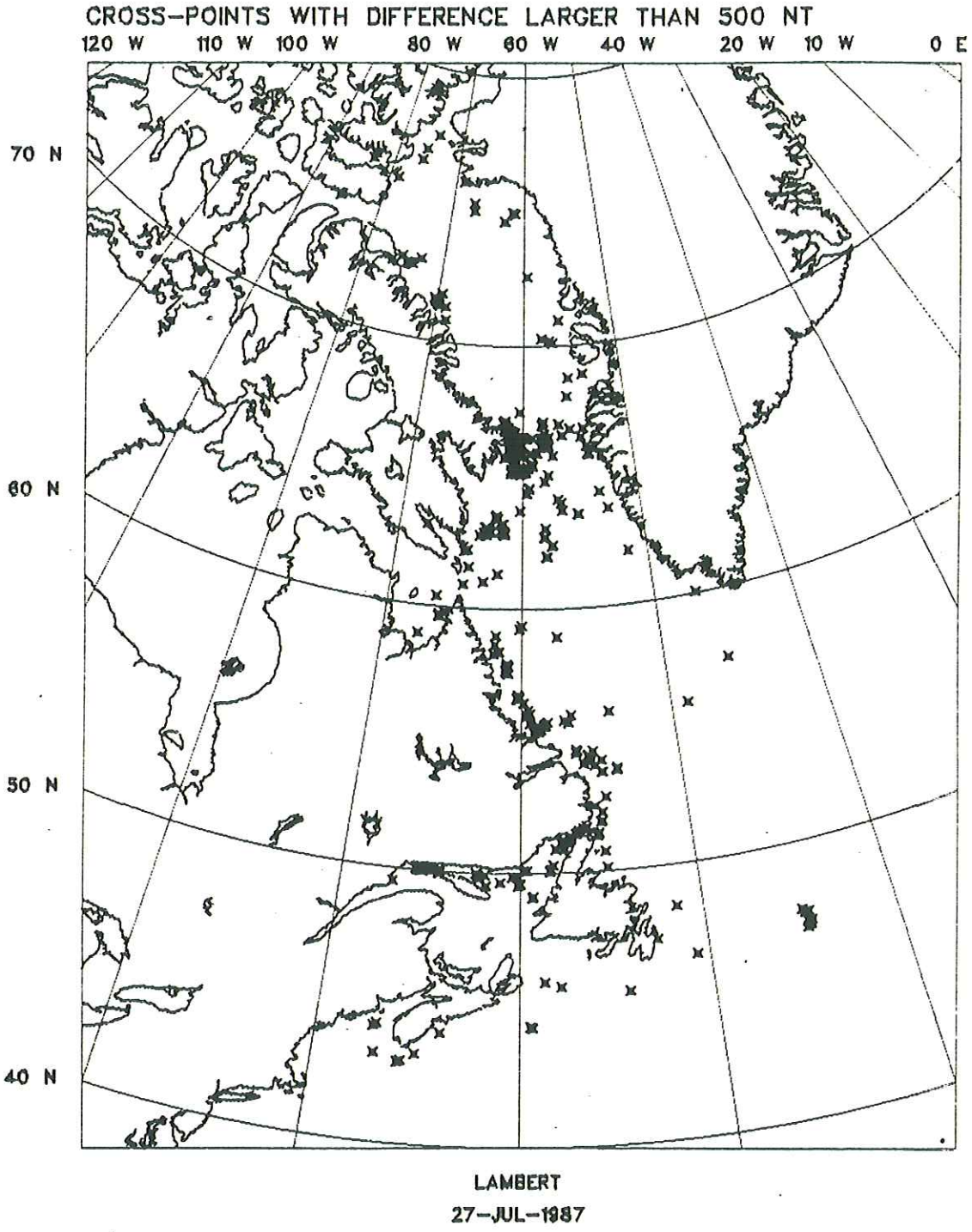

FIGURE 31. Locations of crossover errors exceeding 500 nT (see text for explanation).

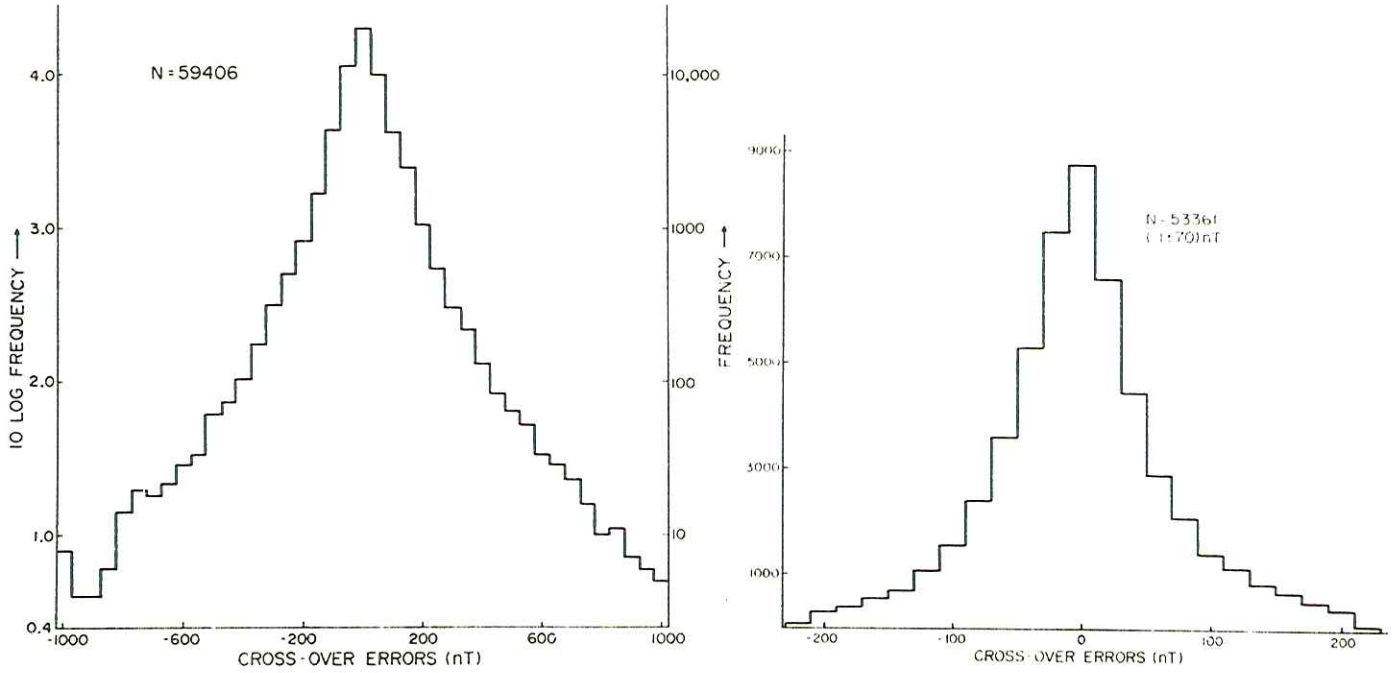

FIGURE 32. Histogram of crossover errors in all data. Left: prior to correction and removal of bad points. Right: after data refinement.

The large number of crossover points (nearly 60,000) suggested a statistical approach. To detect a pattern in the crossover errors, we began by dividing them into yearly groups in order to compute their statistical properties for intercomparison.

For each year, we calculated mean values and standard deviations for two sets of crossover errors: those arising from comparisons of data collected in that year alone, and those arising from comparisons with data collected in other years. For brevity in the following discussion, we will refer to these error sets as internal and external crossover sets, respectively.

Mean values and standard deviations were then re-computed for all crossover sets, excluding those values which fell outside the two sigma confidence level. Standard histograms were constructed for each crossover set, but the sheer volume of plots precluded attempts to make meaningful comparisons.

A new form of display was developed to present this mass of statistical information in a manner that would lend itself to a straightforward visual interpretation. Figure 33 is an example of the display, showing the statistical properties of the internal crossover sets.

The horizontal axis is graduated in years and spans the interval 1962-85. For each year, there is a vertical bar that relates to its particular crossover set: the mid-point of the bar is the mean value, as read off on the vertical axis. The length of the bar is the standard deviation, measured to the scale of the vertical axis. The number at the lower end of the bar is the number of points in that particular crossover set.

With the internal crossover sets, the trend of the mean values is flat, and tends to oscillate at low amplitudes around the zero level. This behaviour is not unexpected, as the same IGRF model was used in any given year to derive the original data pairs from which the internal crossover errors were calculated, and residual time-dependent variations will hardly show up over an interval as short as one year.

Various peaks in this and the following figures can be attributed to unfavourable measurement conditions in certain years, e.g. a high proportion of the observations in 1965, 1970, 1978, and 1981 were made in the auroral zone, under poor navigational control, or in areas where the magnetic field was characterized by high amplitudes and short wavelengths.

Figure 33 also shows the statistical properties of the external crossover sets. The yearly mean values show a slight negative trend: this reveals a tendency for anomaly values to decrease

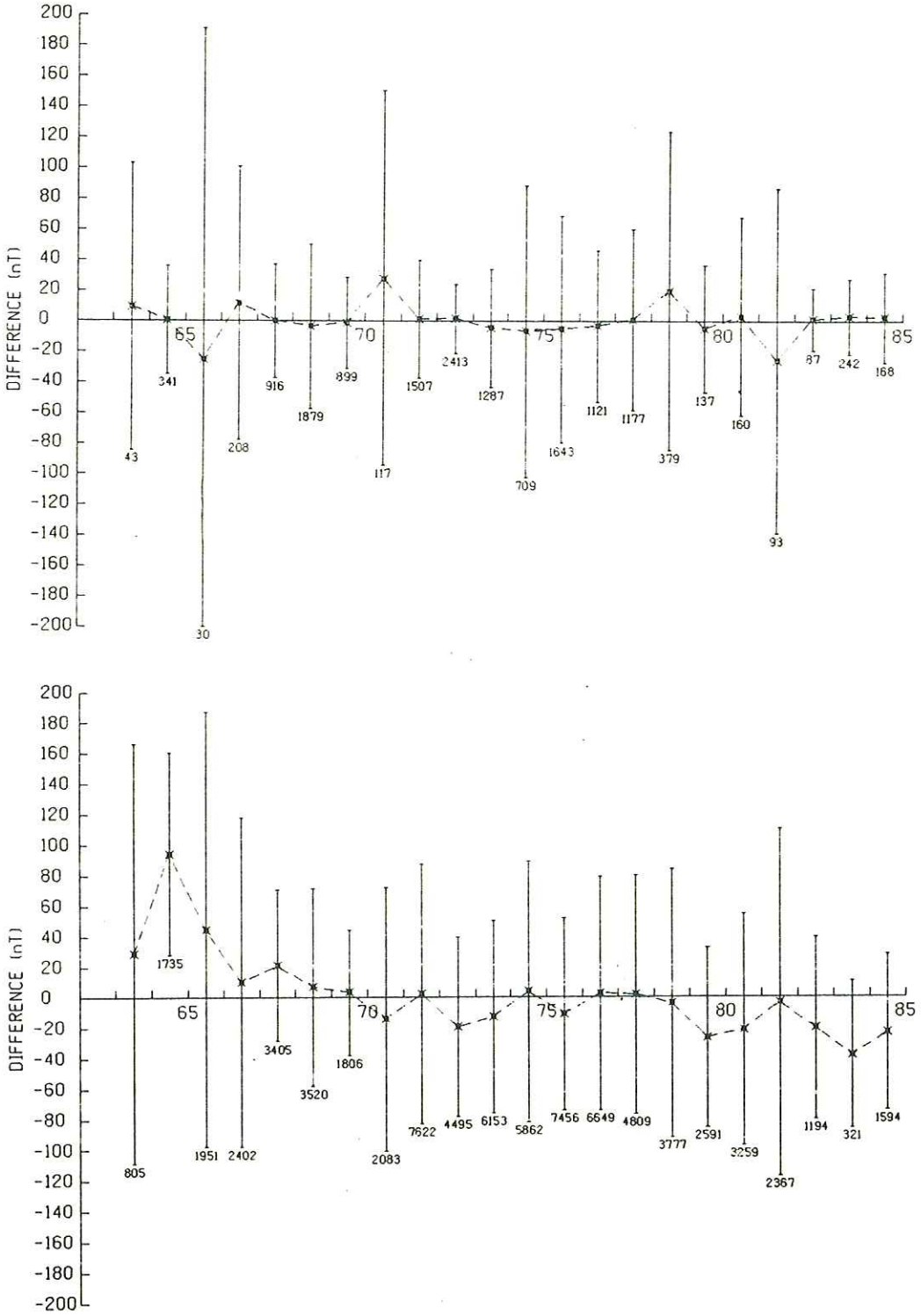

FIGURE 33. Statistical properties of crossover sets (see text for explanation). Top: internal sets. Bottom: external sets.

over time, which would be an indication of a component in the IGRF model that increases with time.

The upper part of Figure 34 shows the statistical properties of the external crossover sets, but excluding those errors where both original observations were made after 1975. The yearly mean values again show a negative trend, leading to a similar conclusion as in the preceding figure.

The lower part of Figure 34 shows the statistical properties of the external crossover set, but this time excluding the errors where both original observations were made prior to 1975. This diagram exhibits a pronounced negative trend prior to 1975, and a flat, near zero-level trend after 1975. This is indicative of a component that increases with time in the pre-1975 IGRF model, but which is absent in the post 1975 implementation.

From the analysis, it seems safe to conclude that the pre-1975 IGRF model contains an artificial time-dependent component that causes the change of the simulated field to increase with time at a higher than actual rate, thereby causing an apparent decrease with time of the magnetic anomaly.

The IGRF model uses linear interpolation to model the field between epochs. Where the simulated field varies slowly and regularly, linear interpolation provides results that are adequate. However in the vicinity of a behavioural discontinuity such as in 1975, linear interpolation may not accurately reflect the behaviour of the function, and might introduce some time-dependent errors in the resulting anomaly field.

An experiment was therefore undertaken to see whether another form of interpolation would improve the modelling of field variations, and so improve the final result. The IGRF model was re-calculated for the entire data set, but using a bicubic spline in lieu of conventional linear interpolation. The dashed lines in Figure 17 illustrate examples of a field so calculated, which is smoother and physically more plausible than the angular approximation rendered by the standard model.

Nevertheless, there was little improvement in the final result, as manifested in the statistical properties of the re-computed crossover errors: where before the mean value and standard deviation were -0.9 and 69.9 respectively, the new figures showed little improvement at -2.4 and 67.2. Clearly the time-dependent errors did not arise from the use of linear interpolation in the standard IGRF.

Having established the existence of a spurious time-dependent factor in the variation of the simulated magnetic field, it was necessary to determine whether this factor also exhibited a location dependence. A statistical analysis similar to the above

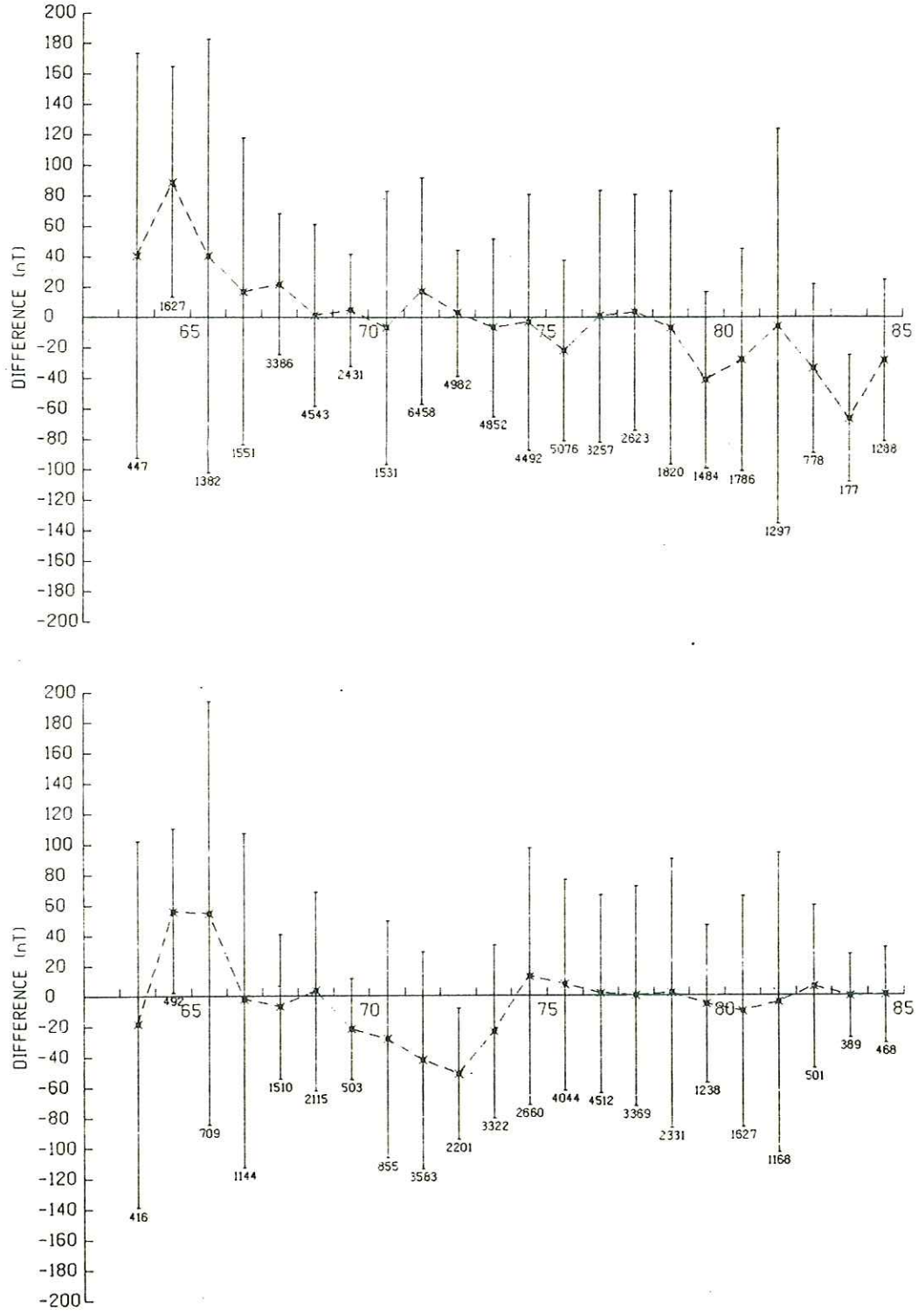

FIGURE 34. Statistical properties of external crossover sets (see text for explanation). Top: excluding pre-1975 crossover pairs. Bottom: excluding pre-1975 crossover pairs.

was carried out, but with the data separated into three zones bounded by latitudes 35N-50N, 50N-65N, and 65N-80N.

The analysis showed that mean values increased in all three zones, but not significantly; standard deviations decreased in the southernmost zone, and increased in the two northernmost zones. (The major increase in the latter is attributed to unfavourable observation conditions in the north: poor navigation, auroral zone disturbances, complex magnetic field.)

The outcome of that analysis is summarized in the table below, which compares the statistical properties of the zoned data with those of the total data set:

Zone	No of points	Average	Std Dev
All data	53361	-0.9	69.9
35N-50N	25556	-4.2	50.8
50N-65N	21335	-1.1	79.1
65N-80N	6556	9.3	116.8

Taking the analysis a step further, histograms of the zoned external crossover sets were constructed and combined as above to display the statistical properties for the interval 1962-85. Two plots were produced for each zone: one excluding errors where both original observations were made after 1975, the other before 1975.

The plots in Figure 35 for Zone 35N-50N show a pattern similar to that observed before in the total data set, and lead to the same conclusion: there is a time-dependent change component in the pre-1975 IGRF model which is absent in the post 1975 version.

On the other hand, Figure 36 for Zone 50N-65N shows no significant change in trend, nor does Figure 37 for Zone 65N-80N. (The latter figure does show increased peaks in the early years, but these are again attributed to measurement conditions in the auroral zone.) The time-dependent change component is absent in these two zones.

We conclude that the IGRF model does not simulate correctly the pre-1975 regional field in the southernmost zone occupied by AGC marine data. The model contains a spurious change-of-field component that is both time- and location-dependent. This might lead to errors in our gridded data set. However, it was decided not to apply any ad hoc corrections to the data, but to keep the well defined level of the reference fields, until further research on this subject leads to an internationally accepted correction.

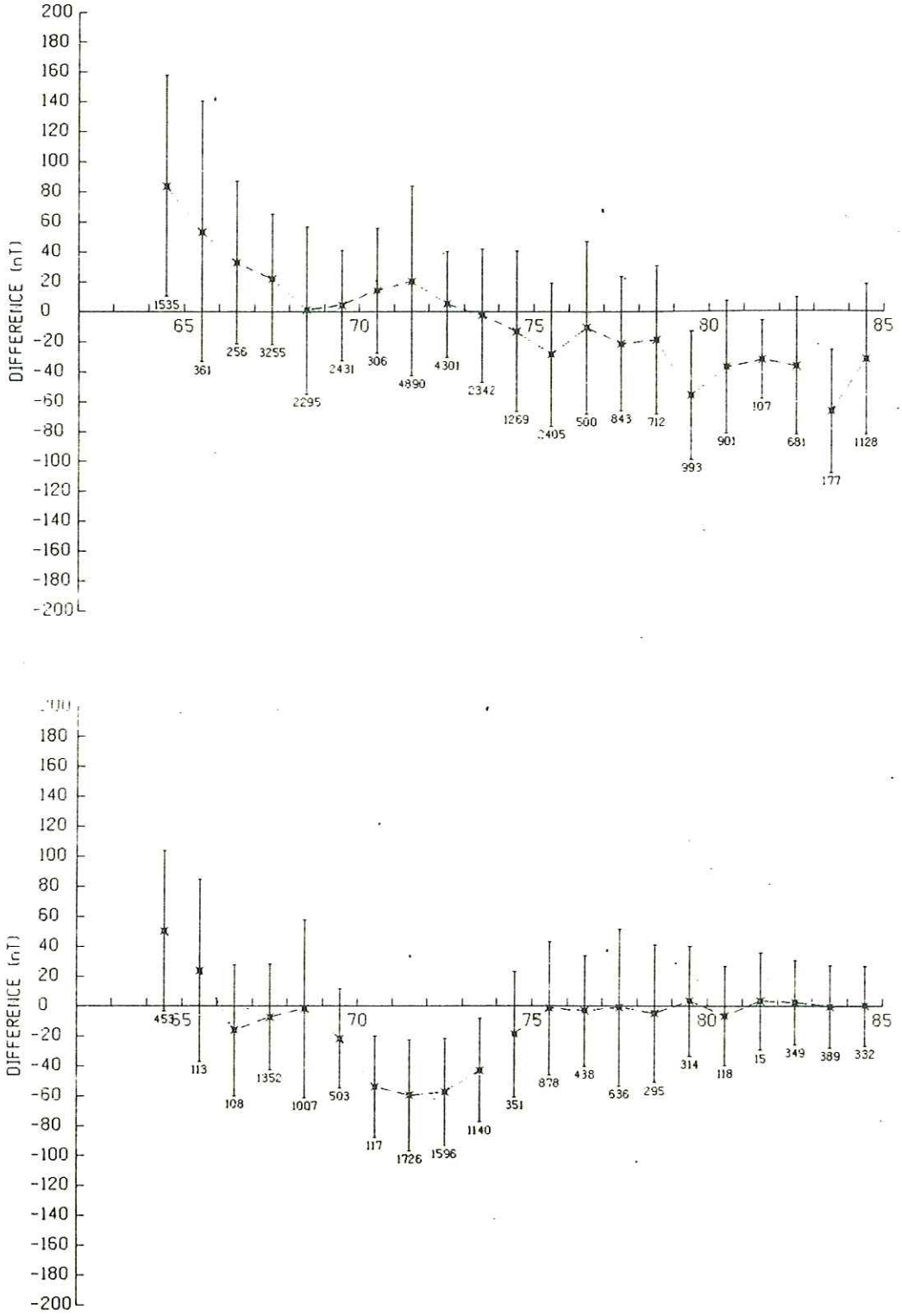

FIGURE 35. Statistical properties of external crossover sets in Zone 35N-50N. Top: excluding post-1975 crossover pairs. Bottom: excluding pre-1975 crossover pairs.

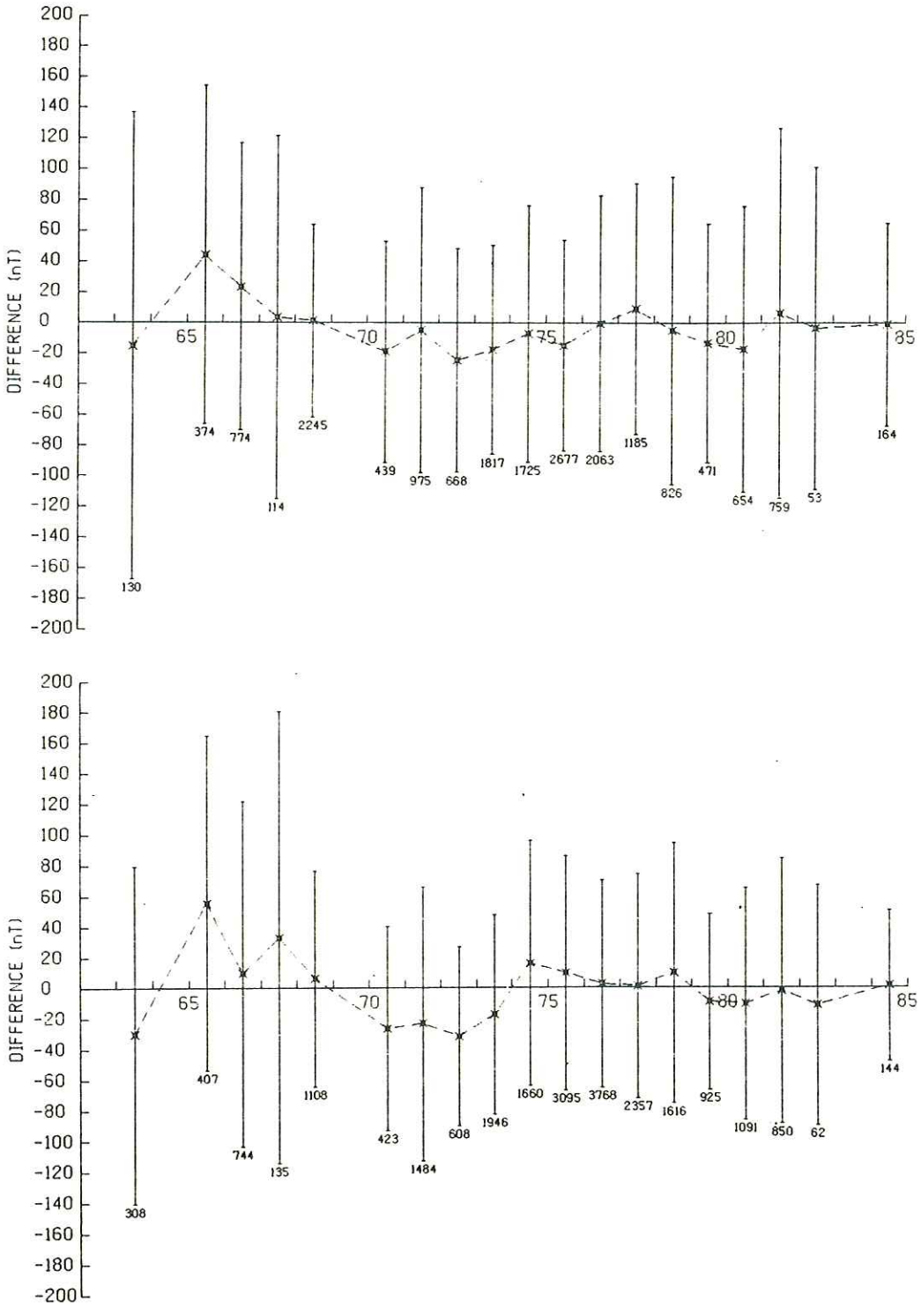

FIGURE 36. Statistical properties of external crossover sets in Zone 50N-65N. Top: excluding post-1975 crossover pairs. Bottom: excluding pre-1975 crossover pairs.

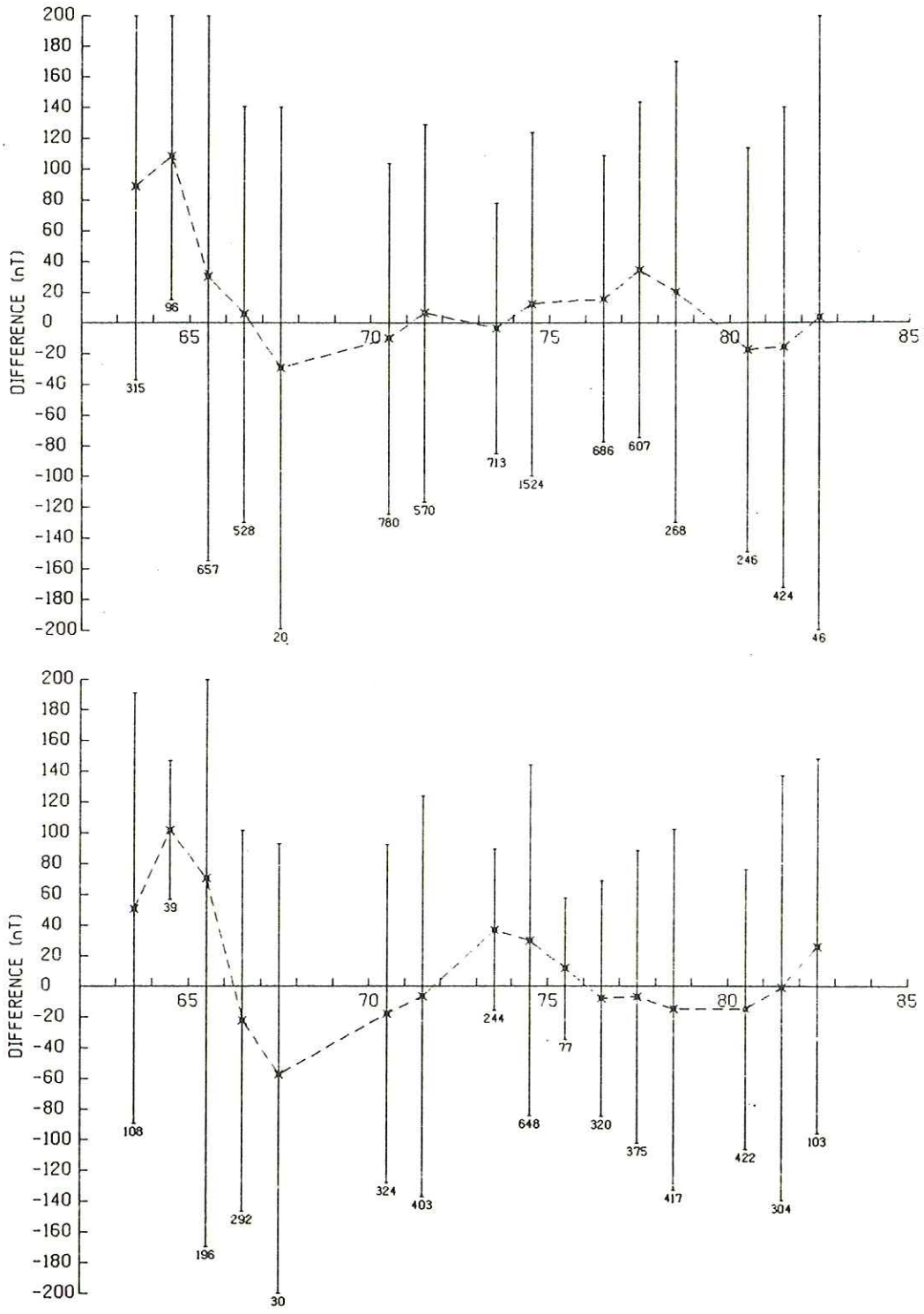

FIGURE 37. Statistical properties of external crossover sets in Zone 65N-80N. Top: excluding post-1975 crossover pairs. Bottom: excluding pre-1975 crossover pairs.

8. COMBINING MARINE AND AEROMAGNETIC DATA SETS

This section describes the procedures that were applied to the various subsets of marine and aeromagnetic data as they were incorporated into a common data base.

The coverage and distribution of the assembled subsets are shown in Figure 38 with identifying labels for the smaller subsets (Zone A, Zone B, etc). The objective was to integrate these subsets in a coherent fashion with reasonable agreement in their levels, and with smooth seams where they joined.

Some procedures were common in combining most or all data sets; other procedures were applied in particular cases in order to deal with specific problems.

8.1. General data preparations

The IGRF was applied or re-applied to all data sets to ensure consistency in the derivation of magnetic anomaly values. The aeromagnetic data that were obtained in flight line format and the marine magnetic data sets were checked for errors; bad data points were eliminated using the methodology described in the preceding sections. Data were all gridded to a common grid, i.e. .05 degree of latitude and longitude. In the case of the aeromagnetic data that had been obtained in already gridded form, usually only a regridding to the common grid was necessary.

At locations where relevelling was necessary between marine and aeromagnetic data, adjustments were as a rule applied to the aeromagnetic data to make them agree with the marine data. This was done because the general level of the marine data set was well defined by consistent application of the IGRF fields, while levels of the individual aeromagnetic subsets were usually not so well defined.

The gridding procedure used at AGC created a 'halo' of pseudo data points outside each subset of data. With a width of about three grid points, the halo had the effect of extrapolating magnetic field values from within a region of valid data into surrounding areas, and introduced the risk of biasing data in adjacent subsets. Where appropriate, the halo was trimmed by a program that removed the three outermost grid points around the periphery of a given subset. This procedure was applied mainly to the subsets of AGC marine data, because most of the aeromagnetic data were provided to us in a gridded form devoid of halos.

Small gaps in the individual data sets were filled with the two-dimensional Gaussian weighting function. A similar procedure was applied to fill openings between adjacent data sets, where they did not quite meet.

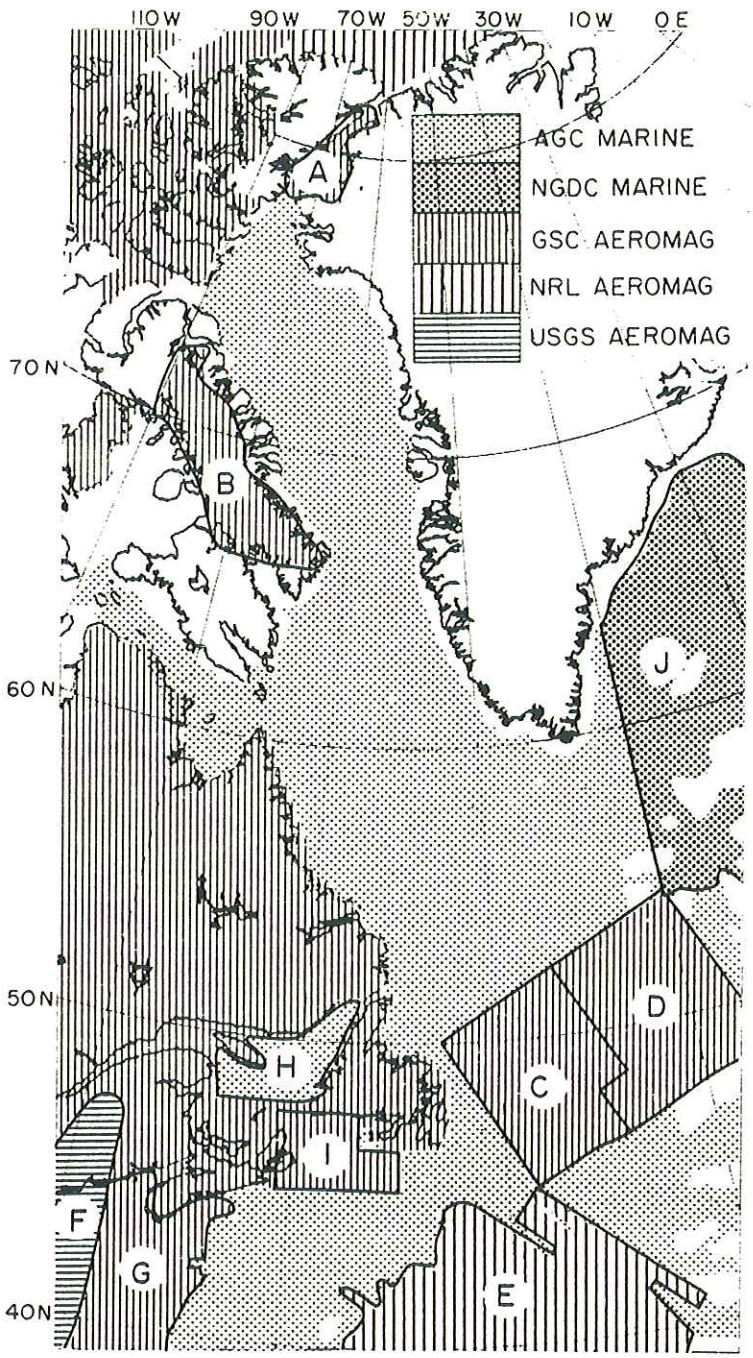

FIGURE 38. Coverage and distribution of the various data subsets that were incorporated into the final data base.

8.2. Methods of combining data

Depending on data quality, distribution, and other factors, marine and aeromagnetic data were combined in one of two fashions: merge, or insert-and-replace.

A merge could be accomplished in two ways: by combining subsets of data in their original track or flight line form, and then gridding all together in order to produce a single grid; by gridding the subsets separately, and then averaging the values of the separate grids in order to produce a single grid.

An insert-and-replace operation involved the discarding of poorer quality data within an area, and replacing with better quality data.

Seams between data sets where the levels did not match smoothly were treated with a cosine taper function, which multiplied grid points in a suitably wide band with values ranging from 0 to 1.

8.3. Primary marine and aeromagnetic data sets

Of the total data base, two primary components covered most of the continental and oceanic regions: the GSC aeromagnetic data over land in Quebec, Newfoundland, and the Maritime Provinces; the AGC marine data in Baffin Bay, the Labrador Sea, and the Northwest Atlantic. Where these data sets met or approached along the coast, their levels were in good overall agreement; no adjustments were required to match them up, and it was only necessary to fill in a few gaps with the two-dimensional Gaussian weighting function.

8.4. Arctic Islands and Ocean

Aeromagnetic information in these regions consisted of two data sets compiled by the GSC. The data over the Arctic Islands were initially assembled from government and industry observations, and published in the Magnetic Anomaly Map of Arctic Canada (McGrath and Fraser, 1981).

Data over the Arctic Ocean were collected by the US Naval Research Laboratory (Taylor et al, 1981; Vogt et al, 1979).

The two data sets were merged and provided to us in gridded form by the Geophysics Division of the GSC. No adjustments or levelling were applied to these data for combining with other data sets in the map area.

8.5. Kane Basin and northern Baffin Bay

Data in Kane Basin (Zone A in Figure 38) consisted of two GSC subsets that partially overlapped in the southern end: aeromagnetic data over the whole of the Basin extending up into Smith Sound; marine data in the southern Basin - this actually comprised the northernmost portion of the larger Baffin Bay data set.

An aeromagnetic data set did exist from an isolated survey in the northern end of Baffin Bay, but it was problematic, in that its level differed considerably from the marine data set; its inclusion would not have improved the quality of coverage in the area. This data set was therefore not included in the compilation.

A comparison of the two data sets in the overlap zone revealed an overall difference of 300 nT, with the aeromagnetic data high. As the marine data in Baffin Bay and southern Kane Basin were already internally consistent, it was judged preferable to adjust the entire aeromagnetic data set downwards by 300 nT, and to match the marine data. This merging was accomplished through a simple averaging of the anomaly values at each grid point.

Data north of 81.75N were eliminated to avoid problems in matching with data in the Lincoln Sea to the north, which also exhibited a substantial level difference.

8.6. Baffin Island

Aeromagnetic data existed over part of Baffin Island (Zone B in Figure 38) and was adjusted downward by 200 nT to achieve good agreement with the marine data in Baffin Bay. The gap along the coast between marine and aeromagnetic data was filled by means of the two dimensional Gaussian weighting function.

8.7. NE Newfoundland Shelf and SE Labrador Sea

This data set resulted from two surveys carried out concurrently: a high resolution operation over the NE Newfoundland Shelf/Orphan Basin, and a contiguous regional survey extending out into the deep ocean (Zones C and D, respectively, in Figure 38).

Data from the high resolution survey were obtained in gridded form at 625 m, and were resampled at .05 degree. Data from the regional survey were acquired in flight line form, already reduced along each line by the average value of the data for that line; they were first reconstituted by adding back their mean values, and then were gridded at .05 degree.

The aeromagnetic data, being more consistent and regular, was then inserted into the area to replace the marine data. Level differences at the perimeter between marine and aeromagnetic data

were smoothed by means of a cosine taper function operating over six grid points.

8.8. J-Anomaly survey

Both the marine and the aeromagnetic data in the J-Anomaly area (Zone E in Figure 38) were relatively sparse, but their levels agreed well. Consequently, the two data sets were combined in their original track and flight line forms, and then gridded together to produce a single grid. No special edge treatment was applied.

8.9. Gulf of Maine - Georges Bank

This region proved to be the most complex to handle, with three sets of aeromagnetic data complementing the marine data.

Initially, the high resolution USGS survey (Figure 13) and the Project MAGNET regional survey (Figure 14) were compared to reveal a level difference of 27nT. The level of the high resolution survey data was then raised by 25 nT to match the MAGNET data, and the former was cut into the latter in an insert-and-replace operation. A cosine taper function was applied to smooth the seam.

Next, that portion of the combined data set that lay east of longitude 65W was discarded, in preparation for eventual combination with the Georges Bank aeromagnetic data set.

Comparison of the combined USGS-MAGNET data set with AGC marine data showed an overall level difference of 11 nT, so the USGS-MAGNET data set was adjusted upward by 10 nT. It was then combined with the marine data in an insert-and-replace operation, where marine data was discarded in favour of the aeromagnetic data. A cosine taper function was applied to smooth the seams. This looked after the situation west of 65W in the Gulf of Maine (Zone F in Figure 38).

Finally, an analysis of the Georges Bank data (Zone G in Figure 38) revealed that an appropriate tilt adjustment would achieve a good fit with surrounding data. Consequently, an inclined plane correction was applied that reduced the level by 80 nT at the south end (40N) and decreased linearly to zero near the north end (44N). This adjusted data set was butt-joined to the combined USGS-MAGNET-marine data set along longitude 65W, with a three-point cosine taper function to smooth the seam.

8.10. Gulf of St. Lawrence

Aeromagnetic data in the southern part of the Gulf of St Lawrence and surrounding land areas were provided on a 2 km grid by Ottawa staff of the GSC, and were re-sampled on a 5 km grid at AGC. A

dense network of marine data covered the northern part of the Gulf (Zone H in Figure 38), complemented by an aeromagnetic survey of Anticosti Island. The latter data set consisted of a grid of N-S and E-W lines (Rolliff, 1968).

No level adjustments were necessary. Marine data were replaced by aeromagnetic data where available, and a three-point cosine taper function was applied to smooth the seam. Minor gaps along the North Shore between marine and aeromagnetic data were filled by means of a Gaussian weighting function. Immediately south of Anticosti Island, gaps between marine magnetic profiles were too wide to be infilled by interpolation, and so were left blank.

8.11. Laurentian Channel

A high resolution aeromagnetic survey provided good coverage south of Newfoundland, and linked areas that had been similarly surveyed over Newfoundland and Cape Breton Island (Zone I in Figure 38).

No level adjustments were necessary. Marine data were replaced with aeromagnetic data, and a three-point cosine taper function was applied to smooth the seam.

8.12. NGDC marine data SE of Greenland

Data were supplied as total field values in track form, and first had to be converted to anomaly values through application of the IGRF. The bulk of the data lay east of longitude 40E (Zone J in Figure 38), with a few tracks traversing the area of primary AGC coverage. These data points were merged with AGC data through production of a single grid. No level adjustments were applied.

8.13. Scotian Margin

As described and illustrated in a previous section, directional filtering was applied to de-corrugate a portion of data in this region. A subset of the original data lying in the quadrangle defined by four corner points 39.5N/60W, 45N/50.5W, 38N/50.5W, and 35N/60W, was removed from the data base. It was replaced with a block of the de-corrugated data that filled the area of the quadrangle, plus an exterior band around its perimeter measuring one-half degree wide. A smooth merge was effected by averaging old and new data in the half-degree band.

8.14. Maine and New England margin

GSC Ottawa staff provided a regional data compilation for the northeastern U.S. that had been assembled from a variety of sources, in preparation for the DNAG Magnetic Anomaly Map of

North America. Supplied in a 2 km grid, the compilation was re-sampled at AGC on a 5 km grid.

Data from the Maine area were then extracted from the re-sampled grid for insertion into the gap that existed in the AGC data base. No level adjustments were necessary north of the oblique line joining 45N/72W and 45.4N/67.5W. South of this line, data were fitted to a NW-dipping plane in order to match the merged data sets along the coast of the Gulf of Maine.

Similarly, data were extracted from the re-sampled grid to insert into the area of the continental margin south of Cape Cod. These were fitted to a NS-dipping plane elevated by 50 nT along the 38th parallel, and 250 nT along the 42th parallel.

9. DNAG MAP PREPARATIONS

The first major project to make use of the data base was the production of a map portraying the magnetic anomaly field over the continental margin of eastern Canada, to accompany the volume prepared by AGC staff as their contribution to the commemorative series for the Decade of North American Geology (DNAG) (Keen and Williams, in press).

Extending from the Gulf of Maine in the south to the Lincoln Sea in the north (see Figure 38 for an illustration of the map's full geographical extent), the map was constructed at a scale of 1:5 million on a Lambert conformal projection. Standard parallels were selected at 49N and 77N, to remain compatible with the conventional 1:5 million maps for the whole of Canada, which are produced for various other purposes.

In a reasonably straightforward process, the geographic grid coordinates of the values in the data base were converted to a Lambert projection grid suitable for processing on the Applicon colour plotter at the Computer Science Centre in Ottawa.

A colour scale was chosen to match the natural spectrum of white light, with blue negative, yellow zero, and red positive. Different shades were used at 25 nT intervals from -350 nT to 300 nT, with intervals increasing to 50, 100, 250, and 500 nT beyond those limits.

Grid conversion and the preparation of input tapes for the Applicon plotter were carried out at AGC, with tapes - and the resulting colour plots - being despatched between Dartmouth and Ottawa by courier. With proper preparation and notification, etc., turnaround time for a typical job (including transit) was about a week, and often less.

Several plots were executed during the course of the project to test software and procedures, and to inspect the state of the data base as it was being put through the various stages of combination, correction, and refinement. These plots featured annotated margins, latitude-longitude grids, and detailed coastlines.

Size restrictions precluded one-pass production of the entire map on the Applicon plotter, so the test maps had to be made up in three pieces which were then taped together. This was satisfactory as long as the maps were only being used for quality control of the data base.

For the final stage, which involved the production of colour separations of the anomaly field alone (i.e. no margin, grid, or coastline) for printer's use, we turned to a larger format Optronics plotter, again situated in the Ottawa area. The colour separations were then handed to cartographic staff at GSC Headquarters, who added other elements, such as a title block with brief descriptive notes, annotations, landforms, etc.
The final version of the map has a modified Lambert projection to the north of 80N.

10. CONCLUDING REMARKS

This report sums up the procedures used to handle numerous sets of marine and aeromagnetic data through various stages: initial collection in the field; editing, correction, and compilation; implementation of a coherent data base; production of a regional map portraying most of the contents of the data base.

The project provided opportunities: to assemble a large quantity of data from a variety of sources; to develop powerful techniques for the manipulation and display of these data; to prepare a body of quality data that readily lends itself to follow-up interpretation; to identify an important problem in the present implementation of the International Geomagnetic Reference Field.

As shown by the crossover analysis, we detected a variation in the IGRF fields that is not present in the anomalies. This variation is not only time dependent , but also location dependent. It might lead to errors in the data set. We have not yet found an acceptable way to correct for the time dependency of the magnetic anomalies, but we expect that further research, done by dividing the data set into smaller segments of 2 years and then using spatial and frequency correlation analysis in order to establish the reliable parts of the anomaly field, will lead to a better definition of these anomalies while increasing their accuracy.

In their present condition, both the data base and the resulting regional map are important and reliable adjuncts to research into

the structure of the continental margin off eastern Canada, and they provide a sound foundation upon which to base future magnetic interpretation.

ACKNOWLEDGEMENTS

The activities described in this report were carried out under the auspices of the East Coast Task of the Frontier Geoscience Program.

The project benefitted from the advice and participation of many people.

From the Potential Fields Group of the Regional Reconnaissance Subdivision of the Atlantic Geoscience Centre who assisted on a day-to-day basis, or who made helpful suggestions: Paul Girouard, Bosko Loncarevic, Gordon Oakey, Wayne Prime, Keh-Gong Shih, Shiri Srivastava, and John Woodside. Myriad details relating to the illustrations, and to their integration with the final text of the report, were handled capably by Claudia Powell.

From staff of the Geophysics Division in Ottawa who provided aeromagnetic data, expertise, or various services, : Dwight Dods, John Halpenny, Bryne Hearty, Peter Hood, Wim Knappers, Ken McConnell, Ed Ready, and Dennis Teskey.

From US colleagues who provided data: Wally Bothner (University of New Hampshire), Kim Klitgord (USGS), and Skip Kovacs (USNRL).

A substantial part of the software that was used throughout the project was developed by workers at the Veining Meinesz Laboratorium, Utrecht University, The Netherlands.

We are pleased also to acknowledge our signicant debt to the great numbers of field and support personnel, ships' crews, and aircraft crews, without whom we would not have had such a magnificent data set to work with.

BIBLIOGRAPHY

Auld, D.R., Law, L.K., and Currie, R.G. 1979: Cross-over error and reference station location for a marine magnetic survey; Mar. Geophys. Res., 4, 167-179.

Barrett, D.L., and Keen, C.E. 1976: Mesozoic magnetic lineations, the Magnetic Quiet Zone, and sea floor spreading in the northwest Atlantic; J. Geophys. Res., 81, 4875-4884.

Bullard, E.C. and Mason, R.G. 1961: The magnetic field astern of a ship; Deep Sea Res., 8, 20-27.

Dods, S.D., Teskey, D.J., and Hood, P.J. 1985: The new series of 1:1,000,000 scale magnetic anomaly maps of the Geological Survey of Canada: Compilation techniques and interpretation. in The Utility of Regional Gravity and Magnetic Anomaly Maps, ed. W.J. Hinze, Society of Exploration Geophysicists, Tulsa, OK.

Earth Physics Branch. 1986: Integration of Atlantic Geoscience Centre marine gravity data into the National Gravity Data Base; EPB Open File 85-32, GSC Open File 1232.

Geoterrex Limited. 1986: Operations and processing report on a high sensitivity aeromagnetic survey over the East Newfoundland Shelf - Orphan Knoll Area; Unpublished contractor's report.

Grant, S.T. and Wells, D.E. 1982: Interactions among integrated navigation system components; International Association of Geodesy Symposium on Marine Geodesy, Tokyo.

Haworth, R.T. 1980: Appalachian structural trends northeast of Newfoundland and their trans-Atlantic correlation; Tectonophysics, 64, 111-130.

Hill, M.N., and Mason, C.S. 1962: Diurnal variation of the earth's magnetic field at sea; Nature, 195, 365-366.

Hood, P.J., McGrath, P.H., and Teskey, D.J. 1985: Evolution of Geological Survey of Canada magnetic-anomaly maps: A Canadian perspective. in The Utility of Regional Gravity and Magnetic Anomaly Maps, ed. W.J. Hinze, Society of Exploration Geophysicists, Tulsa, OK.

Hood, P.J., and Ready, E. 1976: Federal-provincial aeromagnetic survey program of Canada: a progress report. in Report of Activities, Part B, Geological Survey of Canada, Paper 76-1B, 267-272.

IAGA Commission 2, Working Group 4. 1969: International Geomagnetic Reference Field 1965.0; J. Geophys. Res., 74, 4407-4408.

IAGA Division I, Study Group. 1976: International Reference Field 1975; EOS, Trans. AGU, 57, 120-121.

IAGA Division I, Working Group 1. 1981: International Geomagnetic Reference Fields: DGRF 1965, DGRF 1970, DGRF 1975 and IGRF 1980; EOS Trans AGU, 62, 1169.

IAGA Division I, Working Group 1. 1986: International Geomagnetic Reference Field Revision 1985; Eos, Trans. Amer. Geophys. Union, 67, 523-524.

Jackson, H.R., Keen, C.E., Falconer, R.K.H., and Appleton, K.P. 1979: New geophysical evidence for sea-floor spreading in central Baffin Bay; Can. J. Earth Sci., 16, 2122-2135.

Keen, M.J., and Williams, G.L., eds. In press: Geology of the Continental Margin of Eastern Canada; Decade N. Am. Geology (DNAG) Series.

Kenting Earth Sciences Limited. 1982: Report on an aeromagnetic survey in the Georges Bank area, Scotian Shelf, Eastern Canada for the Geological Survey of Canada; Unpublished contractor's report.

Kenting Earth Sciences Limited. 1987: Operations and compilation report on an aeromagnetic survey of the Laurentian Channel area for the Geological Survey of Canada; Unpublished contractor's report.

Macnab, R., 1974: Marine geophysical surveys northeast of Newfoundland and in the St. Lawrence estuary; in Report of Activities, Geological Survey of Canada, Paper 74-1, Part A, 121-122.

Macnab, R., Shih, K.G., and Srivastava, S.P. 1985A: Application of the new International Geomagnetic Reference Field (IGRF80) to large sets of marine magnetometer data; Phys. Earth Planet. Inter., 37, 5-11.

Macnab, R.F., and Srivastava, S.P. 1975: A regional geophysical survey of the Labrador Sea; in Report of Activities, Part A, Geological Survey of Canada, Paper 75-1, Part A, 177-179.

Macnab, R.F. 1983A: Multiparameter mapping off the east coast of Canada; in Current Research, Part A, Geological Survey of Canada, Paper 83-1A, 163- 171.

Macnab, R.F. 1983B: SHIPAC: a software package for the shipboard processing of marine geophysical survey data; in Current Research, Part B, Geological Survey of Canada, Paper 83-1A, 327-330.

Macnab, R., Loncarevic, B.D., Cooper, R.V., Girouard, P.R., Hughes, M.D., and Shouzhi, F. 1985B: A regional marine multi-parameter survey south of Newfoundland; in Current Research, Part B, Geological Survey of Canada, Paper 85-1B, 325-332.

McGrath, P.H., and Fraser, I. 1981: Magnetic Anomaly Map of Arctic Canada, scale 1:3,500,000. Map No. 1512A, Geological Survey of Canada, Ottawa.

Miller, R.O., Macnab, R., Amos, C.L., Fader, G.B. 1983: Canadian east coast multiparameter surveys, 1982. in Current Research, Part B, Geological Survey of Canada, Paper 83-1B, 331-334.

Peddie, N.W. 1982: International Geomagnetic Reference Field: the Third Generation; J. Geomag. Geoelectr., 34, 309-326.

Regan, R.D., and Rodriquez, P. 1981: An overview of the external magnetic field with regard to magnetic surveys; Geophysical Surveys, 4, 255-296.

Roliff, W.A. 1968: Oil and gas exploration - Anticosti Island, Quebec; Proceedings of the Geological Association of Canada, 19, 31-36.

Simpson, R.W., Jachens, R.C., Blakely, R.J., and Saltus, R.W. 1986: A new isostatic residual map of the conterminous United States with a discussion on the significance of isostatic residual anomalies; J. Geophys. Res., 91, 8328--8372.

Slootweg, A.P. 1978: Computer contouring with a digital filter; Mar. Geophys. Res., 3, 401-405.

Taylor, P.T., Kovacs, L.C., Vogt, P.R., and Johnson, G.L. 1981: Detailed aeromagnetic investigation of the Arctic Basin, 2; J. Geophys. Res., v. 86, p. 6323-6333.

Teskey, D.J., Dods, S.D., and Hood, P.J. 1982: Compilation techniques for the 1:1 million magnetic anomaly map series; in Current Research, Part A, Geological Survey of Canada, Paper 82-1A, 351-358.

Verhoef, J., Collette, B.J., Miles, P.R., Searle, R.C., Sibuet, J-C., and Williams, C.A. 1986: Magnetic anomalies in the north-east Atlantic Ocean; Mar. Geophys. Res., 8, 1-25.

Verhoef, J., and Scholten, R.D. 1983: Cross-over analysis of marine magnetic anomalies; Mar. Geophys. Res., 5, 421-435.

Vogt, P.R., Taylor, P.T., Kovacs, L.C., and Johnson, G.,L. 1979: Detailed aeromagnetic investigation of the Arctic Basin; J. Geophys. Res., v. 84, p. 1071-1089.

TABLE 1. MARINE DATA SETS

YR-NUM	VESSEL	LOCALITY	NAVIGATION	OB PTS	KM
63-012	LABRADOR	Kane Basin	Radar, DR	10400	10311
64-018	BAFFIN	Orpheus Basin	Decca	10800	4857
64-019	BAFFIN	Bay of Fundy	Lambda	12400	4827
64-020	LABRADOR	Lancaster Sound	Radar, DR	1200	1518
64-027	HUDSON	Orpheus Basin	Decca	7600	1913
65-006	HUDSON	Scotian Margin	Decca	34800	15789
65-022	LABRADOR	Arctic Channels	Radar, DR	31600	10151
65-024	HUDSON	Hudson Strait	Radar, DR	14800	5883
65-034	HUDSON	Scotian Margin	Decca	3600	1263
66-008	BAFFIN	Tail of the Banks	Lambda	10000	4656
66-010	HUDSON	Scotian Margin	Decca	2000	1578
66-019	HUDSON	Scotian Margin	Decca	32000	13272
66-022	LABRADOR	Ungava Bay	DF	50400	18833
66-099	SHOUP	Labrador Sea	Loran	11200	6558
67-007	BAFFIN	Scotian Margin	Decca	25600	9692
67-014	BAFFIN	Grand Banks	Lambda	82000	29810
67-099	MARIPOSA	Labrador Sea	Loran	2800	1472
68-021	BAFFIN	Gulf St Lawrence	Lambda	74800	29398
68-022	HUDSON	Grand Banks	Satnav	7400	11625
68-023	THETA	Grand Banks	Decca	16800	4578
69-002	BAFFIN	Scotian Margin	Decca	16800	6620
69-021	BAFFIN	Gulf St Lawrence	Lambda	65600	26478
69-025	HUDSON	Grand Banks	Satnav	14400	6031
69-050	HUDSON	Various	Satnav	16400	28613
70-002	BAFFIN	Scotian Margin	Satnav	19200	6341
70-021	BAFFIN	Baffin Bay	Satnav	49600	15485
70-028	DAWSON	Baffin Bay	Satnav	51600	18246
71-000	LYNCH	Labrador Sea	Satnav	11200	4939
71-014	HUDSON	Gulf of Maine	Satnav	35600	12047
71-017	BAFFIN	Flemish Cap	Lambda	94800	37023
71-022	HUDSON	Grand Banks	Satnav	12000	4475
71-030	DAWSON	Labrador Sea	Satnav	30800	6726
71-032	HUDSON	Baffin Bay	Satnav	56400	18720
72-009	DAWSON	S Nfld Shelf	Satnav	30800	7941
72-015	MINNA	Grand Banks	Lambda	75200	24075
72-021	HUDSON	Scotian Margin	Satnav/Loran	30400	8201
72-025	HUDSON	Labrador Sea	Satnav/Loran	40400	12414
72-036	HUDSON	Scotian Margin	Satnav/Loran	5200	1300
73-006	HUDSON	Laurentian Chan	Satnav/Loran	22800	5603
73-011	HUDSON	Scotian Margin	Satnav/Loran	41200	13515
73-014	BAFFIN	Gulf St Lawrence	Hifix	30000	2699
73-019	MINNA	NE Nfld Shelf	Lambda/Loran	85200	25851
73-027	DAWSON	Labrador Sea	Satnav/Loran	40000	13264
73-034	DAWSON	Tail of the Banks	Satnav/Loran	20000	7088
74-002	BAFFIN	Scotian Margin	Satnav/Loran	26400	9318
74-003	HUDSON	Scotian Margin	Satnav	4800	1931
74-015	BAFFIN	Gulf St Lawrence	Hifix	22000	2444
74-019	SACKVILLE	Scotian Margin	Satnav	20400	6288

74-021	HUDSON	Scotian Margin	Satnav/Loran	11200	4584
74-023	MINNA	Labrador Sea	Satnav/Loran	60000	17495
74-026	HUDSON	Various	Satnav	84000	30643
75-009	HUDSON	Various	Satnav/Loran	131600	41830
75-011	BAFFIN	Foxe Basin	Hifix	30000	7060
75-018	M KARLSEN	Labrador Sea	Lam/Sat/Lor	110800	38481
76-001	BAFFIN	Scotian Margin	Satnav/Loran	85200	19136
76-012	BAFFIN	Gulf St Lawrence	Satnav/Loran	33600	6033
76-019	M KARLSEN	Labrador Sea	Satnav/Loran	80400	30092
76-023	HUDSON	Baffin Bay	Satnav	23200	6592
76-025	HUDSON	Lancaster Sound	Satnav	17600	5985
76-029	HUDSON	Baffin Bay	Satnav	33600	10936
76-031	M KARLSEN	Nfld Basin	Satnav/Loran	15600	16490
77-008	BAFFIN	Gulf St Lawrence	Hifix	31200	4755
77-014	HUDSON	NE Nfld Margin	Satnav/Loran	12400	4447
77-019	M KARLSEN	Labrador Sea	Satnav/Loran	43600	11968
77-021	HUDSON	Labrador Sea	Satnav/Loran	18800	5814
77-024	HUDSON	Baffin Bay	Satnav	10400	4306
77-027	HUDSON	Baffin Bay	Satnav	22000	5732
78-010	BAFFIN	Labrador Sea	Satnav/Loran	15200	4703
78-016	HUDSON	NE Nfld Margin	Satnav/Loran	12800	4632
78-019	M KARLSEN	Labrador Sea	Satnav/Loran	24800	7781
78-020	HUDSON	NE Nfld Margin	Satnav/Loran	9200	3937
78-023	HUDSON	NE Nfld Shelf	Satnav/Loran	2400	6392
78-026	HUDSON	Baffin Bay	Satnav	7200	2921
78-029	HUDSON	Baffin Bay	Satnav	36400	9313
79-013	HUDSON	Labrador Sea	Bionav	22400	2922
79-015	BAFFIN	Scotian Margin	Bionav	52800	14826
79-019	HUDSON	Labrador Sea	Bionav	10000	5137
80-001	DAWSON	Scotian Margin	Bionav	1600	404
80-010	HUDSON	Grand Banks	Bionav	23200	2647
80-028	HUDSON	Davis Strait	Bionav/Accu	30400	6517
80-031	BAFFIN	Davis Strait	Bionav/Accu	23600	6112
80-035	HUDSON	Davis Strait	Bionav/Accu	1600	4657
80-037	HUDSON	Labrador Sea	Bionav	2800	925
81-038	DAWSON	Davis Strait	Bionav/Accu	49200	18869
81-045	HUDSON	Davis Strait	Bionav	20000	7492
82-018	HUDSON	Scotian Margin	Bionav	18400	6854
82-034	HUDSON	Baffin Bay	Bionav	9600	2976
82-039	BAFFIN	Scotian Margin	Bionav	54800	10355
83-035	BAFFIN	Scotian Margin	Bionav	26400	7959
84-030	HUDSON	Labrador sea	Bionav	25200	6598
84-044	BAFFIN	S Nfld Margin	Bionav	39200	12163

TABLE 2. AEROMAGNETIC DATA SETS

YEAR	LOCALITY	AGENCY	OPERATOR	NAVIGATION	SPACING	ALT	GRID	REMARKS
1950-80	E Canada	GSC	Various	Various	800 m	305 m	2 km	Compiled by GSC
1950-80	Arctic Is	GSC/Ind	Various	Various	Various	.8-6 km		Compiled by GSC
1964	G Maine	USN	USNOO	Various	10-20 km	500 m		Project MAGNET
1974-78	Arctic O	NRL	NRL	Inertial	Various	150+ m	2 km	Compiled by GSC
1978	G Maine	USGS			2 km	500 m		Provided by USGS
1977	J-Anomaly	NRL	NRL	Inertial	20 km	300 m		Provided by NRL
1981-82	Kane B	GSC	NAE				2 km	Provided by GSC
1982	Georges B	GSC	Kenting	Dopp/Lor	2-6 km	305 m	813 m	
1985	NE Nfld	GSC/Ind	Geoterrex	Lor/GPS/INS	3X9 km	305 m	625 m	
1985	SE Labrador S	GSC	Geoterrex	Lor/GPS/INS	30 km	305 m		
1985	Laurentian C	GSC	Kenting	Lor	1-4 km	305 m		
Various	SE Can/NE US	Various	Various	Various			2 km	Compiled by GSC

Note: Grid column indicates grid spacing of data when received by AGC. A blank signifies that the data were provided ungridded and in flight line form.

TABLE 3. MARINE DATA FLAGGED AS ERRONEOUS

YR-CRU	START DDDHHMM	END DDDHHMM
66-010	1510300	1512000
68-022	0000000	1602000
68-022	1610700	3650000
70-021	2830800	2851200
71-014	1110400	1151400
71-022	0000000	3562359
71-032	2681200	2700130
72-009	1301500	1302359
72-021	2170000	2171200
72-025	2730935	2750700
74-023	2032200	2061600
74-026	2050200	2050900
74-026	2070600	2071600
75-009	1820000	1832300
76-023	2151100	2170000
76-029	2910400	2911600
76-031	2870300	2881340
77-027	2612300	2621800
78-010	2670000	2680800
78-026	0000000	3650000
79-013	1721800	1730000
79-013	1870000	1881200
79-015	2811800	2821900
79-015	2840600	2850300
79-015	2960500	2962200
80-035	2962200	2971000
84-030	2201200	2210400
84-030	2371600	2390000
84-044	2952100	2961000